8-31-2024

A micromagnetic study of skyrmions in thin-film multilayered ferromagnetic materials

Nicholas J. Dubicki
New Jersey Institute of Technology, nickdubicki@gmail.com

ABSTRACT

A MICROMAGNETIC STUDY OF SKYRMIONS IN THIN-FILM MULTILAYERED FERROMAGNETIC MATERIALS

by
Nicholas J. Dubicki

Magnetic skyrmions are topologically protected, localized, nanoscale spin textures in non-centrosymmetric thin ferromagnetic materials and heterostructures. At present they are of great interest to physicists for potential applications in information technology due to their particle-like properties and stability. In a system of multiple thin ferromagnetic layers, the stray field interaction was typically treated with various simplifications and approximations. It is shown that extensive analysis of the micromagnetic equations leads to an exact representation of the stray field interaction energy in the form of layer interaction kernels, a so-called 'finite thickness' representation. This formulation reveals the competition between perpendicular magnetic anisotropy (PMA) and stray field in the stabilization of skyrmions, and gives new existence and collapse criteria. This is demonstrated in detail in the case of a monolayer of finite thickness and compared to past results which cannot reveal the collapse criteria. The layer interaction kernels are then treated asymptotically for thin films to obtain the nonlocal stray field interaction energies of multilayers. It is thereby shown that a system of PMA multilayers interacting with each other only through the stray field can support bound columns of concentric skyrmions in each layer, enabled by the stray field interaction alone. The multilayer skyrmions are shown to be larger than those of a monolayer, and exhibit a full range of Bloch-Néel hybrid combinations depending on certain constraints given by the interlayer volume charge energy. Further solutions are given for Dzyaloshinskii-Moriya interaction enabled skyrmions in a system of multilayers interacting with each other through both ferromagnetic and antiferromagnetic exchange.

A MICROMAGNETIC STUDY OF SKYRMIONS IN THIN-FILM MULTILAYERED FERROMAGNETIC MATERIALS

by
Nicholas J. Dubicki

A Dissertation
Submitted to the Faculty of
New Jersey Institute of Technology
and Rutgers, The State University of New Jersey—Newark
in Partial Fulfillment of the Requirements for the Degree of
Doctor of Philosophy in Mathematical Sciences

Department of Mathematical Sciences

August 2024

A MICROMAGNETIC STUDY OF SKYRMIONS IN THIN-FILM MULTILAYERED FERROMAGNETIC MATERIALS

Nicholas J. Dubicki

Dr. Cyrill Muratov, Dissertation Co-Advisor   Date
Professor of Mathematics, Università di Pisa. Pisa, Italy

Dr. Michael Siegel, Dissertation Co-Advisor   Date
Professor of Mathematical Sciences, NJIT

Dr. Anand Oza, Committee Member   Date
Associate Professor of Mathematical Sciences, NJIT

Dr. David Shirokoff, Committee Member   Date
Associate Professor of Mathematical Sciences, NJIT

Dr. Anne Bernand-Mantel, Committee Member   Date
Senior Research Scientist, Centre d'Élaboration de Matériaux et d'Études
Structurales. Toulouse, FR

Dr. Valeriy Slastikov, Committee Member   Date
Senior Lecturer of Applied Mathematics, University of Bristol. Bristol, UK

BIOGRAPHICAL SKETCH

Author: Nicholas J. Dubicki

Degree: Doctor of Philosophy

Date: August 2024

Undergraduate and Graduate Education:

- Doctor of Philosophy in Mathematical Sciences
  New Jersey Institute of Technology, Newark, NJ, 2024

- Master of Science in Applied Mathematics
  University of New Hampshire, Durham, NH, 2019

- Bachelor of Science in Mechanical Engineering
  University of New Hampshire, Durham, NH, 2017

Major: Mathematical Sciences

For my brother, Daniel.

ACKNOWLEDGMENTS

I am indebted to my advisor, Cyrill Muratov, who gave me guidance and confidence through my exploration of mathematical physics. Because of his tutelage, I emerge with great confidence in my abilities. He has imparted on me a shrewd and critical nature becoming of a modern scientist.

I thank the Committee members, Drs. Valeriy Slastikov, Anne Bernand-Mantel, Michael Siegel, David Shirokoff, and Anand Oza, for taking an interest in me and my work. They have also served as mentors to me and offered their expertise and council.

Invaluable contributions to my work were made by my collaborators Drs. Anne Bernand-Mantel, Theresa Simon, and Valeriy Slastikov.

Meanwhile, my colleagues and friends have supported me in kind and seen me though this endeavor. Pia Sen, Atul Anurag, David Mazowiecki, Nicholas Harty, Andrew White, Rey Sentina, Brian O'Donnell, Ayushi Sangoi, Arseniy Gutnik, Anjali Madgula, Jose Pabón, Jake Brusca, Dr. Tadanaga Takahashi, and Dr. Roy Goodman. There are many others I would like to mention among the NJIT and Rutgers-Newark community, were it not for the limited space available to me.

TABLE OF CONTENTS

Figure   **Page**

Figure   **Page**

CHAPTER 1

INTRODUCTION

The nature of ferromagnetism has its origins in quantum physics. Ideas such as the Pauli exclusion principle were necessary to explain how ferromagnetic materials sustain a net magnetic moment at the atomic level. This is due to their atomic structure consisting of an excess of unpaired d-orbital electrons [26]. The magnetic moment results from the constructive combination of the spin of these unpaired electrons. 'Spin' may equivalently refer to the electron's intrinsic angular momentum, or to its intrinsic magnetic moment. For the limited scope of this dissertation, the term 'spin' may refer to any object with a definable and discrete magnetic dipole moment. Meanwhile, the ferromagnet's essential property is its tendency for neighboring spins in the material structure to come into parallel alignment with one another, promoting an order of uniformly parallel elementary spins. The uniformity promoting mechanism at hand is known as the Heisenberg exchange interaction, or simply 'exchange'.

When examined at the level of an aggregate material, these atomic level interactions give rise to global uniformity promoting behavior in materials which may result in a macroscopically observable magnetic moment. At this scale, however, the material interaction is modulated by the long distance interactions it undergoes through the magnetic field, disrupting the uniformity and leading to complex multiscale organization of the material's magnetic moments. The material's self-interaction through the magnetic field is referred to as the 'stray field interaction'. These basic frameworks were enough for Landau, Lifshitz, and their peers to begin the study of magnetic domains and domain walls [59, 60], domains being examples of large scale regions of a material all magnetized in the same direction, and domain walls, referring to the transition region between domains where the material magnetization

rapidly transitions from one domain's alignment to the other. These advances were a fundamental step in understanding the multiscale structure of ferromagnetics as a consequence of competing magnetic interactions.

The magnetization structure of interest in the present study are the so called magnetic skyrmions. These are localized solitary regions formed in a magnetic material that resemble a nanoscopic circular domain which achieves the opposite magnetization to that of its surroundings at a single point. The circular symmetry imbues them with some stability with respect to fundamental magnetic interactions. The skyrmion's smallness, controllability by electric currents and spin-orbit interactions [25, 70], and stability properties attracted researchers to study and manufacture materials as skyrmion hosts. Advances herein may form the basis for the manufacture of skyrmion based computer memory and logic devices [34, 35, 76, 102, 113]. Such devices have already been proposed [87, 110]. One example is the skyrmion racetrack memory described by Fert et al. [34].

Development of skyrmions as a concept began with T. Skyrme, who described the Skyrme mechanism that gives rise to the formation of topological solitons in 1961, intending to use them as a model of nucleons [98]. In the context of ferromagnetism, Belavin and Polyakov in 1975 first showed the existence of topologically nontrivial energy minimizing structures in 2D ferromagnets under the exchange interaction alone, a result to feature heavily in our work [6]. In 1989 Bogdanov, Kudinov, and Yablonskii were able to characterize stable isolated "vortex" states in magnetic materials with Dzyaloshinskii-Moriya interaction (DMI) [18, 19], which would later be called *magnetic* skyrmions. Bogdanov and Hubert went on to refine the stability properties of skyrmions [16, 17]. Skyrmions have since been observed in experiments, first in 2009 [75] (and see further developments in experimental work summarized by [20, 46, 71, 101, 107]).

Feasibility of any skyrmion device relies on properly assessing the dynamics and stability properties, for which much has been done. Reasonable schemes have been conceived for writing and deleting skyrmions in a sample [89, 97]. Other authors gave sufficient criteria for room temperature stable skyrmions [10, 24] and assesed their thermal stability [3, 44, 68, 104]. More recently, Bernand-Mantel et al. used stochastic analysis to predict expected skyrmion lifetimes depending on material parameters [14]. The same was studied in discrete lattice models by Potkina et al. [85].

We emphasize the problem of multilayered thin ferromagnetic systems, and the use of the micromagnetic model in explaining the role of the stray field interaction in facilitating the existence or nonexistence of skyrmion solutions and their consequent properties in different geometries of ferromagnetic materials.

1.1   On Skyrmions as Topological Solitons

Skyrmions are topologically nontrivial objects, in the sense that when the magnetization configurations are regarded as continuous maps, it is impossible to deform a skyrmion continuously to the uniform state.   We will define its topological characteristics more precisely in Section 3.1. This motivates the search for various other species of isolated topologically nontrivial magnetic structure (see Figure 1.2) [42, 94, 113]. The field has thus enjoyed many contributions from its parallel mathematical disciplines studying topologically nontrivial minimizers of the Dirichlet energy, or so called harmonic maps [47].   Indeed, study of these maps is directly related to the stable states of exchange dominant ferromagnetic films, where a fully realized isolated magnetic texture is understood to be closely approximated in some sense by harmonic maps [8, 93].

Realization and study of degree 1 harmonic maps in two dimensional magnetic structure gives a mathematical basis to begin the study of skyrmions. Immediately, local minimizers of the exchange energy are characterized by several tunable degrees
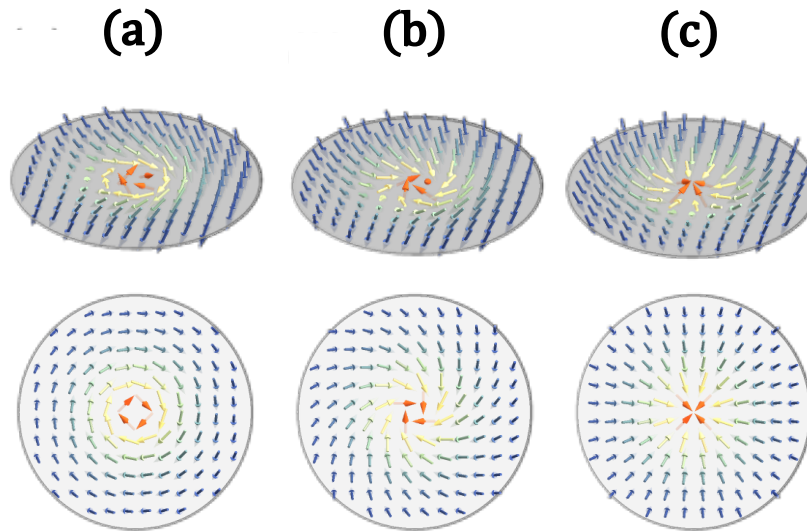
Figure 1.1 Schematic diagrams of magnetic skyrmions in the plane. (a) Bloch skyrmion, (b) Hybrid skyrmion, (c) Néel skyrmion.

of freedom including the profile's dilation, rotational character, and position in the plane (see Chapter 3) [6]. Stable skyrmions in the context of harmonic maps in 2D ferromagnets in the presence of other interactions were first rigorously obtained by Melcher in 2014 [72], and in 2017 shown to converge to harmonic maps in some conformal limit [30]. The skyrmion is endowed with a rotational sense according to how the magnetization vector transitions from the core to the surroundings, and several such species of skyrmion are classified based on this parameter. Such cases are diagrammed in Figure 1.1. Those which acquire a vortex-like character and where, when transitioning from core to surroundings the magnetization rotates about the radial vector, ever perpendicular to it, in a helical path, are called a Bloch skyrmions. When the magnetization, however, rotates toward the radial axis when transitioning from core to surroundings such that it always resides in the same vertical plane containing the radial axis, this is called a Néel skyrmion. Skyrmions may also exhibit a hybrid phase intermediate between the Néel and Bloch cases. Depending on the magnetic system, one or another species of skyrmion may be enabled to the exclusion of others, and this becomes important when studying how they dynamically deform and
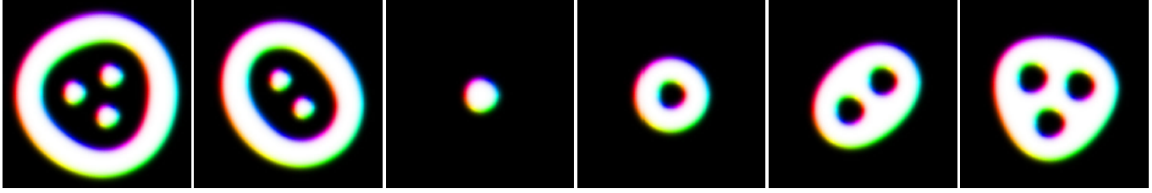
Figure 1.2 Isolated magnetic textures realized in simulations of ultrathin ferromagnetic films. Black and white coloring encode the out-of-plane component of magnetization. Objects (and topological charge) as they appear from the left are: skyrmion bag (3), skyrmion bag (2), isolated skyrmion (1), skyrmionium (0), skyrmions contained in domains (1), (2).
Taken from Rybakov and Kiselev [94].

translate under external inputs [25, 31, 79]. The same dependence on the Néel/Bloch character of dynamics is observed in domain walls [61].

1.2   On Skyrmions in Thin Magnetic Materials

Interest in the diverse behavior of material magnetic structure, and the study of the micromagnetic model, continues to grow, and more rapidly in the age of computers where magnetic materials are essential components of the manufacture of computer memory [51]. This naturally invites the analysis of structure at very small scales, of thin film ferromagnets. Alternative magnetic materials such as ferrimagnets, antiferromagnets, synthetic ferromagnets, and frustrated ferromagnets are also being studied in view of applications to information technology, and are amenable to modifications of the micromagnetic model and admit their own classes of magnetic texture [4, 28, 50, 69, 83]. These advances also inspired the study of other related localized structure like anti-skyrmions and skyrmioniums [54, 56, 65, 66, 80]. We present a small catalogue of select examples of localized texture obtained in simulations by Rybakov and Kiselev in figure 1.2 [94].

Of particular interest in this dissertation are the properties of skyrmions in compound nanometer thin films. The geometry of these systems is such that their behavior is highly dependant on the interactions at its interface. Chiral symmetry
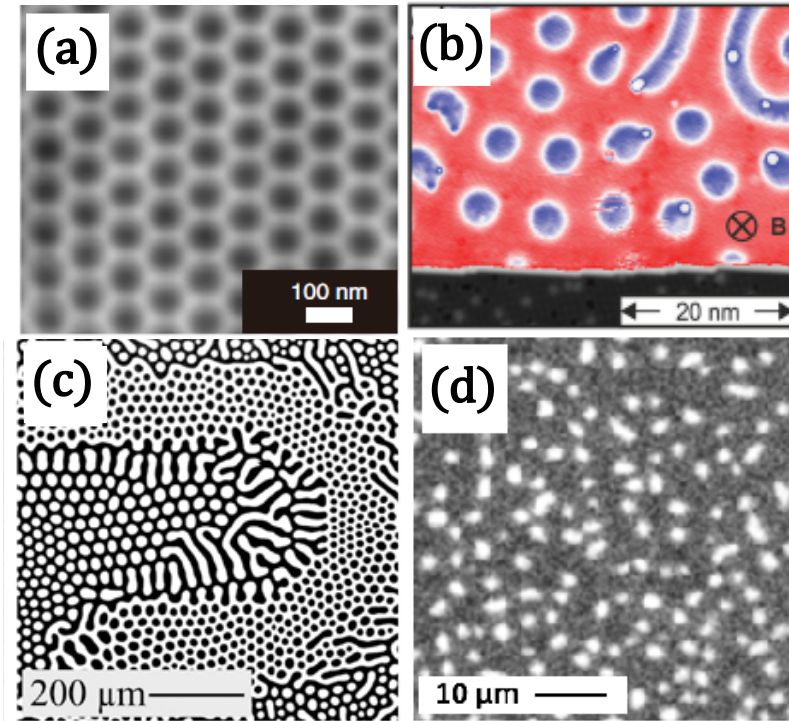
Figure 1.3 Select examples of observed magnetization patterns in thin ferromagnetic films. (a) Lorentz transition electron microscopy image of out-of-plane component of material magnetization in a cooled sample of FeGe of thickness 150nm showing an aggregated Hexagonal skyrmion lattice. (b) spin-polarized scanning tunneling microscopy image of the out-of-plane component of an ultrathin (atomic) PdFe/Ir layer showing nanometer scale skyrmions cohabitating with stripe domains under the influence of applied field. (c) Bubble and stripe domains in a strongly uniaxial $BiLu_2Fe_4GaO_{12}$ sample. Here, the white and Black domains are magnetized antiparallel and out-of-plane. (d) Kerr image of the out-of-plane magnetization, showing skyrmionic bubbles in an ultrathin (Co = 0.4nm) $Pt/Co/AlO_x$ trilayer.

(a) Taken from Yu et al. [109]. (b) Taken from Romming et al. [90]. (c) aggregated by McCord et al. [71] image originally obtained by M. Kustov, Kiel University. (d) provided courtesy of collaborator Anne Bernand-Mantel, Centre d'Élaboration de Matériaux et d'Études Structurales (CEMES), CNRS.

breaking in a ferromagnetic film leading to the Dzyaloshinskii-Moriya Interaction (DMI) is one such property of these films [32, 74]. The DMI is known to arise as a consequence of interfacial interactions [27], and predicted to host skyrmions as energy minimizing configurations [91]. One may observe skyrmions in specially manufactured thin ferromagnetic films grown on a heavy metal substrate to induce the symmetry breaking DMI at the interface which promotes twisting magnetic structure [7, 20, 107]. As shown in figure 1.3, various magnetic imaging techniques can examine the material microstructure and observe skyrmions in various phases, both as isolated bubble like structures and as an aggregated skyrmion lattice. These are obtained in practice with careful manipulation of the sample's temperature as well as out-of-plane applied fields to control the growth and nucleation of both domains and skyrmions [7, 109].

Films with multiple ferromagnetic layers have been synthesized in the past 5 years, and have been observed to support skyrmion-like structures [73]. The presence of several interacting ferromagnetic layers leads to multiple nontrivial effects. In simulation of current driven dynamics of bilayers coupled through a reduced (anti-)ferromagnetic exchange coupling, Koshibae and Nagaosa observed the formation of bound pairs of concentric skyrmions which are greater in size and more stable than their single-layer counterparts [57]. Zhang et al. deduced the cancellation of the skyrmion Hall effect in antiferromagnetically coupled bilayer systems [112]. In the absence of the skyrmion-Hall effect, current driven dynamics will not deflect the skyrmion unfavorably to the boundary of a finite sized system. The Multilayer system with antiferromagnetic coupling may serve as a synthetic antiferromagnet [84], and corresponding antiferromagnetic skyrmions have been studied with similar favorable properties [5, 111]. Hence, multilayer materials represent a promising avenue in the development of controllable systems applicable to computer engineering, and for observing and studying skyrmions.

1.3 On the Use of the Micromagnetic Model

The micromagnetic model is a continuum based variational model which has already seen extraordinary success modeling all of these interactions and giving theoretical insight to observed magnetic structure. This began with Landau and Lifshitz work using the continuum model to study elementary domain structure of ferromagnets. In that era already, the micromagnetic framework was shown to enable diverse interlocking multiscale phenomena such as the interplay between domain walls (micro) and domains (macro) [60]. This theory blossomed into its own field and has since been expounded upon, summarized in the book by W.F. Brown [22], and has been applied to observed magnetic systems of countless types of materials with different geometry and crystal structure; for a more exhaustive catalog of the applications of the micromagnetic theory and associated experimental technique, see the book by Hubert and Schäfer [48]. The theory is adaptable by way of various modifications to modeling ferrimagnetic and antiferromagnetic materials [33, 95].

A ferromagnet is any material that can sustain a spontaneous, macroscopically observable magnetic moment in the absence of external forces. According to the Landau theory of ferromagnetism, such materials can sustain a magnetic moment when cooled below the Curie temperature [59]. As such, in the micromagnetic framework the material is characterized by a magnetic dipole moment density, represented as a vector which is typically taken to have a constant length with respect to space and time. Ferromagnetism is governed, to a first approximation, by the Heisenberg exchange interaction, which is a quantum effect that induces neighboring electron spins to align with one another. It is this interaction that facilitates the emergence of the macroscopically observable magnetic moment. The exchange is modulated by anisotropy, as the crystal lattice may prefer magnetization in certain directions. The presence of noncentrosymmetric crystaline structures can lead to an additional antisymmetric exchange inducing a tendency of the material to form helical magnetic

structures (Dzyaloshinskii-Moriya Interaction (DMI)) [15]. The material will also interact with itself at a distance through the magnetic field they generate, producing a non-local term in the energy equation. Furthermore in heterogeneous materials, the spins of one material will strongly interact at the interface with non ferromagnetic substrates.

The full incorporation of magnetic interactions is required to properly predict and explain skyrmion solutions in thin film systems, especially that of the interfacial DMI [55, 91] and stray magnetic field interactions. At first the leading order stray field interactions in a film were lumped into shape anisotropy, and the thin film system energy was described entirely locally by the model of Gioia and James [41, 106]. Later research began to show the importance of the non-local stray field effects; Indeed, skyrmions enabled by the nonlocal effects of stray field were coming under consideration [24] before their corresponding asymptotic terms were obtained. Further theoretical developments then incorporated the perturbative effects of the stray magnetic field in the thin-film limit. Knüpfer, Muratov, and Nolte expressed nontrivial, nonlocal, stray field energy terms in the expansion with a magnitude of the same order as the dimensionless film thickness [52, 77, 81], which enable the formation of stable skyrmion solutions even in the absence of DMI and compete with weak DMI [9]. These improvements in characterizing the stray field interaction of thin films serve both as fundamental contributions to the greater micromagnetic model, and as the foundation for the present study to further elucidate the role stray field plays in stabilizing skyrmions in thin films.

The methodology of our skyrmion study focuses on determining stable states which feature a skyrmion in each layer of a multilayer material, and mapping out the energy landscape in the neighborhood of these stable states to gain insight into possible dynamics. This approach utilizes an ansatz based calculation of the energy, approximating the profile of a magnetic skyrmion within a restricted class of

topologically nontrivial magnetization profiles; however, due to more recent work the quality of the ansatz is improved, now placed on a more rigid theoretical grounding and enclosed within the context of harmonic maps. An admissible class of localized magnetic textures, close to harmonic maps, and exhibiting all necessary properties of compact skyrmions is proposed according to past work by Bernand-Mantel et al. [8]. This analysis has practical relevance to producing and studying skyrmions in ferrimagnetic systems, as the inherent reduced stray field interaction allows the competition between exchange and stray field interactions to occur over broader length scales than that of ferromagnets, ensuring the resultant structures have length scales greater than that of atomic spacing and thus amenable to the continuum models. Such parameter regimes were studied for a monolayer under applied field, stray field, and DMI by Bernand-Mantel et al. to find stable skyrmions in the low DMI regime [9, 13]. Particular emphasis and discussion shall be given to the role played by the stray magnetic field energy, and deriving the stray field interactions between skyrmions in each layer from the aforementioned ansatz.

1.4   Summary of Results

Modeling thin magnetic systems in the stray-field dominated regime presents its own challenges. In the absence of any modulating effects, the nonlocal nature of the stray field is nonnegligible. Furthermore, in direct simulation of micromagnetic equations, one observes that field dominated systems exhibit numerical stiffness requiring high resolution when studying small structures in simulation [13]. Magnetic structure of multilayered media shows strong dependence of the magnitude of the stray field energy on film thickness and number of layers [99]. We show how to obtain each of the stray field interaction energy terms from a scalar potential theoretic framework, solving Maxwell's equations in the multilayer geometry. This treatment exactly represents the local contribution of stray field, and the so called volume charge (those due to in

plane divergences of the material magnetization), and surface charge (those due to components of magnetization perpendicular to surfaces) energies in the finite-thickness regime of multilayer systems formulating each as combinations of integral kernels, like the analysis done for monolayer systems in [52]. However, for the multilayer system the stray field also facilitates interaction between charges in different layers. In particular, we find the exact representation yields interaction kernels for interlayer surface-volume charges which was since neglected. This improves upon previous approximate schemes for stray field in the multilayer system, for example studies of domain walls conducted by Lemesh et al. neglecting the surface-volume interactions [64]. See also the model used by Büttner et al. for domain walls in multilayered media using only the surface-surface and volume-volume interactions [23]. We compute an exact representation of surface-volume interactions between layers, and show asymptotically that they are negligible compared to all other categories of stray field interaction, completely enclosing past results of the micromagnetic theory in layered systems (see chapter 5).

In the asymptotic thin multilayer system with perpendicular magnetic anisotropy (PMA) we show the existence of energy minimizers within the restricted class of skyrmion profiles (see chapter 6). Due to the layer separation, the exchange interaction between the films is greatly reduced, and represented by a local weak coupling term which favors parallel alignment (or antiparallel in the case of antiferromagnetically coupled layers) after [57]. Already, we may show even in the absence of interlayer exchange coupling, the stray magnetic field interaction alone enables layer-layer coupling and facilitates the formation of bound skyrmions in each layer, concentric in a column and of the same size [12]. These formations are larger and more stable than the stray field driven skyrmions predicted in the monolayer asymptotic model described in [9].

The analysis for asymptotically thin layers is also supplemented with an alternative physical model of a monolayer in which the layer is assumed thin enough that the dominant exchange interaction forces $\partial_z \mathbf{m} = 0$, but does not pass to the asymptotic limit of vanishing film thickness, and rather treats the stray field energy exactly. This is herein referred to as the "finite thickness" film model. Such schemes have been used before in the analysis of domain walls in ferromagnetic films [2, 29, 38]. Analysis of a monolayer under the finite thickness conditions shows competition between the material's perpendicular magnetic anisotropy (PMA) and the stray field. In the restricted class of skyrmion profiles, and with sufficiently strong anisotropy, local minimizers cease to exist, a fact which is not revealed by the asymptotic model, and leading to a more complete understanding of stray field enabled skyrmions. This system is studied further numerically with the mumax3 software [105] to find the critical film thickness upon which the film demagnetizes by way of skyrmions bursting into stripe domains (see chapter 4).

First steps are made introducing exchange coupling to the multilayer model by neglecting the higher order, long range, effects of the stray field interaction in the thin film limit. This leaves the DMI as the skyrmion enabling mechanism. Supposing a two layer system and each layer having a DMI coefficient of identical magnitude, one finds the existence of skyrmions hinges upon the relationship between sign of the coupling constant and the sign of the DMI coefficient. In two ferromagnetically coupled layers, opposite sign DMI terms in each layer cancel out in the total energy, and a coupled bilayer skyrmion solution does not exist. Likewise this is the case for anti-ferromagnetically coupled layers with same sign DMI terms. In the remaining cases coupled and concentric skyrmion columns do minimize the system energy. We further discover that the strength of the interlayer exchange coupling plays no role in determining the skyrmion size at equilibrium, and only induces skyrmion solutions in each layer to align concentrically with one another.

CHAPTER 2

MICROMAGNETIC MODELING

Micromagnetics is a continuum modeling framework that describes the local magnetic moments in a ferromagnet as a three-dimensional vector field $\mathbf{M}$ which has a fixed length and whose properties are governed by an energy functional $E(\mathbf{M})$. It was introduced in 1935 by Landau and Lifshitz to describe the formation of magnetic domains [60] and subsequently expounded upon by many authors (summarized in [22, 48]). As in any variational theory, stable magnetizations $\mathbf{M}$ are defined as those magnetic configurations for which the energy functional is minimized either locally or globally. Local minimizers are called "metastable" states, while global minimizers are referred to as the "ground state". When the magnetization is not stable or metastable the magnetic configuration evolves with time to reduce the energy, unless additional external influences are present.

Where relevant, physical units will follow the SI convention, the basic quantities which are sufficient to derive all other units featuring in this work are as follows: mass (kg), length (m), time (s), and electric current (A). Derived units are force (N), torque (Nm), energy (J), and magnetic induction (T).

2.1 The Landau-Lifshitz-Gilbert Equations

Consider a ferromagnetic solid occupying a domain $\Omega \subseteq \mathbb{R}^3$. With $\mathbf{M} : \Omega \to \mathbb{R}^3$, $\mathbf{M}$ may be extended by defining it to be 0 outside of Ω. The magnitude, $|\mathbf{M}| = M_s$ in Ω, is refered to as the saturation magnetization, and takes physical units A/m, and this is assumed spatially independent.

The differential equation describing the evolution of the magnetization is the Landau-Lifshitz-Gilbert (LLG) equation [40, 60]. The dynamics are governed by the

Landau-Lifshitz-Gilbert equations (LLG). In Landau-Lifshitz form, they are as follows in physical units [48, 59]:

$$\left(1 + \alpha^2\right) \frac{\partial \mathbf{M}}{\partial t} = -\gamma_0 \left(\mathbf{M} \times \mathbf{H}_{\text{eff}} + \frac{\alpha}{M_s} \mathbf{M} \times (\mathbf{M} \times \mathbf{H}_{\text{eff}}) \right); \quad \mathbf{H}_{\text{eff}} = -\frac{1}{\mu_0} \frac{\delta E}{\delta \mathbf{M}}, \quad (2.1)$$

So the evolution depends on the so called effective field H_{eff}, and where $\delta E / \delta \mathbf{M}$ represents the functional derivative of the energy with respect to the magnetization. The three constants are γ_0, the gyromagnetic ratio and α, the LLG damping parameter and μ_0, the magnetic permeability of a vacuum. Each has their respective units: $[\gamma_0] = \frac{\text{m}}{\text{As}}$, $[\alpha] = 1$, and $\mu_0 = 4\pi \cdot 10^{-7} \frac{\text{kg} \cdot \text{m}}{\text{A}^2 \text{s}^2}$; and the field having the same units as magnetization $[\mathbf{H}_{\text{eff}}] = \text{A}/\text{m}$.

Following from the vector geometry, we see that this equation preserves $|\mathbf{M}| = M_s$ constant. When $\mathbf{M}$ is not a stationary state of E this implies the precession of $\mathbf{M}$ about the effective field axis, since $\mathbf{M} \times \mathbf{H}_{\text{eff}} \perp \mathbf{H}_{\text{eff}}$. The precession is then modulated by the damping term, $\mathbf{M} \times (\mathbf{M} \times \mathbf{H}_{\text{eff}})$, which can only evolve $\mathbf{M}$ toward the field axis as it is perpendicular to both $\mathbf{M}$ and $\mathbf{M} \times \mathbf{H}_{\text{eff}}$. This makes α a model energy loss coefficient, and so the trajectories of this equation are monotonically decreasing in E [59]. Then for long enough time, $\mathbf{M}$ must approach a local minimizer of $E(\mathbf{M})$.

2.2   The Micromagnetic Energy

The micromagnetic energy which drives this system is [39]:

$$E(\mathbf{M}) = E_{ex}(\mathbf{M}) + E_{an}(\mathbf{M}) + E_{DMI}(\mathbf{M}) + E_Z(\mathbf{M}) + E_d(\mathbf{M}). \quad (2.2)$$

In the SI units, energy is measured in Joules (J). Each term represents one type of interaction, with functional dependence on the magnetization, $\mathbf{M}$. In order of appearance they are the exchange, E_{ex}; the crystalline anisotropy, E_{an}; the

Dzyaloshinskii-Moriya Interaction, E_{DMI} (also called antisymmetric-exchange); the interaction with applied field, E_Z (this energy is called the Zeeman energy); and the stray field energy, E_d (or demagnetizing energy). The stray field is the magnetic field which is generated by the spins themselves.

2.2.1 Bulk material interactions of a ferromagnet

Exchange energy is defined as

$$E_{ex}(\mathbf{M}) = \frac{A}{M_s^2} \int_\Omega |\nabla \mathbf{M}|^2 d^3r, \qquad (2.3)$$

with the exchange stiffness constant, A, taking units, $[A] = \text{J/m}$, and where the notation $|\nabla\mathbf{M}|$ refers to the Froebenius norm of the Jacobian matrix of the mapping $\mathbf{M} : \mathbb{R}^3 \to \mathbb{R}^3$. This penalizes nonuniformity in the magnetic structure. The presence of this effect is what defines a ferromagnet. Mathematically, insisting the exchange energy be bounded guarantees some regularity on $\mathbf{M}$. At the nanoscale, it cannot be neglected. Due to this central role it is typically the point of comparison in dimensional analysis when analyzing the orders of magnitude of any other interaction [48]. The study of this energy and its critical points in and of itself already represents a fruitful domain of mathematics known as "harmonic maps" [47], which are indispensable for the study of skyrmions. We summarize the relevant theory on harmonic maps in Section 3.1.

Anisotropy energy is defined as

$$E_{an}(\mathbf{M}) = K \int_\Omega \Phi_{an}\left(\frac{\mathbf{M}}{M_s}\right) d^3r, \qquad (2.4)$$

with the constant K having units $[K] = \text{J/m}^3$. The function Φ_{an} may be chosen based on the material's crystal structure, and should be invariant with respect to reversal of the direction of magnetization, and such that it grows when $\mathbf{M}$ deviates from favorable

directions. One prominent example is uniaxial anisotropy: supposing the 3rd-axis is favored, one may write $\Phi_u(\mathbf{M}) = M_1^2 + M_2^2$, which vanishes for $\mathbf{M} = \pm\hat{\mathbf{e}}_3$, [59].

Dzyaloshinskii-Moriya Interaction energy (DMI) is defined generally,

$$E_{DMI}(\mathbf{M}) = \frac{D}{M_s^2} \int_\Omega F_{DMI}(\mathbf{M}, \nabla\mathbf{M}) d^3r, \tag{2.5}$$

for some bilinear form F_{DMI}, and with the constant D having units $[D] = \text{J/m}^2$. Named after the authors describing the effect, the DMI induces a spatial twisting effect leading to helical magnetic textures [32, 74]. It may be due to the material's crystalline structure in which case it is called bulk DMI [15, 59]. The energy density is such that it is quadratic in $\mathbf{M}$, while also changing sign with reversal of the coordinate directions, $\mathbf{r} \to -\mathbf{r}$. The bilinear forms available take the form of linear combinations of the quantities

$$M_j \frac{\partial M_k}{\partial x_i} - M_k \frac{\partial M_j}{\partial x_i}. \tag{2.6}$$

which are the so-called Lifshitz invariants. They were characterized by Bogdanov and Yablonskii for different instances of DMI [18]. For example, in non-cenntrosymmetric materials with cubic crystalline symmetry, F_{DMI} takes a particularly simple form:

$$F_{DMI}(\mathbf{M}, \nabla\mathbf{M}) = \mathbf{M} \cdot (\nabla \times \mathbf{M}). \tag{2.7}$$

The **Zeeman** energy is that which is stored in the interaction between the material magnetization and an applied magnetic field, $\mathbf{H}_a$, and is given by

$$E_Z(\mathbf{M}) = -\mu_0 \int_{\mathbb{R}^3} \mathbf{M} \cdot \mathbf{H}_a d^3r, \tag{2.8}$$

and so is minimal when the material is magnetized in the same direction as the applied field.

The magnetic **stray field** energy is given by,

$$E_d(\mathbf{M}) = \frac{\mu_0}{2} \int_{\mathbb{R}^3} |\mathbf{H}_d(\mathbf{M})|^2 d^3 r, \tag{2.9}$$

with $\mathbf{H}_d$ being distinctly the portion of the magnetic field which the material generates by itself. Where the subscript d stands for 'demagnetizing' due to the tendency of this interaction to compete with the exchange to frustrate the ferromagnetic order [48]. By separating the applied and stray fields, the latter is related to $\mathbf{M}$ by the stationary Maxwell's equations. First, one has the constitutive equation relating field, magnetization, and magnetic induction ($\mathbf{B}$) at a point in a material. In the SI unit system this is given by

$$\mathbf{B} = \mu_0(\mathbf{H}_a + \mathbf{H}_d + \mathbf{M}). \tag{2.10}$$

Then we must have $\mathbf{B}_a = \mu_0 \mathbf{H}_a$ not depending on $\mathbf{M}$, since it is external to the system, and so applied and stray fields are separated. Then follow the stationary Maxwell's equations describing the stray field:

$$\mathbf{B}_d = \mu_0(\mathbf{H}_d + \mathbf{M}),$$
$$\nabla \cdot \mathbf{B}_d = 0 \ , \quad \nabla \times \mathbf{H}_d = 0. \tag{2.11}$$

These give the existence of a magnetic scalar potential, U_d, such that $\mathbf{H}_d = -\nabla U_d$, which obeys Poisson's equation [36]

$$\Delta U_d = \nabla \cdot \mathbf{M}. \tag{2.12}$$

Understanding that $\mathbf{M}$ has a discontinuity at the boundary, this must be considered in the distributional sense. This leads to the distinction between interactions due to bulk divergences, referred to as volume charges, in the material and those due to the divergence singularities acquired at the boundaries of the material, called surface

charges. Such structures are fundamental to understanding the role of stray field in thin film systems, and expounded upon in Chapter 5. Using the fundamental solution for the Laplacian in $\mathbb{R}^3$ formally yields

$$U_d = -\frac{1}{4\pi} \int_{\mathbb{R}^3} \frac{\nabla \cdot \mathbf{M}(\mathbf{r}')}{|\mathbf{r} - \mathbf{r}'|} d^3 r'. \tag{2.13}$$

in particular, the stray field energy may be rewritten as $E_d = \frac{\mu_0 M_s^2}{2} \int_{\mathbb{R}^3} |\nabla U_d|^2 d^3 r$. It is clear that E_d is always positive. The tendency of materials to reduce the energy of the stray field by locally reducing $\nabla \cdot \mathbf{M}$ has been called "the principle of pole avoidance" or "flux-closure" [48], see Figure 1.3c for examples of close anti-parallel domain formation following this tendency.

Having characterized each interaction energy, the total energy may then be written

$$E(\mathbf{M}) = \frac{A}{M_s^2} \int_{\Omega} |\nabla \mathbf{M}|^2 d^3 r + K \int_{\Omega} \Phi_{an}\left(\frac{\mathbf{M}}{M_s}\right) d^3 r + \frac{D}{M_s^2} \int_{\Omega} F_{DMI}(\mathbf{M}, \nabla \mathbf{M}) d^3 r$$
$$- \mu_0 \int_{\Omega} \mathbf{M} \cdot \mathbf{H}_a \, d^3 r + \frac{\mu_0}{2} \int_{\mathbb{R}^3} |\nabla U_d|^2 d^3 r. \tag{2.14}$$

This together with the Landau-Lifshitz Equations completes the general micromagnetic model.

2.2.2 Nondimensionalization of the 3D micromagnetic energy

Begin nondimensionalizing the equations by taking $\mathbf{M} = M_s \mathbf{m}$. With foresight the stray magnetic field energy is characterized by the constant energy density

$$K_d = \frac{\mu_0 M_s^2}{2}. \tag{2.15}$$

We define the exchange length, l_{ex} in meters, to be the length scale for which the exchange and stray field interactions balance each other [48]:

$$l_{ex} = \sqrt{\frac{2A}{\mu_0 M_s^2}} = \sqrt{\frac{A}{K_d}}. \tag{2.16}$$

Taking $\mathbf{r} \to l_{ex}\mathbf{r}$, we acquire the following dimensionless groups,

$$\tilde{K} = \frac{K l_{ex}^2}{A}, \quad \tilde{D} = \frac{D l_{ex}^2}{A}, \quad \mathbf{h}_a = \frac{\mathbf{H}_a}{M_s}. \tag{2.17}$$

So, the energy, now measured in the units of Al_{ex}, is as follows:

$$\begin{aligned} \tilde{E}(\mathbf{m}) = \frac{E(\mathbf{M})}{Al_{ex}} &= \int_\Omega |\nabla \mathbf{m}|^2 d^3r + \tilde{K} \int_\Omega \Phi_{an}(\mathbf{m}) \, d^3r \\ &+ \tilde{D} \int_\Omega F_{DMI}(\mathbf{m}, \nabla\mathbf{m}) d^3r - 2 \int_\Omega \mathbf{m} \cdot \mathbf{h}_a \, d^3r \\ &+ \int_{\mathbb{R}^3} |\nabla U_d|^2 d^3r. \end{aligned} \tag{2.18}$$

2.3   Modeling Ferromagnetic Films

Thin ferromagnetic films are very sensitive to surface effects due to their broad free surface compared to their volume. In fact, any ferromagnetic body in general, In addition to the bulk material effects, will experience strong nontrivial interactions which are due to its geometry, and the shape of its boundary. These geometric effects can be induced by nearest neighbor interactions with a material of a different species in direct contact with the ferromagnetic sample and then transformed to a continuous model by appropriate treatment leading to different forms of anisotropy and DMI [7]. Such a configuration is presented in the form of a thin-film in figure 2.1 leading to the interfacial DMI. For surface induced anisotropy, the effects have been long studied, and for the purposes of the thin film model it is sufficient to lump it in simultaneously with the bulk anisotropy [45].

Figure 2.1 Schematic example of an antisymmetric film. The ferromagnetic layer (FM) is sandwiched between two unlike non-ferromagnetic (NM) layers. The lack of cancelation between surface interactions at the top and bottom of the FM layer gives rise to interfacial DMI.

Additionally, the most obvious interfacial effect is the stray field interaction, since $\mathbf{M}$ is defined to be 0 outside the material domain, the jump in the surface-normal component of $\mathbf{M}$ creates a divergence singularity in (2.13) leading to an excess stray field in free space in which the system stores energy. This effect plays an important and nontrivial role in the analysis of thin ferromagnetic films [41].

The reduction to the thin-film model involves first the enumeration of bulk and interfacial interaction energies in a cylindrical domain with base $\Omega \subseteq \mathbb{R}^2$ and finite extent, d, in the third coordinate direction. Then follows a rigorous treatment of the stray field energy that it may be rendered as a convergent integral and that distinct effects acquired by the stray field in this system geometry are properly identified and classified. This involves asymptotic analysis in the limit as the film thickness approaches zero. Variations of this model and process are fundamental to the results of this dissertation. Alternate and more detailed analyses of the stray field are presented in Chapter 4 for monolayer systems and in Chapter 5 for multilayer systems.

2.3.1 Antisymmetric interfacial interactions (DMI)

In the thin-film system, DMI often results from presence of a heavy metal in contact with one side of the film, thereby breaking inversion symmetry, [32, 74] as shown in

figure 2.1. In this case it is called interfacial DMI.

$$F_{DMI} = \left(M_3 \frac{\partial M_1}{\partial x_1} - M_1 \frac{\partial M_3}{\partial x_1} \right) + \left(M_3 \frac{\partial M_2}{\partial x_2} - M_2 \frac{\partial M_3}{\partial x_2} \right). \tag{2.19}$$

It features prominently in stabilizing magnetic skyrmions in noncentrosymmetric materials [17].

Accordingly, the definition of the DMI energy must change to a surface integral, since this interaction is no longer defined as an energy density in three-space. Only occurring on one or both interfaces, consider the thin system with thickness d and integrate the following surface energy density over the other two coordinates in $\Omega \subseteq \mathbb{R}^2$ [77, 88]:

$$E_{DMI}(\mathbf{M}) = \frac{Dd}{M_s^2} \int_\Omega \left[\left(M_3 \frac{\partial M_1}{\partial x_1} - M_1 \frac{\partial M_3}{\partial x_1} \right) + \left(M_3 \frac{\partial M_2}{\partial x_2} - M_2 \frac{\partial M_3}{\partial x_2} \right) \right] d^2 r. \tag{2.20}$$

This is such that D may take on the same dimensional units as that defined in the bulk-DMI. The presence or absence of competing interactions with nonmagnetic layers on the top or bottom surfaces of the ferromagnetic film is already contained within the constant D. For the given choice of Lifshitz invariant, this particular species of interfacial DMI induces the magnetic texture to tilt toward the axis of transition such that all the $\mathbf{M}$ vectors tend to be coplanar (also called Néel-type rotation), promoting the formation of cycloidal structures to the exclusion of helical structures, and the sense of rotation promoted is determined by the sign of D.

2.3.2 Total energy of thin films with uniaxial anisotropy

We show the calculation of the energy of the thin-film ferromagnetic system with uniaxial out-of-plane anisotropy and with interfacial DMI. In particular this involves properly nondimensionalizing according to the film thickness, and treatment and
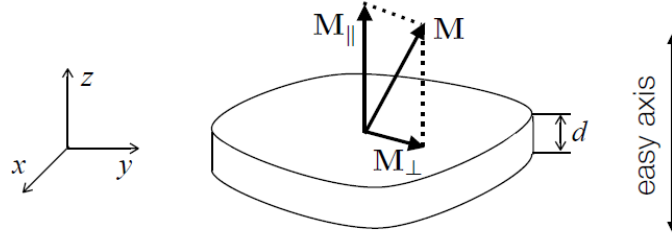
Figure 2.2 Schematic thin-film system and decomposition of **M** into in-plane and out-of-plane components, subscripts -$\perp$ and -$\parallel$ respectively denoting components of **M** which are perpendicular and parallel to the preferred direction of crystaline anisotropy (easy-axis).

Taken from Bernand-Mantel et. al. [9].

classification of the various effects obtained from analysis of the stray field energy before passing to the asymptotic limit.

The chosen orientation of anisotropy motivates a coordinate system with the magnetization vector decomposed into in-plane and out-of-plane components: $\mathbf{m} = (\mathbf{m}_\perp, m_\parallel)$, as is diagrammed in figure 2.2. Each are of course functions over all of $\mathbb{R}^3$ and are defined to be zero outside of the material domain. For perpendicular uniaxial anisotropy and the DMI interaction we let, $\Phi_{an} = |\mathbf{m}_\perp|^2$, and $F_{DMI} = m_\parallel \nabla \cdot \mathbf{m}_\perp - \mathbf{m}_\perp \cdot \nabla m_\parallel$. We introduce the assumption that the magnetization does not vary significantly in the vertical direction, $\mathbf{m}(x, y, z) = \mathbf{m}(x, y)\chi_{(0,d)}(z)$ [38], where χ is the characteristic function and d is the film thickness. This is consistent with d being small in some sense. An early rigorous treatment of the asymptotic reduction to the thin-film equations was given by Gioia and James, in which none of the constants depend on d [41]. The boundaries $z = 0$ and $z = d$ will cause discontinuities in $\mathbf{m}$, and as a consequence, one must treat the stray field carefully while passing to the thin film limit. Other authors refined this approach [37, 38, 52, 53, 78].

The micromagnetic energy of a ferromagnetic film of infinite extent is thus:

$$\mathcal{E}_0(\mathbf{m}) = A \int_{\mathbb{R}^2 \times (0,d)} |\nabla \mathbf{m}|^2 d^3\tilde{r} + K_u \int_{\mathbb{R}^2 \times (0,d)} |\mathbf{m}_\perp|^2 \, d^3\tilde{r}$$

$$+ D \int_{\mathbb{R}^2 \times (0,d)} \left(m_\parallel \nabla \cdot \mathbf{m}_\perp - \mathbf{m}_\perp \cdot \nabla m_\parallel \right) d^3\tilde{r} \qquad (2.21)$$

$$+ \frac{\mu_0 M_s^2}{2} \int_{\mathbb{R}^3} \left(|\nabla U_d|^2 - \chi_{(0,d)}(z) \right) d^3\tilde{r},$$

where a constant has been subtracted from $|\nabla U_d|^2$ in the material domain to ensure convergence of the integral.

Now, we may define the characteristic exchange length, l_{ex} and introduce the following relevant dimensionless quantities which appear in the final result:

$$l_{ex} = \sqrt{\frac{2A}{\mu_0 M_s^2}}, \quad Q = \frac{2K_u}{\mu_0 M_s^2}, \quad \kappa = D\sqrt{\frac{2}{\mu_0 M_s^2 A}}, \quad \delta = \frac{d}{l_{ex}}, \qquad (2.22)$$

which represent the strengths of the anisotropy, DMI, and the stray field, respectively. The energy becomes

$$E(\mathbf{m}) = \frac{\mathcal{E}_0(\mathbf{m})}{Ad} = \int_{\mathbb{R}^2} |\nabla \mathbf{m}|^2 d^2r + Q \int_{\mathbb{R}^2} |\mathbf{m}_\perp|^2 d^2r$$

$$+ \frac{1}{\delta} \int_{\mathbb{R}^3} \left(|\nabla U_d|^2 - \chi_{(0,\delta)}(z) \right) d^3r \qquad (2.23)$$

$$+ \kappa \int_{\mathbb{R}^2} \left(m_\parallel \nabla \cdot \mathbf{m}_\perp - \mathbf{m}_\perp \cdot \nabla m_\parallel \right) d^2r.$$

Hence, the film thickness, δ, serves to characterize the relative strength of the stray field interaction, though its role is not obvious until a full treatment of the energy is obtained.

For U_d, formally, we are solving a distributional Poisson equation. The process is elaborated in more detail in Section 5.2 where the multilayer system is treated. Using

the shorthand $\chi = \chi_{(0,\delta)}(z)$, we may employ the fundamental solution:

$$U_d = -\frac{1}{4\pi} \int_{\mathbb{R}^3} \frac{\left[\nabla \cdot (\chi(z')\mathbf{m}(x',y'))\right]}{\sqrt{(x-x')^2 + (y-y')^2 + (z-z')^2}} dx' dy' dz'. \qquad (2.24)$$

Assume that $m_\parallel \to -1$ as $|\mathbf{r}| \to \infty$. Then one may expand in δ, as is done in [38, 52] to obtain the formula:

$$\begin{aligned}
\frac{1}{\delta} \int_{\mathbb{R}^3} \left(|\nabla U_d|^2 - \chi_{(0,d)}(z)\right) d^3 r = & -\int_{\mathbb{R}^2} |\mathbf{m}_\perp|^2 d^2 r \\
& + \frac{\delta}{4\pi} \int_{\mathbb{R}^2} \int_{\mathbb{R}^2} \frac{\nabla \cdot \mathbf{m}_\perp(\mathbf{r}) \nabla \cdot \mathbf{m}_\perp(\mathbf{r}')}{|\mathbf{r} - \mathbf{r}'|} d^2 r' d^2 r \\
& - \frac{\delta}{8\pi} \int_{\mathbb{R}^2} \int_{\mathbb{R}^2} \frac{(m_\parallel(\mathbf{r}) - m_\parallel(\mathbf{r}'))^2}{|\mathbf{r} - \mathbf{r}'|^3} d^2 r' d^2 r + \mathcal{O}(\delta^2).
\end{aligned}$$

$$(2.25)$$

Note the leading order term which competes with the ansiotropy [41]. Since we are modeling strong perpendicular anisotropy (having assumed $\mathbf{m} \to -\hat{\mathbf{e}}_3$ as $|\mathbf{r}| \to \infty$, where $\mathbf{m} = \pm\hat{\mathbf{e}}_3$ is the ground state for $\kappa = \delta = 0$) the analysis is restricted to systems with $Q > 1$. The stray field energy also contributes two nonlocal terms, respectively called "volume charge energy" and "surface charge energy", which are controlled by the film's thickness and can sometimes be neglected. These $\mathcal{O}(\delta)$ terms were rigorously obtained in [52, 77, 78]. We may denote them as $E_{vol}(\mathbf{m}, \delta)$ and $E_{surf}(\mathbf{m}, \delta)$. Respectively, they are

$$E_{vol}(\mathbf{m}, \delta) = \frac{\delta}{4\pi} \int_{\mathbb{R}^2} \int_{\mathbb{R}^2} \frac{\nabla \cdot \mathbf{m}_\perp(\mathbf{r}) \nabla \cdot \mathbf{m}_\perp(\mathbf{r}')}{|\mathbf{r} - \mathbf{r}'|} d^2 r' d^2 r, \qquad (2.26)$$

$$E_{surf}(\mathbf{m}, \delta) = -\frac{\delta}{8\pi} \int_{\mathbb{R}^2} \int_{\mathbb{R}^2} \frac{(m_\parallel(\mathbf{r}) - m_\parallel(\mathbf{r}'))^2}{|\mathbf{r} - \mathbf{r}'|^3} d^2 r' d^2 r. \qquad (2.27)$$

Note that both take the form of norms of components of $\mathbf{m}$. Hence, the volume charge energy is always positive and the surface charge energy is always negative. The physical action of these energy terms is such: reduction of the volume charge energy promotes the vanishing of in-plane divergence (A phenomenon observed when

obtaining Bloch skyrmions from a system with $\kappa = 0$, see Section 3.3). Meanwhile, since the surface charge energy is negative, this term promotes antiparallel alignment of the magnetization profile at a distance, competing with the exchange energy. As shown in subsequent sections it is this interaction which enables the formation of skyrmions in the absence of DMI ($\kappa = 0$).

Plugging these back into the total energy, we obtain

$$
\begin{aligned}
E_0(\mathbf{m}) = {} & \int_{\mathbb{R}^2} |\nabla \mathbf{m}|^2 d^2 r + (Q-1) \int_{\mathbb{R}^2} |\mathbf{m}_\perp|^2 d^2 r \\
& + \kappa \int_{\mathbb{R}^2} \left(m_\parallel \nabla \cdot \mathbf{m}_\perp - \mathbf{m}_\perp \cdot \nabla m_\parallel \right) d^2 r \\
& + \frac{\delta}{4\pi} \int_{\mathbb{R}^2} \int_{\mathbb{R}^2} \frac{\nabla \cdot \mathbf{m}_\perp(\mathbf{r}) \nabla \cdot \mathbf{m}_\perp(\mathbf{r}')}{|\mathbf{r} - \mathbf{r}'|} d^2 r' d^2 r \\
& - \frac{\delta}{8\pi} \int_{\mathbb{R}^2} \int_{\mathbb{R}^2} \frac{(m_\parallel(\mathbf{r}) - m_\parallel(\mathbf{r}'))^2}{|\mathbf{r} - \mathbf{r}'|^3} d^2 r' d^2 r.
\end{aligned}
\tag{2.28}
$$

This energy equation has some immediate consequences which are evocative of the subsequent chapters. Note that the stray field has been split into three parts. Having assumed $Q > 1$ and $\mathbf{m} \to -\hat{\mathbf{e}}_3$ in the far field, the excess energy stored in the magnetic field generated by this out-of-plane alignment contributes everywhere, locally, to a reduction of the anisotropy strength, hence $Q - 1$ is now its coefficient.

We remark that in this form, the energy can allow a regrouping of parameters to eliminate the anisotropy coefficient. Rescale the coordinates $r \to r/\sqrt{Q-1}$. Then introducing

$$
\bar{\kappa} = \kappa/\sqrt{Q-1}\,, \quad \bar{\delta} = \delta/\sqrt{Q-1},
\tag{2.29}
$$

one obtains an energy of the same form as in (2.28), with $\bar{\kappa}$ and $\bar{\delta}$ in place of κ and δ, and with $Q - 1$ set to 1. We will alternately use the barred and un-barred quantities where convenient and endeavor to remind the reader of changes in notation. In particular, results for Chapter 4 do not allow this regrouping.

This models the thin monolayer system with asymptotics for the stray field energy, and skyrmion solutions of this equation are studied in [9]. The mathematical methodology for analysis of skyrmions in this system are discussed in Section 3.3.

CHAPTER 3

MATHEMATICAL CHARACTERIZATION OF MAGNETIC SKYRMIONS

For a continuous map from the compactified plane to the sphere, $f : \mathbb{R}^2 \cup \{\infty\} \to \mathbb{S}^2$, one may define the Brouwer degree, q, which is the number of points in the preimage, $x \in f^{-1}(y)$, for which the orientation of a neighborhood of x is preserved under f, minus the number of points for which the orientation is reversed [82]. It is a fundamental result of topology that q will be independent of y for almost every choice of $y \in \text{im}\{f\}$ [82]. We refer to this as the topological degree, also called "skyrmion number". A configuration with one skyrmion has $q = 1$ [58]. When we enforce $\mathbf{m} \to -\hat{\mathbf{e}}_3$ as $|\mathbf{r}| \to \infty$ then the topological degree may be expressed as

$$q(\mathbf{m}) = \frac{1}{4\pi} \int_{\mathbb{R}^2} \mathbf{m} \cdot (\partial_1 \mathbf{m} \times \partial_2 \mathbf{m}) \, d^2r, \tag{3.1}$$

which is just the integral of the Jacobian of $\mathbf{m}$ as a map from $\mathbb{R}^2$ to $\mathbb{S}^2$ [8, 21].

Alternatively, the output of the mapping $\mathbf{m} \in \mathbb{S}^2$ may be regarded after stereographic projection $\mathcal{P}\mathbf{m} = (u, v)$ in which case we may represent the pullback of this projection as

$$\mathbf{m} = \left(\frac{2u}{u^2 + v^2 + 1}, \ \frac{2v}{u^2 + v^2 + 1}, \ \frac{u^2 + v^2 - 1}{u^2 + v^2 + 1} \right). \tag{3.2}$$

In these coordinates the topological degree is given by

$$q(\mathbf{m}) = \frac{1}{\pi} \int_{\mathbb{R}^2} \frac{(\partial_2 u \, \partial_1 v) - (\partial_1 u \, \partial_2 v)}{1 + u^2 + v^2} d^2r. \tag{3.3}$$

3.1 Topologically Nontrivial Magnetic Structure in Two Dimensions

In 1975 Belavin and Polyakov showed the existence of topologically nontrivial, energy minimizing profiles for a 2D ferromagnet which arise under the exchange only, and derived lower bounds on the exchange energy as a function of topological degree [6]. The solution thus obtained exhibited rotational, dilational, and translational invariance. This result is the so called "Belavin-Polyakov profile" and forms the basis for a whole class of ansätze of more complicated skyrmion problems, starting with Ivanov et. al. [49].

The symmetry properties of Belavin-Polyakov profiles follow from their being exchange energy minimizers. Take the following problem set up with the constraint that $|\mathbf{m}| = 1$, consistent with the micromagnetic model, one will derive the "Harmonic map equation" and from that obtain each symmetry [8]. Pose

$$\text{minimize} \quad E(\mathbf{m}) = \int_{\mathbb{R}^2} |\nabla \mathbf{m}|^2 \, d^2 r,$$

$$\text{subj. to} \quad 0 = |\mathbf{m}(\mathbf{r})|^2 - 1 \text{ for } \mathbf{r} \in \mathbb{R}^2, \tag{3.4}$$

$$\text{and} \quad \mathbf{m} \to \text{cnst. as } \mathbf{r} \to \infty.$$

The Euler-Lagrange equations of this system take the form.

$$\Delta \mathbf{m} + |\nabla \mathbf{m}|^2 \mathbf{m} = 0. \tag{3.5}$$

Let the reader be reminded of the notation, that $|\nabla \mathbf{m}|$ represents the Froebenius norm of this Jacobian matrix. The presence of the unit-vector constraint $|\mathbf{m}| = 1$, which is not convex, gives rise to a nonlinear Euler-Lagrange equation. Non-constant solutions do exist, and it is a fact that they must cover $\mathbb{S}^2$ at least once [47, 96]. Therefore we may hope to find solutions with $q = 1$.

The harmonic map equation yields several helpful symmetry properties for its solutions. Since this is solved over all of $\mathbb{R}^2$, (3.5) is translation invariant. For if $\mathbf{m}(\mathbf{r})$ is

a solution, so is $\mathbf{m}(\mathbf{r}-\mathbf{r}_0)$, because the location of the origin is completely arbitrary. The equation admits dilations as well, notice each term contains two derivatives. So when $\mathbf{m}(\mathbf{r})$ is a solution, we let $\mathbf{m}(a\mathbf{r})$ and have $a^2\Delta\mathbf{m}(a\mathbf{r}) + a^2|\nabla\mathbf{m}(a\mathbf{r})|^2\mathbf{m}(a\mathbf{r}) = 0$, and the lengthscale a is factored out. One may show rotational invariance by multiplying the field by a constant rotation matrix, $R \in \mathrm{SO}(3)$. So pose $\mathbf{m} = R\tilde{\mathbf{m}}$, and we can interchange R with derivative operators to show the same equation is obtained for any R.

Moving by an alternative route we will obtain and classify the solutions of (3.5) and show they have integer values for the topological degree, $q(\mathbf{m})$. Owing to the fact that $|\mathbf{m}| = 1$, simple vector calculus gives

$$|\nabla\mathbf{m}|^2 \pm 2\mathbf{m} \cdot (\partial_1\mathbf{m} \times \partial_2\mathbf{m}) = |\partial_1\mathbf{m} \mp \mathbf{m} \times \partial_2\mathbf{m}|^2. \tag{3.6}$$

Integrating this and dropping the always positive right hand side gives an important lower bound on the energy [6],

$$E_{ex}(\mathbf{m}) \geq 8\pi|q(\mathbf{m})|. \tag{3.7}$$

Supposing the bound were saturated, $E_{ex}(\mathbf{m}) - 8\pi q(\mathbf{m}) = 0$, one then obtains the equations:

$$
\begin{aligned}
0 &= \partial_1\mathbf{m} + \mathbf{m} \times \partial_2\mathbf{m}, \\
0 &= \partial_2\mathbf{m} - \mathbf{m} \times \partial_1\mathbf{m}.
\end{aligned}
\tag{3.8}
$$

It may be checked that the solutions of this system are a subset of the solutions of the harmonic map equation by differentiating, and therefore inherit all of the associated symmetry properties, and conversely all solutions of the harmonic map equation will therefore saturate the topological lower bound and the systems (3.5) and (3.8) are equivalent [63].

Taking the system (3.8) and applying the pullback of the stereographic projection given in equation (3.2), one acquires the Cauchy-Riemann equations for u and v,

$$\partial_1 u = \partial_2 v \ , \quad \partial_2 u = -\partial_1 v. \tag{3.9}$$

Thus, $w = u + iv$, is an analytic function almost everywhere. This combined with the constant far field conditions on $\mathbf{m}$ implies that the result is a meromorphic function given by [6]:

$$w = \frac{P(z)}{Q(z)} \text{ for } z \in \mathbb{C}, \tag{3.10}$$

for polynomials P, Q such that P/Q is irreducible. The topological degree q may be directly inferred from (3.3) [108]:

$$q(\mathbf{m}) = \max\left\{\deg(P), \deg(Q)\right\}. \tag{3.11}$$

For the case $q = 1$, we have

$$w = \frac{az + b}{cz + d}. \tag{3.12}$$

Therefore, after returning to the $\mathbf{m}$ coordinates, the degree 1 solution of (3.8) is

$$\mathbf{m}(\mathbf{r}) = \mathcal{R}\mathbf{m}_\infty\left(\frac{\mathbf{r} - \mathbf{r}_0}{\rho}\right), \tag{3.13}$$

where $\rho > 0$, $\mathbf{r}_0 \in \mathbb{R}^2$, $\mathcal{R} \in \mathrm{SO}(3)$, and

$$\mathbf{m}_\infty(\mathbf{r}) = -\frac{2\mathbf{r}}{1 + |\mathbf{r}|^2} + \frac{1 - |\mathbf{r}|^2}{1 + |\mathbf{r}|^2}\hat{\mathbf{e}}_3. \tag{3.14}$$

This is a 6 parameter family of all solutions that represents all degree 1 harmonic maps from the plane to the unit sphere [8, 108]. Examples of these profiles are illustrated in figure 1.1. We will more precisely define the relationship between BP-profiles and skyrmions in the next section.

This motivates the definition of an appropriate search space which encloses skyrmion profiles as a subset of magnetization functions in two dimensions, and appropriately excludes extraneous functions. We therefore define the so called restricted class with desirable properties, let

$$\mathcal{A} = \left\{ \mathbf{m} \in H^1_{\text{loc}}(\mathbb{R}^2; \mathbb{S}^2) \;\middle|\; \mathbf{m} + \hat{\mathbf{e}}_3 \in H^1(\mathbb{R}^2; \mathbb{R}^3), \int_{\mathbb{R}^2} |\nabla \mathbf{m}|^2 d^2 r < 16\pi, q(\mathbf{m}) = 1 \right\},$$

(3.15)

as in [8]. Without loss of generality, and with an eye toward modeling materials with perpendicular magnetic anisotropy (PMA) this selects textures which have a downward out-of-plane alignment in the far field, i.e. $\mathbf{m} \to -\hat{\mathbf{e}}_3$.

3.2   The Belavin-Polyakov profile as a Skyrmion ansatz

The shape of a skyrmion solution arising through the minimization of E_0 defined in (2.28) will be close to a BP-profile for small $(Q - 1)$, δ, and κ [8]. This is reasonable since we have established it as the unique minimizer of exchange energy. We hence use a perturbed BP-profile in an ansatz based calculation of the interaction energies, and minimize over the degrees of freedom to discover the properties of the skyrmion. For that we need to introduce a truncation at scale L relative to the skyrmion core, for $L \gg 1$, which is necessary to result in a bounded anisotropy energy, for otherwise (3.14) is not an $L^2(\mathbb{R}^2)$ function. One may interpret this as dividing the plane into characteristic regions (interior and exterior of a circle of radius $\ll \rho\sqrt{L}$) where exchange and anisotropy effects are respectively dominant. One may also define the radius of the skyrmion to be the point in the magnetization profile where the out-of-plane component vanishes. In equation (3.13) the dilation parameter ρ will serve this purpose.
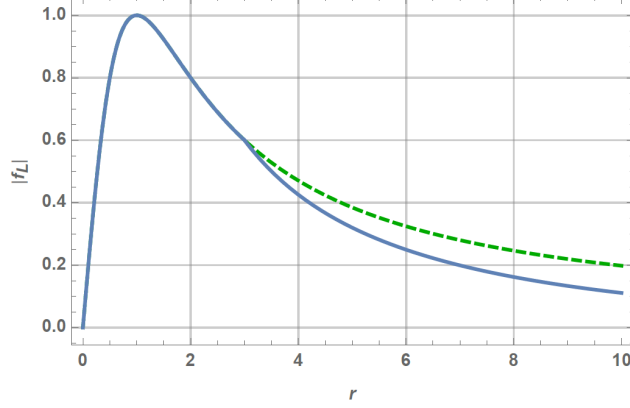
Figure 3.1 Truncated Belavin-Polyakov profile, $f_L(r)$, given in equation (3.17) (blue). Here the profile is truncated after $L = 9$, after which it decays exponentially. The green line represents the profile in the absence of truncation, $f(r)$.

Figure taken from Bernand-Mantel et al. [9].

Define f to be the in-plane modulus of the profile in equation (3.14),

$$f(r) = \frac{2r}{1 + r^2}. \tag{3.16}$$

i.e. $\mathbf{m}_{\infty,\perp} = -f(|\mathbf{r}|)\hat{\mathbf{e}}_r$, where $\hat{\mathbf{e}}_r = \mathbf{r}/|\mathbf{r}|$. Then, introduce the truncation:

$$f_L(r) = \begin{cases} f(r), & r \leq \sqrt{L} \\ \frac{f(\sqrt{L})}{K_1(1/\sqrt{L})} K_1(r/L), & r > \sqrt{L} \end{cases}. \tag{3.17}$$

Then define the ansatz

$$\mathbf{m}_L(\mathbf{r}) = -f_L\left(|\mathbf{r}|/\rho\right) R_\theta \hat{\mathbf{e}}_r + \mathrm{sgn}(\rho - |\mathbf{r}|)\sqrt{1 - f_L^2\left(|\mathbf{r}|/\rho\right)}\ \hat{\mathbf{e}}_3. \tag{3.18}$$

Here $R_\theta \in \mathrm{SO}(2)$ is a rotation matrix acting on the in-plane component. This loses two rotational degrees of freedom from (3.13) since we force $\mathbf{m} \to -\hat{\mathbf{e}}_3$ as $\mathbf{r} \to \infty$. We

have simply,

$$R_\theta = \begin{pmatrix} \cos\theta & -\sin\theta \\ \sin\theta & \cos\theta \end{pmatrix}. \tag{3.19}$$

We call $\theta \in [-\pi, \pi]$ the in-plane angle. This allows us to define the two characteristic types of skyrmions illustrated in figure 1.1: Néel skyrmions are those with $\theta = 0$ or $\pm\pi$, and Bloch skyrmions have $\theta = \pm\pi/2$, and Hybrid skyrmions for all in-between angles.

3.3   Skyrmions in a Thin Ferromagnetic Monolayer

The restricted class and the Belavin-Polyakov profile based ansatz are among the principal mathematical tools for carrying out the study of skyrmions and feature in the calculation of the energy of the ferromagnetic system leading to the results obtained in the subsequent chapters. We show now how the ansatz can be used to identify and classify skyrmion solutions in a thin ferromagnetic monolayer.

The thin film energy (2.28) with $\delta = 0$ has been studied by Komineas et al. who carried out a formal asymptotic analysis of the associated radial Euler-Lagrange equation [55]. Gustafson and Li were able to contextualize their result by studying the radial energy minimizers in the above problem and showing them to be close to a Belavin-Polyakov profile and quantified differences in the energy of the two results [43]. Other results have established solutions of the energy in the restricted class with minimal assumptions, such as Bernand-Mantel et al. who were able to arrive at a skyrmion solution without the assumption of radial symmetry and obtain a result close to the BP-profile [8]. We therefore find the theory of harmonic maps is directly applicable to skyrmions and justified by its ability to recapitulate the results obtained by other techniques.

Quoting results from [9], we may calculate the respective energies. The truncation is only relevant, to leading order, for the exchange and anisotropy. We derive the

following asymptotic expressions for large L:

$$E_{ex}(\mathbf{m}_L) \simeq 8\pi + \frac{4\pi}{L^2}, \tag{3.20}$$

$$E_{an}(\mathbf{m}_L) \simeq 4\pi(Q-1)\rho^2 \log\left(\frac{4L^2}{e^{2(1+\gamma)}}\right), \tag{3.21}$$

$$E_{DMI}(\mathbf{m}_L) \simeq -8\pi\kappa\rho\cos\theta, \tag{3.22}$$

$$E_{vol}(\mathbf{m}_L) \simeq \delta\rho\cos^2\theta\frac{3\pi^3}{8}, \tag{3.23}$$

$$E_{surf}(\mathbf{m}_L) \simeq -\delta\rho\frac{\pi^3}{8}. \tag{3.24}$$

If subject to lower bounds on L such that the exchange is not too large, the truncated BP-profile now satisfies all properties of the restricted class, (3.15). These asymptotic formulas were rigorously justified in [8]. Plugging into (2.28), one may write the total energy of the skyrmion as

$$\begin{aligned}
E_0(\mathbf{m}_L) \simeq E_{\rho,\theta,L} = {} & 8\pi + \frac{4\pi}{L^2} + 4\pi(Q-1)\rho^2\log\left(\frac{4L^2}{e^{2(1+\gamma)}}\right) \\
& - 8\pi\kappa\rho\cos\theta + \delta\frac{\pi^3}{8}\rho(3\cos^2\theta - 1).
\end{aligned} \tag{3.25}$$

Upon minimizing this energy with respect to all degrees of freedom, Bernand-Mantel et al. described the shape of the skyrmion [9]. They further find the competition between DMI and stray field which decides the degree to which the result resembles a Néel or Bloch skyrmion . Let $\theta^\star$, $\rho^\star$, and $L^\star$ be the minimizers of (3.25). Then, $L^\star = 1/(\rho^\star\sqrt{Q-1})$, with

$$\rho^\star\sqrt{Q-1} \simeq \frac{1}{16\pi}\frac{\bar{\varepsilon}(\bar{\kappa},\bar{\delta})}{\left|\ln\left(\beta\bar{\varepsilon}(\bar{\kappa},\bar{\delta})\right)\right|}, \tag{3.26}$$

$$\theta^\star = \begin{cases} 0 & \text{if } \bar{\kappa} \geq \frac{3\pi^2}{32}\bar{\delta} \\[2mm] -\pi & \text{if } \bar{\kappa} \leq -\frac{3\pi^2}{32}\bar{\delta} \\[2mm] \pm\arccos\left(\frac{32\bar{\kappa}}{3\pi^2\bar{\delta}}\right) & \text{else} \end{cases} \tag{3.27}$$

for $\beta\bar{\varepsilon} \ll 1$ and

$$\bar{\varepsilon}(\bar{\kappa},\bar{\delta}) = \begin{cases} 8\pi|\bar{\kappa}| - \frac{\pi^3}{4}\bar{\delta} & \text{if } |\bar{\kappa}| \geq \frac{3\pi^2}{32}\bar{\delta}, \\[2mm] \frac{128\bar{\kappa}^2}{3\pi\bar{\delta}} + \frac{\pi^3}{8}\bar{\delta} & \text{else.} \end{cases} \tag{3.28}$$

This is using the rescaled parameters $\bar{\kappa}$, $\bar{\delta}$ defined in (2.29).

These formulas show how the constants $\bar{\kappa}$ and $\bar{\delta}$ control the size and shape of the skyrmion. When $\bar{\kappa} = 0$ we obtain a Bloch skyrmion, otherwise, when $\bar{\kappa} > 0$ the DMI and stray field compete and the solution is a Bloch-Néel hybrid skyrmion. For increasing $\bar{\kappa}$ this hybrid state will approach a Néel skyrmion until the threshold, $\bar{\kappa}_{th} = \frac{3\pi^2}{32}\bar{\delta}$. When $\bar{\kappa} \geq \bar{\kappa}_{th}$ the DMI is the dominant effect, and the solution is properly a Néel skyrmion.

CHAPTER 4

EXISTENCE OF SKYRMIONS IN THE FINITE-THICKNESS REGIME

By analyzing the stray field integral in the thin film model without asymptotically expanding in the parameter, δ, one reveals the relationship between the stray field interaction and the anisotropy strength, Q. It is shown that in the regime with small δ and small $\frac{\delta}{Q-1}$ there exists a critical $Q = Q_c(\delta)$ for which the system energy for truncated BP-profiles undergoes a bifurcation after which skyrmion solutions fail to exist. This disappearance regime is not revealed in the asymptotic model. The result contributes toward a complete description of skyrmion existence in the (Q, δ) phase space, the other boundary being the critical value of $\delta = \delta_b(Q)$ for which the skyrmion cannot be a stable compact object and bursts into magnetic domains.

For this study, begin with the model energy equation of a monolayer which includes the usual exchange and perpendicular magnetic anisotropy (PMA) and a general expression of the stray field. Let $\tilde{\mathbf{m}} : \mathbb{R}^2 \times (0, \delta) \to \mathbb{R}^3$ and $\partial_3 \mathbf{m} = 0$, that integration may be carried out in the third coordinate trivially for all local energy terms. In other words $\tilde{\mathbf{m}} = \mathbf{m}(x, y)\chi_{(0,\delta)}(z)$. Simplifying from (2.21), the energy is

$$E(\tilde{\mathbf{m}}) = \int_{\mathbb{R}^2} \left(|\nabla \mathbf{m}|^2 + Q|\mathbf{m}_\perp|^2 \right) d^2 r + E_d\left(\tilde{\mathbf{m}}, \delta\right), \tag{4.1}$$

having integrated in the vertical coordinate (except for E_d) and applied the same nondimensional scheme as the energy equation, (2.28). Arguing physically from the point of view of the dominant exchange energy, we have implicitly assumed that δ is small to enable $\partial_3 \mathbf{m} = 0$ everywhere in the material, but the asymptotic expansion of E_d will not be performed, instead the stray field energy is to be evaluated exactly after computing it on the finite thickness film of infinite extent. This resembles the finite thickness model presented in [38]. After separating the local and nonlocal contributions

of the stray field in the subsequent sections we find the physical implications of this scheme are the same as, but serve as an augmentation to the asymptotic model of [52].

4.1 Stray Field Energy in Monolayers of Finite-Thickness

While some of this derivation is redundant with the treatment of the asymptotically thin systems in Chapters 2, 3 and 5, it is necessary to repeat the steps to show the relatedness of the various problems considered, and to flesh out the relevant technical details required for this study.

The energy may be represented explicitly in terms of the material magnetization, as follows. For $\tilde{\mathbf{m}}(x, y, z) = \mathbf{m}(x, y)\chi_{(0,\delta)}(z)$ with $(x, y) \in \Omega = \mathbb{R}^2$ and $\mathbf{m}(x, y) \to -\hat{\mathbf{e}}_3$ as $x^2 + y^2 \to \infty$, we have to renormalize the stray field energy by subtracting the far field behavior of $\mathbf{m}$. Define the uniform magnetization state $\tilde{\mathbf{m}}_\star = -\hat{\mathbf{e}}_3\chi_{(0,\delta)}$, whose magnetostatic potential is

$$
U_\star(x, y, z) = \begin{cases} 0, & z < 0, \\ -z, & 0 \le z \le \delta, \\ -\delta, & z > \delta, \end{cases} \tag{4.2}
$$

and let $\tilde{\mathbf{m}}_r = \tilde{\mathbf{m}} - \tilde{\mathbf{m}}_\star$ and $U_r = U - U_\star$, where U is given by the nondimensional form of (2.13). Subtracting the background field in the material domain, the stray field energy is redefined accordingly as

$$
\begin{aligned}
E_d(\mathbf{m}, \delta) &= \frac{1}{\delta} \int_{\mathbb{R}^3} \left(|\nabla U|^2 - \chi_{(0,\delta)}(r_3) \right) d^3r, \\
&= \frac{1}{\delta} \int_{\mathbb{R}^3} \left(|\nabla U_r|^2 - 2\partial_3 U_r \right) d^3r, \\
&= E_d' + E_d''.
\end{aligned} \tag{4.3}
$$

We can transform the second term by integrating Poisson's equation on a 2D plane at arbitrary height, z, after multiplication by, f, an appropriate rapidly decaying test function. Take $\Delta U_r = \nabla \cdot \tilde{\mathbf{m}}_r$ and proceed by multiplying it with f and integrating over (x, y):

$$\int_{\mathbb{R}^2} \Delta U_r(x, y, z) f(x, y) d^2 r = \int_{\mathbb{R}^2} \nabla \cdot \tilde{\mathbf{m}}_r(x, y, z) f(x, y) d^2 r. \qquad (4.4)$$

Breaking it into in-plane and out-of-plane parts gives

$$\int_{\mathbb{R}^2} \left[(\partial_1^2 + \partial_2^2) U_r f(x, y) + \partial_3^2 U_r f(x, y) \right] d^2 r = \int_{\mathbb{R}^2} \left[\nabla \cdot \tilde{\mathbf{m}}_{r,\perp} + \partial_3 \tilde{m}_{r,\parallel} \right] f(x, y) d^2 r. $$
$$(4.5)$$

Move all out-of-plane components to the righthand side to find

$$\int_{\mathbb{R}^2} \nabla \cdot \left[(\hat{\mathbf{e}}_1 \partial_1 + \hat{\mathbf{e}}_2 \partial_2) U_r - \tilde{\mathbf{m}}_{r,\perp} \right] f(x, y) d^2 r = \int_{\mathbb{R}^2} \left[\partial_3 \tilde{m}_{r,\parallel} - \partial_3^2 U_r \right] f(x, y) d^2 r, \quad (4.6)$$

where the left hand side is zero by way of the divergence theorem, and the right hand side has no derivatives in the integrated variables We now have

$$0 = \partial_3 \int_{\mathbb{R}^2} \left[\tilde{m}_{r,\parallel} - \partial_3 U_r \right] f(x, y) d^2 r. \qquad (4.7)$$

This expression gives equality in the integral when $f(x, y)$ is traded for a sequence $f_n(x, y)$ that approaches 1 pointwise almost everywhere. Therefore, integrating the above identity gives

$$E_d'' = -\frac{2}{\delta} \int_{\mathbb{R}^3} (\partial_3 U_r) d^3 r = \frac{2}{\delta} \int_{\mathbb{R}^3} \tilde{m}_{r,\parallel} d^3 r. \qquad (4.8)$$

Now since $\tilde{m}_{r,\parallel} = \tilde{m}_\parallel + 1$, and using the fact that $|\tilde{\mathbf{m}}| = 1$, we may compute

$$2(\tilde{m}_\parallel + 1) = |\tilde{\mathbf{m}}_\perp|^2 + |\tilde{m}_\parallel + 1|^2, \tag{4.9}$$

$$2(\tilde{m}_\parallel(x,y,z) + 1) = \chi_{(0,\delta)}(z)\left\{|\mathbf{m}_\perp(x,y)|^2 + |m_\parallel(x,y) + 1|^2\right\}. \tag{4.10}$$

Then integrating E''_d in z amounts to integrating a constant over $(0,\delta)$ and we obtain

$$E''_d = -\int_{\mathbb{R}^2} \left(|\mathbf{m}_\perp|^2 + |m_\parallel + 1|^2\right) d^2r. \tag{4.11}$$

We now investigate

$$E'_d = \frac{1}{\delta}\int_{\mathbb{R}^3} |\nabla U_r|^2 d^3r = \frac{1}{\delta}\int_{\mathbb{R}^3}\int_{\mathbb{R}^3} \frac{\nabla \cdot \tilde{\mathbf{m}}_r(\mathbf{r})\nabla \cdot \tilde{\mathbf{m}}_r(\mathbf{s})}{4\pi|\mathbf{r} - \mathbf{s}|} d^3r d^3s. \tag{4.12}$$

Use the following convention for the Fourier transform:

$$\hat{f}(\mathbf{q}) = \int_{\mathbb{R}^3} f(\mathbf{r})e^{-i\mathbf{q}\cdot\mathbf{r}} d^3r \ , \quad f(\mathbf{r}) = \int_{\mathbb{R}^3} \hat{f}(\mathbf{k})e^{i\mathbf{q}\cdot\mathbf{r}} \frac{d^3q}{(2\pi)^3}. \tag{4.13}$$

Following from the fact $\mathcal{F}\{1/(4\pi|\mathbf{r}|)\} = 1/|\mathbf{q}|^2$ for the $\mathbb{R}^3$ Fourier transform, we may proceed via Plancherel's theorem and the convolution theorem to render this expression in Fourier space as

$$E'_d = \frac{1}{\delta}\int_{\mathbb{R}^3} \frac{\overline{i\mathbf{q}\cdot\hat{\tilde{\mathbf{m}}}_r(\mathbf{q})}\ i\mathbf{q}\cdot\hat{\tilde{\mathbf{m}}}_r(\mathbf{q})}{|\mathbf{q}|^2} \frac{d^3q}{(2\pi)^3}. \tag{4.14}$$

Now separating the vertical coordinate, recall

$$\tilde{\mathbf{m}}_r(x,y,z) = (\mathbf{m}(x,y) + \hat{\mathbf{e}}_3)\chi_{(0,\delta)}(z). \tag{4.15}$$

Let $\mathbf{q} = \mathbf{k} + \omega\hat{\mathbf{e}}_3$. Now, using the shorthand $\chi = \chi_{(0,\delta)}$, we have

$$i\mathbf{q} \cdot \hat{\tilde{\mathbf{m}}}_r(\mathbf{k}, \omega) = \left(i\mathbf{k} \cdot \hat{\mathbf{m}}_\perp(\mathbf{k})\hat{\chi}(\omega) + \widehat{(m_\parallel + 1)}(\mathbf{k})(\widehat{\partial_z \chi})(\omega) \right). \tag{4.16}$$

with $\hat{\chi} = \frac{1 - e^{-i\delta\omega}}{i\omega}$. Assuming nothing further, we compute the component parts of (4.14) by substituting for $\mathbf{q} \cdot \hat{\tilde{\mathbf{m}}}_r$ and multiplying out each term.

$$\begin{aligned}
E'_d = \frac{1}{\delta} \int_{\mathbb{R}^2} \int_{\mathbb{R}} & \left(\frac{1}{|\mathbf{k}|^2 + \omega^2} \right) \left(\overline{(i\omega\hat{\chi})(\widehat{m_\parallel + 1})} \, (i\omega\hat{\chi})(\widehat{m_\parallel + 1}) \right. \\
& + \overline{(\hat{\chi})\mathbf{k}\cdot\hat{\mathbf{m}}_\perp} \, (i\omega\hat{\chi})(\widehat{m_\parallel + 1}) + \overline{i\omega\hat{\chi})(\widehat{m_\parallel + 1})} \, (\hat{\chi})\mathbf{k}\cdot\hat{\mathbf{m}}_\perp \\
& \left. + \overline{(\hat{\chi})\mathbf{k}\cdot\hat{\mathbf{m}}_\perp} \, (\hat{\chi})\mathbf{k}\cdot\hat{\mathbf{m}}_\perp \right) \frac{d\omega}{(2\pi)} \frac{d^2k}{(2\pi)^2}.
\end{aligned} \tag{4.17}$$

Where all characteristic functions may be factored out, and $\overline{\hat{\chi}}\hat{\chi} = \frac{2}{\omega^2}(1 - \cos(\delta\omega))$, arrive at the following representation for the energy,

$$\begin{aligned}
E'_d = \frac{1}{\delta} \int_{\mathbb{R}^2} \int_{\mathbb{R}} & \left(\frac{2(1 - \cos(\delta\omega))}{|\mathbf{k}|^2 + \omega^2} \right) \left(\overline{(\widehat{m_\parallel + 1})} \, (\widehat{m_\parallel + 1}) + \frac{\overline{\mathbf{k}\cdot\hat{\mathbf{m}}_\perp} \, \mathbf{k}\cdot\hat{\mathbf{m}}_\perp}{\omega^2} \right. \\
& \left. + \frac{\overline{\mathbf{k}\cdot\hat{\mathbf{m}}_\perp} \, (\widehat{m_\parallel + 1}) + \overline{(\widehat{m_\parallel + 1})} \, \mathbf{k}\cdot\hat{\mathbf{m}}_\perp}{\omega} \right) \frac{d\omega}{(2\pi)} \frac{d^2k}{(2\pi)^2},
\end{aligned} \tag{4.18}$$

provided these integrals are well defined. One can break up the ω integrals term-by-term into the following kernels

$$K_r(\mathbf{k}) = \int_{\mathbb{R}} \left(\frac{2(1 - \cos(\delta\omega))}{(|\mathbf{k}|^2 + \omega^2)\,\omega^r} \right) \frac{d\omega}{(2\pi)}. \tag{4.19}$$

with $r \in \{0, 1, 2\}$. And we find:

$$K_0(\mathbf{k}) = \frac{1 - e^{-\delta|\mathbf{k}|}}{|\mathbf{k}|}, \tag{4.20}$$

$$K_1(\mathbf{k}) = 0, \tag{4.21}$$

$$K_2(\mathbf{k}) = \frac{\delta|\mathbf{k}| - 1 + e^{-\delta|\mathbf{k}|}}{|\mathbf{k}|^3}. \tag{4.22}$$

In this case the energy is

$$E'_d = \frac{1}{\delta} \int_{\mathbb{R}^2} \left\{ \frac{1 - e^{-\delta|\mathbf{k}|}}{|\mathbf{k}|} |\widehat{m_\| + 1}|^2 + \frac{\delta|\mathbf{k}| - 1 + e^{-\delta|\mathbf{k}|}}{|\mathbf{k}|^3} |\mathbf{k} \cdot \hat{\mathbf{m}}_\perp|^2 \right\} \frac{d^2k}{(2\pi)^2}, \qquad (4.23)$$

As obtained in [38]. Adding and subtracting the local term gives

$$E'_d = \int_{\mathbb{R}^2} \left(m_\| + 1 \right)^2 d^2r + \int_{\mathbb{R}^2} \left\{ \left(\frac{1 - e^{-\delta|\mathbf{k}|}}{\delta|\mathbf{k}|} - 1 \right) |\widehat{m_\| + 1}|^2 \right.$$
$$\left. + \frac{\delta|\mathbf{k}| - 1 + e^{-\delta|\mathbf{k}|}}{\delta|\mathbf{k}|^3} |\mathbf{k} \cdot \hat{\mathbf{m}}_\perp|^2 \right\} \frac{d^2k}{(2\pi)^2}. \qquad (4.24)$$

Combining together with (4.11) one obtains the total stray field energy:

$$E_d(\mathbf{m}, \delta) = -\int_\Omega |\mathbf{m}_\perp|^2 d^2r + \int_{\mathbb{R}^2} \left\{ \left(\frac{1 - e^{-\delta|\mathbf{k}|}}{\delta|\mathbf{k}|} - 1 \right) |\widehat{m_\| + 1}|^2 \right.$$
$$\left. + \frac{\delta|\mathbf{k}| - 1 + e^{-\delta|\mathbf{k}|}}{\delta|\mathbf{k}|^3} |\mathbf{k} \cdot \hat{\mathbf{m}}_\perp|^2 \right\} \frac{d^2k}{(2\pi)^2}. \qquad (4.25)$$

As an aside, note its asymptotic expansion in δ recovers the energy of Section 2.3.2 [10]:

$$E_d(\mathbf{m}, \delta) \simeq -\int_\Omega |\mathbf{m}_\perp|^2 d^2r + \delta \int_{\mathbb{R}^2} \left\{ -|\mathbf{k}||\widehat{m_\| + 1}|^2 + \frac{|\mathbf{k} \cdot \hat{\mathbf{m}}_\perp|^2}{|\mathbf{k}|} \right\} \frac{d^2k}{(2\pi)^2}. \qquad (4.26)$$

From here, Plancharel's Theorem will give (2.25).

Let us conclude by introducing a more universal kernel, let

$$F(k) = \frac{e^{-k} - 1 + k}{k^2}, \qquad (4.27)$$

and it is clear that (4.25) becomes

$$E_d(\mathbf{m}, \delta) = -\int_\Omega |\mathbf{m}_\perp|^2 d^2r + \delta \int_{\mathbb{R}^2} F(\delta|\mathbf{k}|) \left\{ \frac{|\mathbf{k} \cdot \hat{\mathbf{m}}_\perp|^2}{|\mathbf{k}|} - |\mathbf{k}||\widehat{m_\| + 1}|^2 \right\} \frac{d^2k}{(2\pi)^2}. \qquad (4.28)$$

We may refer to component terms of this energy integral as the shape anisotropy, volume charge energy, and surface charge energy respectively.

$$E_{vol}(\mathbf{m}, \delta) = \delta \int_{\mathbb{R}^2} F(\delta|\mathbf{k}|) \frac{|\mathbf{k} \cdot \hat{\mathbf{m}}_\perp|^2}{|\mathbf{k}|} \frac{d^2k}{(2\pi)^2}, \tag{4.29}$$

$$E_{surf}(\mathbf{m}, \delta) = -\delta \int_{\mathbb{R}^2} F(\delta|\mathbf{k}|)|\mathbf{k}||\widehat{m_\parallel + 1}|^2 \frac{d^2k}{(2\pi)^2}. \tag{4.30}$$

Completing the finite thickness model of the stray field interaction energy for one layer. The same can be obtained for multiple interacting layers in Chapter 5.

4.2 Stray Field Energy of BP-profiles in the Finite-Thickness Regime

We proceed to the reduced energy. Recalling Section 3.2, our representation of skyrmions is given by the Belavin-Polyakov profiles ansatz based calculations of magnetic skyrmions. While technically beginning with the truncated profile, (3.17), the stray field energy is asymptotic to that calculated for the untruncated profile, (3.14), for $L \to \infty$. Thus,

$$E_d(R_\theta \mathbf{m}_L(\mathbf{r}/\rho), \delta) \simeq E_d(R_\theta \mathbf{m}_\infty(\mathbf{r}/\rho), \delta), \tag{4.31}$$

with in-plane rotations characterized by the rotation angle θ. Recall when $\theta = \pi n$ this is called a Néel skyrmion, and when $\theta = \pi n + \pi/2$, a Bloch skyrmion. We may now easily render the profiles in Fourier space by their well known $\mathbb{R}^2$ transforms as obtained in [9]. One obtains

$$i\mathbf{k} \cdot \hat{\mathbf{m}}_{\infty,\perp} = -4\pi|\mathbf{k}|K_1(|\mathbf{k}|), \tag{4.32}$$

$$(\widehat{m_{\infty,\parallel} + 1}) = 4\pi K_0(|\mathbf{k}|), \tag{4.33}$$

where K_0, K_1 are the modified Bessel functions of the second kind [1]. When applying the in-plane rotation, one obtains

$$\mathbf{m}_\perp(\mathbf{r}) = \cos(\theta)\mathbf{m}_{\infty,\perp}(\mathbf{r}/\rho) + \sin(\theta)\mathbf{m}_{\infty,\perp}^\perp(\mathbf{r}/\rho). \tag{4.34}$$

with $\mathbf{m}_{\infty,\perp}^\perp = f(|\mathbf{r}|)\hat{\mathbf{e}}_\phi$, this term vanishes under the divergence, therefore,

$$i\mathbf{k} \cdot \mathbf{m}(\mathbf{k}) = \rho^2 \cos(\theta) i\mathbf{k} \cdot \mathbf{m}_\infty(\rho\mathbf{k}). \tag{4.35}$$

This untruncated variant is sufficient for calculation of the stray field energy of the BP profiles, as we calculate only to leading order for truncation distance, $L \to \infty$.

$$E_{vol} = \delta(4\pi)^2 \rho^4 \cos^2\theta \int_{\mathbb{R}^2} F(\delta|\mathbf{k}|) \ |\mathbf{k}| K_1^2(\rho|\mathbf{k}|) \frac{d^2k}{(2\pi)^2}, \tag{4.36}$$

$$E_{surf} = -\delta(4\pi)^2 \rho^4 \int_{\mathbb{R}^2} F(\delta|\mathbf{k}|) \ |\mathbf{k}| K_0^2(\rho|\mathbf{k}|) \frac{d^2k}{(2\pi)^2}. \tag{4.37}$$

Further simplification of the surface charge energy is necessary, as it is a main ingredient in the stabilization of skyrmion solutions (Section 4.3). Using polar coordinates $|\mathbf{k}| = k$, and renormalizing by letting $\rho k = s$, and defining $\eta = \rho/\delta$. The surface charge energy becomes

$$E_{surf} = -(4\pi)^2 \delta\rho \int_0^\infty F\left(\frac{s}{\eta}\right) \ K_0^2(s) s^2 \frac{ds}{(2\pi)^2}, \tag{4.38}$$

$$= -8\pi\delta\rho\eta^2 \int_0^\infty \left(\frac{s}{\eta} - 1 + e^{-s/\eta}\right) K_0^2(s) ds, \tag{4.39}$$

$$= -\delta\rho H(\eta). \tag{4.40}$$

with

$$H(\eta) = 4\pi\eta - 2\pi^3\eta^2 + 8\pi\eta^2 \int_0^\infty e^{-s/\eta} K_0^2(s) ds. \tag{4.41}$$

This is compared to that which is obtained asymptotically for small δ in (3.24), in Figure 4.2.

It will be useful for us to establish properties of this function H. We find that since $0 < F(k) \leq \frac{1}{2}$, it follows from (4.38) that H is always positive and bounded from above for all $\eta > 0$, hence

$$0 < H(\eta) \leq 4\pi \int_0^\infty s^2 \, K_0^2(s)ds = \frac{\pi^3}{8}. \tag{4.42}$$

We further deduce that $F(k)$ is monotonically decreasing with $k > 0$ and decays like $1/k$. We refine the estimate

$$F(k) \leq \min\left\{\frac{1}{2}, \frac{1}{k}\right\}, \tag{4.43}$$

and acquire another bound for H by the same technique. One obtains

$$0 < H(\eta) \leq 8\pi\eta \int_0^\infty s \, K_0^2(s)ds = 4\pi\eta. \tag{4.44}$$

Then we may put

$$H(\eta) \leq \min\left\{4\pi\eta, \frac{\pi^3}{8}\right\}. \tag{4.45}$$

Due to the Lebesgue dominated convergence theorem and $\frac{|k|}{\eta}F\left(\frac{|k|}{\eta}\right) \to 1$ as $\eta \to 0$, we have

$$\lim_{\eta \to 0} \frac{H(\eta)}{\eta} = 4\pi. \tag{4.46}$$

When enacting the minimization of the total energy we will need the derivative

$$-\left(\frac{H(\eta)}{\eta}\right)' = 8\pi \int_0^\infty \left(1 - (e^{-\frac{k}{\eta}})\left(1 + \frac{k}{\eta}\right)\right) K_0^2(k)dk. \tag{4.47}$$

We note that $-\lim_{\eta\to 0}\left(\frac{H(\eta)}{\eta}\right)' = 2\pi^3$. Given that it has a strictly positive integrand, we find this expression is always positive. This implies $\frac{H(\eta)}{\eta}$ is strictly monotone decreasing. Furthermore, observe for all $k > 0$ that

$$\left(1 - e^{-k}(1+k)\right)' = ke^{-k} > 0, \tag{4.48}$$

so that $-\left(\frac{H(\eta)}{\eta}\right)'$ is strictly monotone decreasing as well. We now aim to show the quantity is log-concave. Denote

$$M(\gamma) = -\left(\frac{H(e^\gamma)}{e^\gamma}\right)'. \tag{4.49}$$

We then have

$$M(\gamma) = 8\pi \int_{\mathbb{R}} \left(1 - e^{-e^{s-\gamma}}\left(1 + e^{s-\gamma}\right)\right) e^s K_0^2(e^s) ds. \tag{4.50}$$

It is a fact that convolutions of log-concave functions are themselves log-concave [62, 86]. Furthermore, since products of log-concave functions are log-concave, we may split this task into proving that for $s \in \mathbb{R}$ the two functions

$$f_1(s) := 1 - e^{-e^s}\left(1 + e^s\right), \tag{4.51}$$

$$f_2(s) := K_0(e^s) \tag{4.52}$$

are log-concave.

By explicit calculation, we have that

$$(\log \circ f_1)'(s) = \frac{1}{f_3(e^s)}, \tag{4.53}$$

with $f_3(k) = \frac{e^k - 1 - k}{k}$ for $k > 0$ which can be seen to be strictly monotone increasing in k by the series expansion of the exponential. Consequently, f_1 is strictly log-concave.

For the second function, we compute

$$(\log \circ f_2)'(s) = e^s \frac{K_0'(e^s)}{K_0(e^s)}, \tag{4.54}$$

which is strictly decreasing [1]. Hence, f_2 is strictly log-concave. Therefore, $M(\gamma)$ is log-concave. It follows from the strict monotonicity of $M(\log(\eta))$ that the quantity is strictly log-concave.

4.2.1 Numerical evaluation of surface charge energy

For practical computation of the energy we turn to numerical methods. The surface charge energy, (4.41), must be evaluated accurately for small values of ρ in order to properly capture the nature of this energy landscape. Note first, it admits an analytical solution in the form of the complete elliptic integral, K, and the $_3F_2$-hypergeometric function [1].

$$E_{surf} = -\delta\rho \left(4\pi\eta - 2\pi^3\eta^2 + 2\pi\eta^2 K\left(\frac{1}{4\eta^2}\right) - 2\,_3F_2\left[\begin{matrix}1,1,1\\\frac{3}{2},\frac{3}{2}\end{matrix}\middle|\frac{1}{4\eta^2}\right]\right). \tag{4.55}$$

While interesting, this could never be evaluated efficiently due to the singular nature of the resultant functions, and we turn to numerical methods. Trefethen gives an appropriate scheme for accurately evaluating integrals on semiinfinite domains using Gauss-Legendre polynomials on a truncated domain, where the truncation distance is scaled $P^{1/3}$, with P number of quadrature nodes, this will be far more efficient than Gauss-LaGuerre or Gauss-Hermite type schemes [103]. It may be observed that for $\eta = \rho/\delta$ very small, the Bessel function is dilated very far from the origin while $\left(\frac{1-e^{-|\mathbf{k}|}}{|\mathbf{k}|} - 1\right)$ is nearly unity in the far field. Therefore, for a certain cutoff of $\eta < \eta_c$ the truncation distance is extended past Trefethen's recommendation, proportionally to η^{-1}. This methods stands up well compared to the analytical representation, (4.55), and a test of the numerical evaluation is given in Figure 4.1.
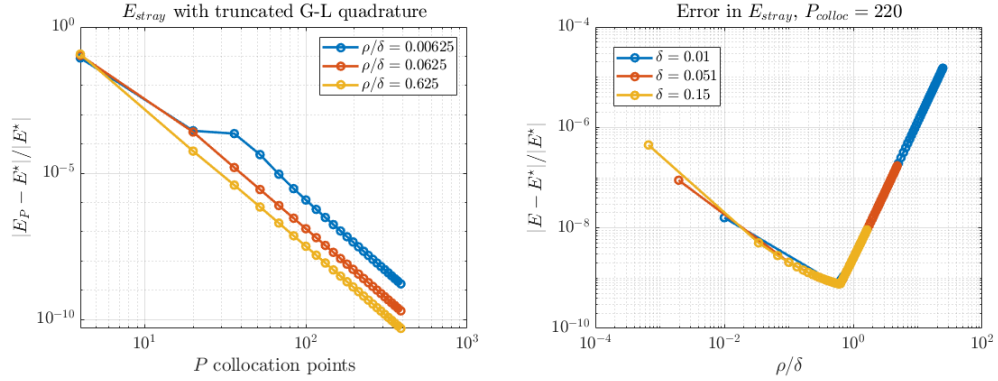
Figure 4.1 Relative errors in evaluation of (4.40) across nominal values of ρ and δ using the truncated Gauss-Legendre quadrature. Left: Performance of the G-L quadrature showing error decrements of 5 decades per decade of collocation points, P. Right: Performance of quadrature method for $P_{colloc} = 220$ across values of ρ/δ guaranteeing errors below 10^{-5} for nominal values of ρ and δ. In practice $P_{colloc} = 400$ is used for the energy minimization procedure.
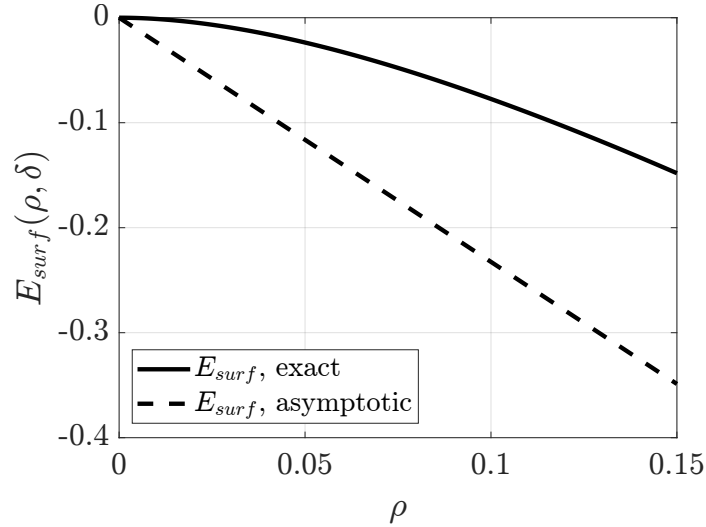
Figure 4.2 Comparison of asymptotic, (3.24), and finite-thickness, (4.40), forms of the surface charge energy vs skyrmion radius. Chosen parameter $\delta = 0.6$. Though having similar slopes for intermediate ranges of ρ, the finite thickness form of the surface charge energy has high negative curvature in the low ρ region. Stray field dominates in this form for low values of ρ, enabling the formation of a local maximum in the total energy.

4.3 Locus of Stable Skyrmions in Finite-Thickness Monolayers

We turn to study the problem of skyrmions in a monolayer using the representation of the energy formulated in the finite thickness regime. The resultant minimizers of energy are to be contrasted with those obtained from the asymptotic formulation given by the thin asymptotic model in Section 3.3.

The use of the finite thickness stray field energy leads to a fundamentally different energy landscape which enables the formation of a local maximizer for a value of ρ smaller than that representing the skyrmion solution (see Figure 4.3d). For a fixed δ and increasing Q, the maximizer and minimizer may join together leading to a bifurcation where skyrmion solutions no longer exist. This was not predicted by the asymptotic model in [9] which guarantees existence of skyrmion solutions so long as $\delta < \sqrt{2(Q-1)}$. Therefore, this anti-simplification accomplished by using the exact stray field energy leads to the discovery of a family of bifurcation points on the right hand side of the (Q, δ)-parameter space which bounds the region of existence of skyrmion solutions (see Figure 4.3a). We denote those critical values as Q_c and δ_c, and may represent them as a curve in the plane $\delta_c = \delta_c(Q)$.

We use a film with exchange and anisotropy interactions, so the energy takes the form of (4.1), evaluated on a truncated BP-profile, (3.17), described above with radius ρ, rotation θ and the necessary truncation at a distance $\sqrt{L}$ from the core. Quoting equations (3.20) (3.21), and (4.28), asymptotically the BP-profile energies are

$$E_{ex} = 8\pi + \frac{4\pi}{L^2}, \tag{4.56}$$

$$E_{an} = 4\pi Q \rho^2 \log\left(\frac{4L^2}{e^{2(1+\gamma)}}\right), \tag{4.57}$$

$$E_d = -4\pi \rho^2 \log\left(\frac{4L^2}{e^{2(1+\gamma)}}\right) + E_{vol}(\rho, \theta, \delta) + E_{surf}(\rho, \delta). \tag{4.58}$$

The total energy is

$$E = 8\pi + \frac{4\pi}{L^2} + 4\pi(Q-1)\rho^2 \log\left(\frac{4L^2}{e^{2(1+\gamma)}}\right) + E_{vol}(\rho, \theta, \delta) - \delta\rho H\left(\rho/\delta\right). \qquad (4.59)$$

4.3.1   Energy minimization: Bloch skyrmions in the (Q, δ) phase space

The energy begins simplifying right away. We see from (4.36), that E_{vol} is always positive and is the only term depending on the angular quality of the skyrmion, $\cos(\theta)$. This minimizes to zero when $\theta = \pi/2 \pm \pi n$, for integers n, and thus may be dropped from the energy equation. Therefore the solution will take the form of a Bloch skyrmion. We are left with the total energy

$$E = 8\pi + \frac{4\pi}{L^2} + 4\pi(Q-1)\rho^2 \log\left(\frac{4L^2}{e^{2(1+\gamma)}}\right) - \delta\rho H\left(\rho/\delta\right). \qquad (4.60)$$

and picking $L = (\rho\sqrt{Q-1})^{-1}$, minimizes this expression in L, amounting to balancing the exchange and anisotropy energy. The energy, (4.60) now depends only on the skyrmion radius ρ. We take the numerical computation of the surface charge energy (4.40), and solve for the critical points by Newton's method iteration. For any given combination of δ and Q studied herein, the energy may yield up to three critical points.

There exists a central parameter region in the (Q, δ) plane where the energy has all three critical points (Figure 4.3a), one observes a local maximum ρ_{sad}, a local minimizer ρ_{sky} denoting the skyrmion solution, and a local maximum ρ_{burst}. The final, ρ_{burst} also appears in the thin film asymptotic formulation, far flung of the asymptotic assumptions, yet here it plays a role in characterizing the physics at the boundary of the obtainable skyrmion solutions. Increasing δ until ρ_{burst} and ρ_{sky} annihilate one another results in an energy which has no minimizer and decreases without bound as ρ increases. This may be called the "Bursting" phase, as the calculation being done for BP-profiles suggests any BP profile will dynamically expand into a domain until

it exits the restricted class, (3.15), by violating $\int_{\mathbb{R}^2} |\nabla\mathbf{m}|^2 d^2r < 16\pi$. Analysis of the thin film equations (3.25) finds this bursting bifurcation at the following locus:

$$\delta_b = \bar{\delta}_b \sqrt{(Q_b - 1)}, \tag{4.61}$$

for a constant $\bar{\delta}_b = 1.97$. However, micromagnetic simulations are able to resolve skyrmion solutions far aflung of this estimate (see Figure 4.5). We estimate the critical parameters for this bursting by extrapolating from numerical solutions of the LLG equations in Section 4.3.3 to find $\bar{\delta}_b = 2.953$.

Meanwhile, decreasing δ until ρ_{sad} and ρ_{sky} annihilate gives a system with only the maximizer ρ_{burst}, as illustrated in Figure 4.3d. Thus, a BP profile as an initial condition, and subject to asymptotic assumptions, ρ may be taken smaller than ρ_{burst}, cannot minimize the energy to a radius greater than zero, suggesting these profiles dynamically shrink and find no stable state within the restricted class. As such we call this the "collapse" phase. In this case the collapse energy is

$$\Delta E = E(\rho_{sad}) - E(\rho_{sky}). \tag{4.62}$$

when the local maximizer, ρ_{sad}, does not exist, the collapse energy is just

$$\Delta E = 8\pi - E(\rho_{sky}). \tag{4.63}$$

4.3.2 Existence of skyrmions and the collapse line

With some work and study of the surface charge energy, (4.40), one can show the existence of a critical line in the (Q, δ) plane beyond which skyrmion solutions cease to exist. This relies on several properties given for the surface charge energy.

For $L = \rho^{-2}(Q-1)^{-1}$ the energy is parametrically minimized in L as discussed, becoming

$$E = 4\pi(Q-1)\rho^2 \log\left(\frac{eK^\star}{(Q-1)\rho^2}\right) - \delta\rho H\left(\frac{\rho}{\delta}\right), \tag{4.64}$$

with $K^\star = \frac{4}{\exp(2(1+\gamma))}$. Switching to $\eta = \rho/\delta$, the equation can be rewritten

$$\frac{E}{4\pi\delta^2} = g_1(\eta) = (Q-1)\rho^2 \log\left(\frac{eK^\star}{(Q-1)\delta^2\eta}\right) - \frac{H(\eta)}{4\pi\eta}. \tag{4.65}$$

Differentiating we find

$$g_1'(\eta) = -\frac{2}{\eta}(Q-1) - \left(\frac{H(\eta)}{4\pi\eta}\right)'. \tag{4.66}$$

which vanishes on the following curve relating Q and η

$$(Q-1) = g_2(\eta) = -\frac{\eta}{2}\left(\frac{H(\eta)}{4\pi\eta}\right)'. \tag{4.67}$$

The function $\log(g_2(\eta))$ is strictly concave given that we have already shown that $-\left(\frac{H(e^\gamma)}{e^\gamma}\right)'$ is strictly log-concave in γ. Therefore, g_2 has at most one critical point. We also have $\lim_{\eta\to 0} g_2(\eta) = \lim_{\eta\to\infty} g_2(\eta) = 0$ and $g_2(\eta) \geq 0$. It follows that there exists $Q_c > 1$ and η_c such that

$$Q_c - 1 = g_2(\eta_c). \tag{4.68}$$

Therefore, for $Q < Q_c$, (4.67) has two solutions $\eta_1 < \eta_c < \eta_2$. With η_1 corresponding to an energy minimizing skyrmion solution. Hence, for $Q > Q_c$, minimizers of (4.59) cease to exist.

Our collaborators have refined this analysis to give a more precise form of the boundary and present the following theorem [11].
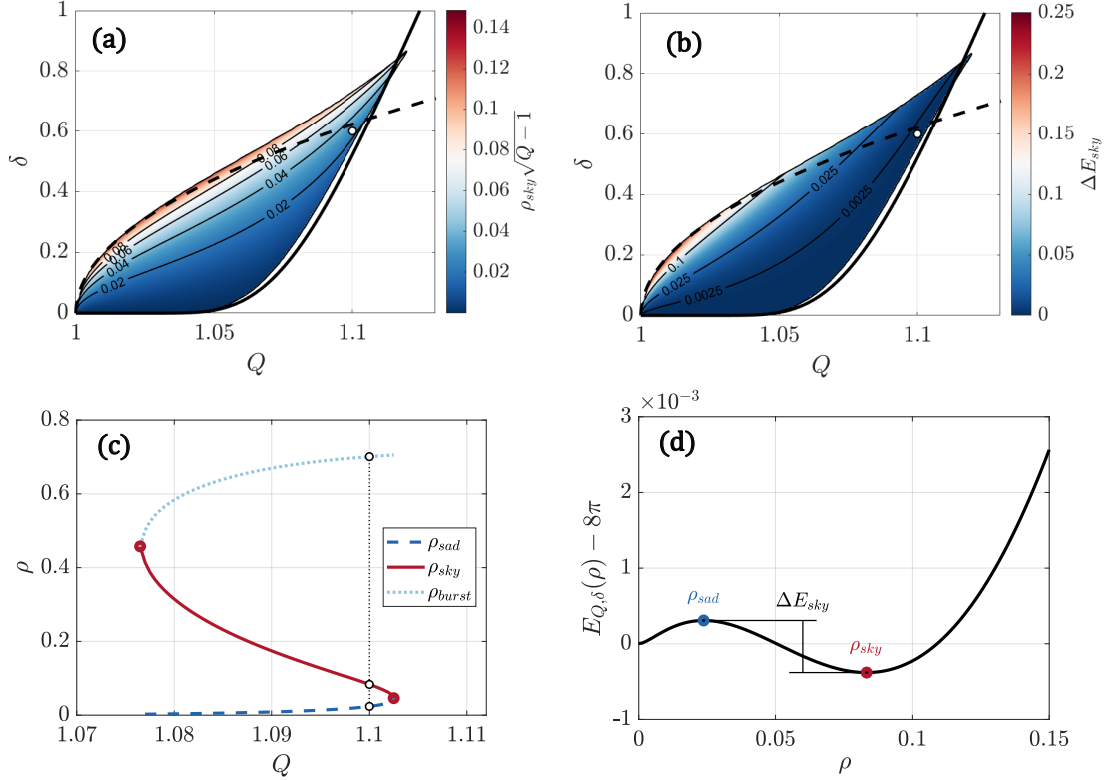
Figure 4.3 All skyrmion solutions for the finite-thickness model. (a) Phase diagram showing obtained skyrmion radius $\rho_{sky}\sqrt{Q-1}$ on the colormap. (b) Phase diagram showing collapse energy (4.62) on the colormap. (c) A locus of energy critical points for a chosen $\delta = 0.6$, and Q on the abscissa. (d) Energy landscape for parameters $Q = 1.10$ and $\delta = 0.6$ (this point in parameter space is marked with white dots on (a-b-c)). On the phase diagrams (a-b), the solid line shows the formula, (4.70), fitted to the collapse curve with $B = 35.18$. The dotted line shows the transition to the bursting phase predicted by the thin-film equations, (4.61).

Theorem 1 *The reduced energy equation calculated for BP profiles, (4.60), admits a minimizer over $(0,1) \times (L_0, \infty)$ for δ and $\frac{\delta}{\sqrt{Q-1}}$ sufficiently small and $L_0 > 1$ sufficiently big (all universal) if and only if for some universal constant $B > 0$ we have*

$$\beta = (Q-1) \left| \log \frac{BK^\star}{(Q-1)^3 \delta^2} \right| < 1, \tag{4.69}$$

and $Q - 1$ sufficiently small depending on $1 - \beta$.

We remark that from this inequality we obtain a form to estimate the boundary of skyrmion existence by saturating this inequality on the positive side of the absolute value. We thereby derive the following relationship between the coordinates, (Q_c, δ_c), of the bifurcation defined by (4.68).

$$\delta_c^2 = \frac{1}{BK^\star} \frac{\exp\left(-\frac{1}{Q_c - 1}\right)}{(Q_c - 1)^3}. \tag{4.70}$$

This critical line is shown on Figure 4.3.

4.3.3 Numerical simulations and skyrmion bursting

Simulations carried out via the MuMax3 software [105] on thin film geometries discretized on a square grid and evolved with finite difference methods. The simulations solve the full unsimplified LLG equations (2.1) on a GPU with a precomputed Fourier kernel for the stray field interaction. From suitable initial conditions, the skyrmions are obtained by direct simulation, and run until judged to have arrived at its stationary state. The parameters here chosen are meant to model a ferrimagnetic material, with $M_s = 10^5$ A/m, and $l_{ex} = 56.4$ nm being characteristic values which weaken the stray field effects compared with exchange and promote variations over broad length scales [9][13]. These simulations are carried out in families identified by a value of K_u and successively decreasing the film thickness, d after obtaining an equilibrium state, using the previously resolved solution as the initial condition for the next. This is continued

until the skyrmion collapses. Due to the size of the skyrmions compared to the discretization step, a small enough skyrmion falls beneath the threshold of resolution, i.e. at this point the gradients become too steep for the discrete grid. We observe this happening for skyrmions of radius around 40 nm in this case for a gridspacing of 4 nm (see Figure 4.4).

The obtained data qualitatively recapitulates the same trends as observed for the theoretical solutions of the finite thickness model. In fact they exhibit grouping around a universal curve depending on $\delta/\sqrt{Q-1}$ as predicted by the asymptotic theory see Figure 4.5. As a first step toward unifying the theoretical and the simulation results a fit may be performed on a suitable function where the simulation data for large $\delta/\sqrt{Q-1}$ are interpreted as approaching a saddle node bifurcation where skyrmions cease to exist. This function would also have to match the asymptotic regime resolved for small $\delta/\sqrt{Q-1}$. We conclude the form

$$f(\bar{\delta}) = \frac{C_0\bar{\delta}}{\log(\beta\bar{\delta})}\left(1 - c\sqrt{\bar{\delta}_b - \bar{\delta}}\right) \tag{4.71}$$

would be a suitable candidate, where $\bar{\delta} = \frac{\delta}{\sqrt{Q-1}}$, and where C_0, c, and $\bar{\delta}_b$ are fit constants . The choice of the factor $\frac{\bar{\delta}}{\log(\beta\bar{\delta})}$ comes directly from (3.26), respecting the asymptotics. From there, we can estimate the appearance of the skyrmion bursting regime $\bar{\delta}_b$, denoted on Figure 4.5.
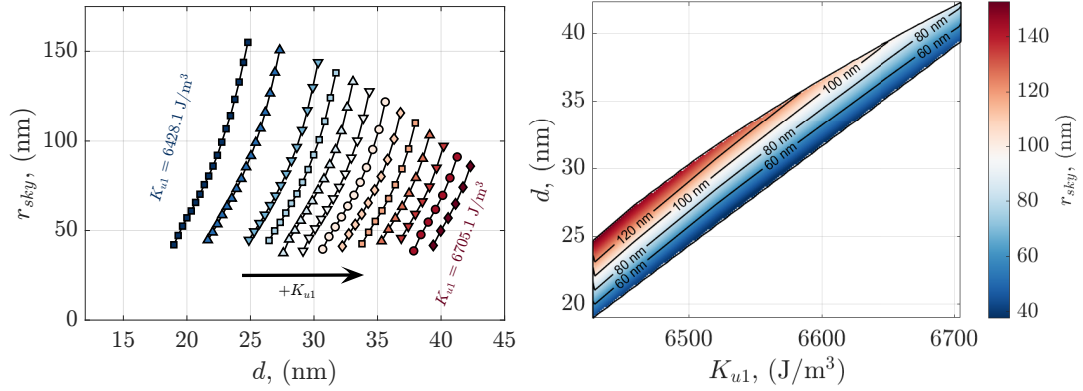
Figure 4.4 Numerical simulations of the LLG equations, (2.1), with skyrmions resolved on a grid of 516×516 points with discretization length 4 nm. Parameters are $A = 20$ pJ/m, $M_s = 10^5$ A/m. Film thickness, d, and anisotropy strength, K_u, are varied between characteristic values. d is taken between 19.0 nm and 42.3 nm, and K_u between 6428.1 J/m^3 and 6705.1 J/m^3 corresponding to values of δ between 0.337 and 0.750 and Q between 1.023 and 1.067. Left: radius of resolved skyrmions depending on film thickness for select values of anisotropy strength. Right: The same interpolated over the (K_u, d) plane.
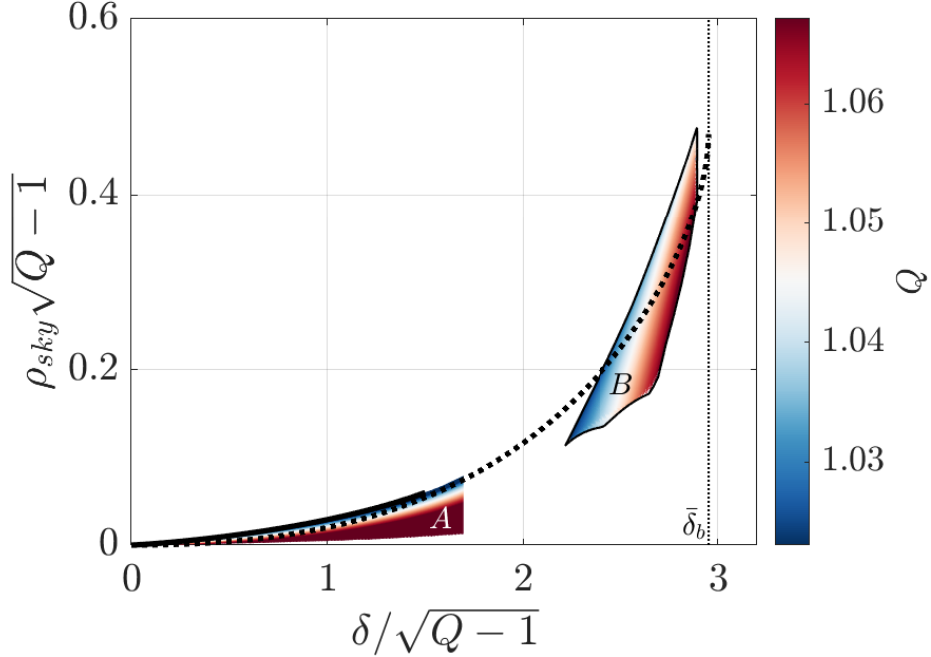
Figure 4.5 Simulation results compared with theoretical solutions. Dashed line: Fit between asymptotic theory and simulation results. Thin dotted line: critical value of $\bar{\delta}_b = 2.953$ obtained from fit. Region (A): skyrmion solutions resolved by the finite-thickness film theory, truncated to $\bar{\delta} \leq 1.6$. Region (B): skyrmions resolved in numerical simulation as Figure 4.4.

CHAPTER 5

STRAY FIELD INTERACTION ENERGY IN A THIN MULTILAYER SYSTEM

We present the derivation of a working thin multilayer model, beginning from the general micromagnetic theory, as given in Chapter 2, and solving it within the thin film geometry. The result includes extra energy terms that differentiate this from the single-layer problem studied by [9] and summarized in Sections 2.3.2 and 3.3. These are the local exchange coupling interaction terms and the stray-field coupling terms acquired from the asymptotic expansion, both facilitating inter-layer interactions. This chapter is dedicated to the treatment of the stray field energy in the multilayer model which will be used to study skyrmions in the subsequent chapters.

5.1 Multilayer Thin-Film Model

The model is characterized by having multiple magnetization fields, $\mathbf{m}_i : \mathbb{R}^2 \to \mathbb{S}^2$, one for each layer. The principal subscript will always be used to identify the field $\mathbf{m}_i$. When components need to be referenced, a secondary subscript will be introduced, $\mathbf{m}_i = (\mathbf{m}_{i,\perp}, m_{i,\parallel})$. There are N layers of non-dimensional thickness δ separated by nonmagnetic layers of thickness $(a-1)\delta$, as diagrammed in Figure 5.1. As such, the thickness of the entire system will be $\mathcal{O}(N\delta)$. We assume the ferromagnetic layers are the same material, and therefore have the same exchange stiffness, interfacial DMI strength, and anisotropy. Separate layers may differ in the sign of κ_i. The reduction to the thin-film equations a la equation (2.25) can be performed much in the same way, and is demonstrated in Section 5.2. The result includes extra energy terms that differentiate this from the single-layer problem. These are the local exchange coupling interaction terms and the stray-field coupling terms. The energy may be expressed as

the multilayered version of (2.23). Each layer has its own fundamental self-interaction energies, resulting in a summation, and an additional $N-1$ interlayer exchange coupling interactions between a layer and its neighbors. The energy, measured in the units Ad is

$$
E\left(\{\mathbf{m}_i\}\right) = \sum_{i=1}^{N} \int_{\mathbb{R}^2} \left(|\nabla\mathbf{m}_i|^2 + Q\,|\mathbf{m}_{i,\perp}|^2 - 2\kappa_i\mathbf{m}_{i,\perp}\cdot\nabla m_{i,\|}\right) d^2r
$$
$$
+ E_d\left(\{\mathbf{m}_i\},\delta\right) + \sigma\sum_{i=1}^{N-1} \int_{\mathbb{R}^2} |\mathbf{m}_{i+1} - \mathbf{m}_i|^2\, d^2r,
$$
(5.1)

where the last term is the interlayer exchange coupling with the constant σ, and the stray field energy, E_d shall be treated in the subsequent sections.

Here, the exchange coupling may be obtained from the nondimensionalization of

$$
\mathcal{E}_{ec,i} = \frac{J_{ec,i}d}{M_s^2} \int_{\mathbb{R}^2} |\mathbf{M}_{i+1} - \mathbf{M}_i|^2 d^2r,
$$
(5.2)

where $J_{ec,i}$ has units J/m^3 [57, 92]. For all layers having the same exchange coupling constant, $J_{ec} = J_{ec,i}$, one obtains the nondimensional parameter

$$
\sigma = \frac{J_{ec}}{K_d},
$$
(5.3)

resulting in the expression included in (5.1).

The exchange coupling may change the problem dramatically, as $\sigma > 0$ and $\sigma < 0$ are both possible choices. We refer to these respective systems as ferromagnetically coupled and antiferromagnetically coupled, since in the latter case the coupling energy would be minimized by an anti-parallel order: $\mathbf{m}_{j+1} = -\mathbf{m}_j$. This interaction is studied in view of skyrmions in Chapter 7.

We may now refer to "self-interactions" as those terms which depend only on one $\mathbf{m}_i$ and "interlayer-interactions" which include dependence on two different

$\mathbf{m}_i$'s. Note a layer i will have an inter-layer stray field interaction with all other layers, while the exchange coupling interaction occurs only between neighboring layers. The inter-layer stray field interaction types are: surface-surface, surface-volume, and volume-volume respectively, $E_{\text{surf}}(\mathbf{m}_i, \mathbf{m}_j)$, $E_{\text{vs}}(\mathbf{m}_i, \mathbf{m}_j)$, $E_{\text{vol}}(\mathbf{m}_i, \mathbf{m}_j)$. We may calculate these interactions exactly in terms of integral kernels. Due to the proximity of the layers, $\mathcal{O}(\delta)$, the asymptotic model will lack surface-volume inter-layer interactions as they are found to be of $\mathcal{O}(\delta^2)$, (see Equation 5.31).

5.2 Reduction and Asymptotics of the Stray-Field Energy in Thin Multilayer Systems

We assume that a ferromagnetic sample occupies domain, $Y \subseteq \mathbb{R}^3$ consisting of N thin layers of thickness δ. The distance between the centers of the neighboring layers is $a\delta$, where $a > 1$ so that the domains do not overlap:

$$Y = \Omega \times \bigcup_{i=1}^{N} [(i-1)a\delta, (1+(i-1)a)\delta], \tag{5.4}$$

with $\Omega \subseteq \mathbb{R}^2$. The micromagnetic stray field energy is,

$$E_d = \frac{1}{\delta} \int_{\mathbb{R}^3} \int_{\mathbb{R}^3} \frac{\nabla \cdot \tilde{\mathbf{m}}(\mathbf{r}) \nabla \cdot \tilde{\mathbf{m}}(\mathbf{r}')}{4\pi |\mathbf{r} - \mathbf{r}'|} d^3 r d^3 r', \tag{5.5}$$

assuming magnetization does not vary in the vertical direction. Here we also employ a shorthand where χ_i is the characteristic function of i-th layer. Then we have

$$\tilde{\mathbf{m}}(x, y, z) = \sum_{i=1}^{N} \mathbf{m}_i(x, y) \chi_i(z) = \sum_{i=1}^{N} \left(\mathbf{m}_i^{\perp}(x, y) + \hat{\mathbf{e}}_3 m_i^{\|}(x, y) \right) \chi_i(z). \tag{5.6}$$

For $\Omega = \mathbb{R}^2$ and $\mathbf{m}_i \to -\hat{\mathbf{e}}_3$ as $\mathbf{r} \to \infty$ we have to renormalize the stray field energy for the integrals to make sense. We define the uniform magnetization state $\tilde{\mathbf{m}}_{\star} = -\hat{\mathbf{e}}_3 \sum_i \chi_i$ and let $\tilde{\mathbf{m}}_r = \tilde{\mathbf{m}} - \tilde{\mathbf{m}}_{\star}$ and $U_r = U - U_{\star}$. The stray field energy is
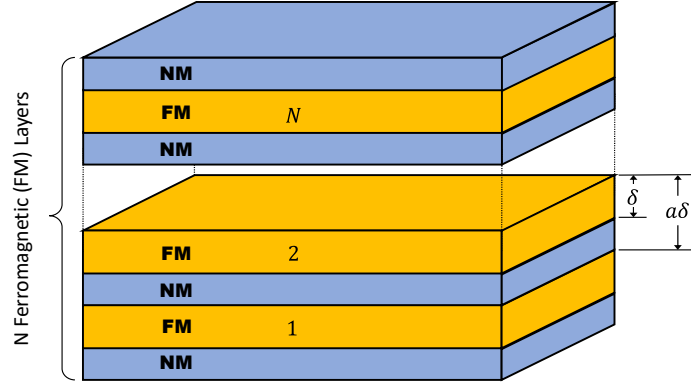
Figure 5.1 Schematic of a characteristic N-layer ferromagnetic (FM) system with identical layers of thickness δ. Each ferromagnetic layer is separated by $(a-1)\delta$ by non-magnetic (NM) spacer layers.

redefined accordingly

$$
\begin{aligned}
E_d &= \frac{1}{\delta} \int_{\mathbb{R}^3} \left(|\nabla U|^2 - \sum_i \chi_i \right) d^3 r, \\
&= \frac{1}{\delta} \int_{\mathbb{R}^3} \left(|\nabla U_r|^2 - 2\partial_3 U_r \right) d^3 r, \\
&= E_d' + E_d''.
\end{aligned}
\tag{5.7}
$$

We can transform the second term much in the same way as we obtained (4.8). Given that the result was obtained with identical assumptions on $\tilde{m}_{r,\parallel}$ we may simply quote

$$
E_d'' = -\frac{2}{\delta} \int_{\mathbb{R}^3} \left(\partial_3 U_r \right) d^3 r = \frac{2}{\delta} \int_{\mathbb{R}^3} \tilde{m}_{r,\parallel} d^3 r.
\tag{5.8}
$$

Now since $\tilde{m}_{r,\|} = \sum_i \chi_i(m_{i,\|} + 1)$, and using the fact that $|\mathbf{m}_i| = 1$ for all i, we may compute

$$2(m_i^\| + 1) = |\mathbf{m}_i^\perp|^2 + |m_i^\| + 1|^2,$$

$$2(\tilde{m}^\|(x, y, z) + 1) = \sum_{i=1}^N \chi_i(z) \left\{ |\mathbf{m}_i^\perp(x, y)|^2 + |m_i^\|(x, y) + 1|^2 \right\}. \tag{5.9}$$

Then integrating in z amounts to integrating disjoint characteristic functions, each having height, δ and we obtain

$$E_d'' = -\sum_{i=1}^N \int_{\mathbb{R}^2} \left(|\mathbf{m}_i^\perp|^2 + |m_i^\| + 1|^2 \right) d^2 r. \tag{5.10}$$

We now investigate

$$E_d' = \frac{1}{\delta} \int_{\mathbb{R}^3} |\nabla U_r|^2 d^3 r = \frac{1}{\delta} \int_{\mathbb{R}^3} \int_{\mathbb{R}^3} \frac{\nabla \cdot \tilde{\mathbf{m}}_r(\mathbf{r}) \nabla \cdot \tilde{\mathbf{m}}_r(\mathbf{s})}{4\pi |\mathbf{r} - \mathbf{s}|} d^3 r d^3 s. \tag{5.11}$$

Switching to cylindrical coordinates, take $\mathbf{r}, \mathbf{s} \in \mathbb{R}^2$ to obtain

$$E_d' = \frac{1}{\delta} \int_{\mathbb{R}} \int_{\mathbb{R}} \int_{\mathbb{R}^2} \int_{\mathbb{R}^2} \frac{\nabla \cdot \tilde{\mathbf{m}}_r(\mathbf{r}, z) \nabla \cdot \tilde{\mathbf{m}}_r(\mathbf{s}, \zeta)}{4\pi \sqrt{|\mathbf{r} - \mathbf{s}|^2 + (z - \zeta)^2}} d^2 r \; d^2 s \; dz \; d\zeta. \tag{5.12}$$

Use the following convention for the Fourier transform:

$$\hat{f}(\omega) = \int_{\mathbb{R}} f(z) e^{i\omega z} dz. \tag{5.13}$$

Applying Fourier transform in vertical variable, $z\hat{\mathbf{e}}_3 \to \omega\hat{\mathbf{e}}_3$, and using the convolution theorem and Parseval's formula we obtain

$$E_d' = \frac{1}{\delta} \int_{\mathbb{R}^2} \int_{\mathbb{R}^2} \int_{\mathbb{R}} \left(\overline{\widehat{\nabla \cdot \tilde{\mathbf{m}}_r}(\mathbf{r}, \omega)} \left(\frac{\widehat{K_0(|\mathbf{r} - \mathbf{s}||\omega|)}}{2\pi} \right) \widehat{\nabla \cdot \tilde{\mathbf{m}}_r}(\mathbf{s}, \omega) \right) \frac{d\omega}{2\pi} \; d^2 r \; d^2 s, \tag{5.14}$$

with

$$\widehat{\nabla \cdot \tilde{\mathbf{m}}_r}(\mathbf{r}, \omega) = \sum_{i=1}^{N} \left[\nabla \cdot \mathbf{m}_i^{\perp}(\mathbf{r}) \hat{\chi}_i(\omega) + (m_i^{\parallel}(\mathbf{r}) + 1) i\omega \hat{\chi}_i(\omega) \right], \tag{5.15}$$

and $K_0(r)$ being the modified Bessel function of the second kind [1]. The characteristic functions are,

$$\chi_0(z) = \chi_{(0,\delta)}(z), \quad \hat{\chi}_0(\omega) = \frac{1 - e^{-i\delta\omega}}{i\omega}. \tag{5.16}$$

We note that χ_i is just an appropriate shift of χ_0 and rewrite

$$\begin{aligned}
\widehat{\nabla \cdot \tilde{\mathbf{m}}_r}(\mathbf{r}, \omega) = \sum_{i=1}^{N} \Big[& \nabla \cdot \mathbf{m}_i^{\perp}(\mathbf{r}) \left(e^{-ia\delta(i-1)\omega} \hat{\chi}_0(\omega) \right) \\
& + (m_i^{\parallel}(\mathbf{r}) + 1) \left(i\omega e^{-ia\delta(i-1)\omega} \hat{\chi}_0(\omega) \right) \Big].
\end{aligned} \tag{5.17}$$

We can plug this expression into the energy and integrate out dependence on vertical variable ω to obtain

$$\begin{aligned}
E_d' = \frac{1}{\delta} \sum_{p=1}^{N} \sum_{q=1}^{N} \int_{\mathbb{R}^2} \int_{\mathbb{R}^2} \Big\{ & K_{vv}^{a(q-p)}(|\mathbf{r} - \mathbf{s}|) \, \nabla \cdot \mathbf{m}_p^{\perp}(\mathbf{r}) \nabla \cdot \mathbf{m}_q^{\perp}(\mathbf{s}) \\
& + K_{vs}^{a(q-p)}(|\mathbf{r} - \mathbf{s}|) \, \nabla \cdot \mathbf{m}_p^{\perp}(\mathbf{r})(m_q^{\parallel}(\mathbf{s}) + 1) \\
& + K_{sv}^{a(q-p)}(|\mathbf{r} - \mathbf{s}|) \, (m_p^{\parallel}(\mathbf{r}) + 1) \nabla \cdot \mathbf{m}_q^{\perp}(\mathbf{s}) \\
& + K_{ss}^{a(q-p)}(|\mathbf{r} - \mathbf{s}|) \, (m_p^{\parallel}(\mathbf{r}) + 1)(m_q^{\parallel}(\mathbf{s}) + 1) \Big\} d^2r \, d^2s.
\end{aligned} \tag{5.18}$$

Here we defined volume-volume, volume-surface and surface-surface interaction kernels as

$$K_{vv}^u(r) = \int_{\mathbb{R}} \frac{K_0(r|\omega|)}{2\pi} \left| \frac{1 - e^{-i\delta\omega}}{i\omega} \right|^2 e^{-i\delta u\omega} \frac{d\omega}{2\pi}, \tag{5.19}$$

$$K_{vs}^u(r) = \int_{\mathbb{R}} i\omega \frac{K_0(r|\omega|)}{2\pi} \left| \frac{1 - e^{-i\delta\omega}}{i\omega} \right|^2 e^{-i\delta u\omega} \frac{d\omega}{2\pi}, \tag{5.20}$$

$$K_{sv}^u(r) = \int_{\mathbb{R}} \overline{i\omega} \frac{K_0(r|\omega|)}{2\pi} \left| \frac{1 - e^{-i\delta\omega}}{i\omega} \right|^2 e^{-i\delta u\omega} \frac{d\omega}{2\pi}, \tag{5.21}$$

$$K_{ss}^u(r) = \int_{\mathbb{R}} \omega^2 \frac{K_0(r|\omega|)}{2\pi} \left| \frac{1 - e^{-i\delta\omega}}{i\omega} \right|^2 e^{-i\delta u\omega} \frac{d\omega}{2\pi}. \tag{5.22}$$

We see clearly, $K_{vs}^u(r) = -K_{sv}^u(r)$, allowing these terms to be combined in the expression for E_d'. For simplicity, we express the energy as the sum of interaction energies,

$$E_d' = \sum_{p=1}^{N} \sum_{q=1}^{N} \left\{ E_{vol}'^{(pq)} + E_{vs}'^{(pq)} + E_{surf}'^{(pq)} \right\}, \tag{5.23}$$

where

$$E_{vol}'^{(pq)} = \frac{1}{\delta} \left((\nabla \cdot \mathbf{m}_p^\perp), K_{vv}^{a(q-p)} * (\nabla \cdot \mathbf{m}_q^\perp) \right)_{L^2}, \tag{5.24}$$

$$E_{vs}'^{(pq)} = \frac{1}{\delta} \left((\nabla \cdot \mathbf{m}_p^\perp), K_{vs}^{a(q-p)} * (m_q^\| + 1) \right)_{L^2}$$
$$- \frac{1}{\delta} \left((m_p^\| + 1), K_{vs}^{a(q-p)} * (\nabla \cdot \mathbf{m}_q^\perp) \right)_{L^2}, \tag{5.25}$$

$$E_{surf}'^{(pq)} = \frac{1}{\delta} \left((m_p^\| + 1), K_{ss}^{a(q-p)} * (m_q^\| + 1) \right)_{L^2}. \tag{5.26}$$

We can explicitly evaluate the interaction kernels with the mathematica software to find

$$K_{vv}^u(r) = -\frac{1}{4\pi}\Bigg[-2\sqrt{r^2 + \delta^2 u^2} + \sqrt{r^2 + (\delta + \delta u)^2} + \sqrt{r^2 + (\delta - \delta u)^2} \tag{5.27}$$

$$- \delta(u+1)\sinh^{-1}\left(\frac{\delta(u+1)}{r}\right) + \delta(u-1)\sinh^{-1}\left(\frac{\delta - \delta u}{r}\right)$$

$$+ 2\delta|u|\sinh^{-1}\left(\frac{\delta|u|}{r}\right)\Bigg],$$

$$K_{vs}^u(r) = \frac{1}{4\pi}\Bigg[2\sinh^{-1}\left(\frac{\delta u}{r}\right) - \sinh^{-1}\left(\frac{\delta(u+1)}{r}\right) + \sinh^{-1}\left(\frac{(1-u)\delta}{r}\right)\Bigg], \tag{5.28}$$

$$K_{ss}^u(r) = \frac{1}{4\pi\sqrt{(r^2 + \delta^2(u-1)^2)(r^2 + \delta^2 u^2)(r^2 + (\delta + \delta u)^2)}}\Bigg[\tag{5.29}$$

$$- \sqrt{(r^2 + \delta^2(u-1)^2)(r^2 + \delta^2 u^2)} - \sqrt{(r^2 + \delta^2 u^2)(r^2 + (\delta + \delta u)^2)}$$

$$+ 2\sqrt{r^4 + 2\delta^2 r^2(u^2 + 1) + \delta^4(u^2 - 1)^2}\Bigg].$$

Since the layer displacement parameter, u, is understood to be $\mathcal{O}(1)$ with respect to δ, one expands to find the following

$$K_{vv}^u(r) \simeq \frac{\delta^2}{4\pi r} + \mathcal{O}(\delta^4), \tag{5.30}$$

$$K_{vs}^u(r) \simeq \frac{u\delta^3}{4\pi r^3} + \mathcal{O}(\delta^4), \tag{5.31}$$

$$K_{ss}^u(r) \simeq \frac{\delta^2}{4\pi r^3} + \mathcal{O}(\delta^4). \tag{5.32}$$

And note that the volume-surface interactions are a higher order effect. We can further simplify surface-surface interaction term. First we observe

$$\left(m_p^{||}(\mathbf{r}) - m_p^{||}(\mathbf{s})\right)\left(m_q^{||}(\mathbf{r}) - m_q^{||}(\mathbf{s})\right) = \left(m_p^{||}(\mathbf{r}) + 1\right)\left(m_q^{||}(\mathbf{r}) + 1\right)$$

$$+ \left(m_p^{||}(\mathbf{s}) + 1\right)\left(m_q^{||}(\mathbf{s}) + 1\right)$$

$$- \left(m_p^{||}(\mathbf{r}) + 1\right)\left(m_q^{||}(\mathbf{s}) + 1\right) \tag{5.33}$$

$$- \left(m_p^{||}(\mathbf{s}) + 1\right)\left(m_q^{||}(\mathbf{r}) + 1\right).$$

Integrating with the kernel, $K^u_{ss}(|\mathbf{r} - \mathbf{s}|)$, for $u = a(q - p)$, we find due to the invariance of K^u_{ss} with interchanges of $\mathbf{r}$ and $\mathbf{s}$,

$$\int_{\mathbb{R}^2} \int_{\mathbb{R}^2} K^u_{ss}(|\mathbf{r} - \mathbf{s}|) \left(m^\|_p(\mathbf{r}) - m^\|_p(\mathbf{s})\right) \left(m^\|_q(\mathbf{r}) - m^\|_q(\mathbf{s})\right) \, d^2r \, d^2s$$

$$= 2 \int_{\mathbb{R}^2} \int_{\mathbb{R}^2} K^u_{ss}(|\mathbf{r} - \mathbf{s}|) \left(m^\|_p(\mathbf{r}) + 1\right) \left(m^\|_q(\mathbf{r}) + 1\right) \, d^2r \, d^2s \,. \qquad (5.34)$$

$$- 2 \int_{\mathbb{R}^2} \int_{\mathbb{R}^2} K^u_{ss}(|\mathbf{r} - \mathbf{s}|) \left(m^\|_p(\mathbf{r}) + 1\right) \left(m^\|_q(\mathbf{s}) + 1\right) \, d^2r \, d^2s.$$

Therefore, the surface-surface interaction energies may be written as

$$E'^{(pp)}_{surf} = ||m^\|_p + 1||^2_{L^2} - \frac{1}{2\delta} \int_{\mathbb{R}^2} \int_{\mathbb{R}^2} K^u_{ss}(|\mathbf{r} - \mathbf{s}|) \left(m^\|_p(\mathbf{r}) - m^\|_p(\mathbf{s})\right)^2 \, d^2r \, d^2s, \text{ for } p = q,$$

$$E'^{(pq)}_{surf} = -\frac{1}{2\delta} \int_{\mathbb{R}^2} \int_{\mathbb{R}^2} K^u_{ss}(|\mathbf{r} - \mathbf{s}|) \left(m^\|_p(\mathbf{r}) - m^\|_p(\mathbf{s})\right) \left(m^\|_q(\mathbf{r}) - m^\|_q(\mathbf{s})\right) \, d^2r \, d^2s,$$

$$\text{for } p \neq q.$$

$$(5.35)$$

Asymptotically this may be rendered,

$$E'^{(pp)}_{surf} \simeq ||m^\|_p + 1||^2_{L^2} - \delta \int_{\mathbb{R}^2} \int_{\mathbb{R}^2} \frac{\left(m^\|_p(\mathbf{r}) - m^\|_p(\mathbf{s})\right)^2}{8\pi|\mathbf{r} - \mathbf{s}|^3} \, d^2r \, d^2s + \mathcal{O}(\delta^2), \text{ for } p = q,$$

$$E'^{(pq)}_{surf} \simeq -\delta \int_{\mathbb{R}^2} \int_{\mathbb{R}^2} \frac{\left(m^\|_p(\mathbf{r}) - m^\|_p(\mathbf{s})\right)\left(m^\|_q(\mathbf{r}) - m^\|_q(\mathbf{s})\right)}{8\pi|\mathbf{r} - \mathbf{s}|^3} \, d^2r \, d^2s + \mathcal{O}(\delta^2),$$

$$\text{for } p \neq q.$$

$$(5.36)$$

Meanwhile, the volume-volume interactions can be asymptotically expressed as

$$E'^{(pq)}_{vol} = \frac{1}{\delta} \int_{\mathbb{R}^2} \int_{\mathbb{R}^2} K^u_{vv}(|\mathbf{r} - \mathbf{s}|) \nabla \cdot \mathbf{m}^\perp_p(\mathbf{r}) \nabla \cdot \mathbf{m}^\perp_q(\mathbf{s}) \, d^2r \, d^2s$$

$$\simeq \delta \int_{\mathbb{R}^2} \int_{\mathbb{R}^2} \frac{\nabla \cdot \mathbf{m}^\perp_p(\mathbf{r}) \nabla \cdot \mathbf{m}^\perp_q(\mathbf{s})}{4\pi|\mathbf{r} - \mathbf{s}|} \, d^2r \, d^2s + \mathcal{O}(\delta^2). \qquad (5.37)$$

Using (5.31) it is clear that all volume-surface interaction energies are of order δ^2

$$E'^{(pq)}_{vs} \simeq \mathcal{O}(\delta^2). \qquad (5.38)$$

Combining all three interactions we obtain

$$
\begin{aligned}
E_d' \simeq \sum_{p=1}^{N} \Bigg\{ &||m_p^\parallel + 1||_{L^2}^2 + \delta \sum_{q=1}^{N} \int_{\mathbb{R}^2} \int_{\mathbb{R}^2} \Bigg(\\
&\frac{\nabla \cdot \mathbf{m}_p^\perp(\mathbf{r}) \nabla \cdot \mathbf{m}_q^\perp(\mathbf{s})}{4\pi|\mathbf{r}-\mathbf{s}|} - \frac{(m_p^\parallel(\mathbf{r}) - m_p^\parallel(\mathbf{s}))(m_q^\parallel(\mathbf{r}) - m_q^\parallel(\mathbf{s}))}{8\pi|\mathbf{r}-\mathbf{s}|^3} \Bigg) d^2r \; d^2s \Bigg\}.
\end{aligned}
\tag{5.39}
$$

Combining with (5.10), the total stray-field energy may finally be expressed as

$$
E_d = E_d' - \sum_{n=1}^{N} \int_{\mathbb{R}^2} \left(|\mathbf{m}_n^\perp|^2 + |m_n^\parallel + 1|^2 \right) d^2r.
\tag{5.40}
$$

Finally, we arrive at in the asymptotic representation of stray field energy

$$
\begin{aligned}
E_d \simeq \sum_{p=1}^{N} \Bigg\{ &-||\mathbf{m}_p^\perp||_{L^2}^2 + \delta \sum_{q=1}^{N} \int_{\mathbb{R}^2} \int_{\mathbb{R}^2} \Bigg(\\
&\frac{\nabla \cdot \mathbf{m}_p^\perp(\mathbf{r}) \nabla \cdot \mathbf{m}_q^\perp(\mathbf{s})}{4\pi|\mathbf{r}-\mathbf{s}|} - \frac{(m_p^\parallel(\mathbf{r}) - m_p^\parallel(\mathbf{s}))(m_q^\parallel(\mathbf{r}) - m_q^\parallel(\mathbf{s}))}{8\pi|\mathbf{r}-\mathbf{s}|^3} \Bigg) d^2r \; d^2s \Bigg\}.
\end{aligned}
\tag{5.41}
$$

This completes the derivation of the multilayer stray-field energy. Therefore, the total energy of the thin film system, without exchange interaction between films, is as follows.

$$
\begin{aligned}
E \simeq \sum_{p=1}^{N} \Bigg\{ &\int_{\mathbb{R}^2} |\nabla \mathbf{m}_p|^2 d^2r + (Q-1) \int_{\mathbb{R}^2} |\mathbf{m}_p^\perp|^2 d^2r \\
&+ \kappa \int_{\mathbb{R}^2} \left(m_\parallel^p \nabla \cdot \mathbf{m}_p^\perp - \mathbf{m}_p^\perp \cdot \nabla m_p^\parallel \right) d^2r \Bigg\} \\
&+ \delta \sum_{p=1}^{N} \sum_{q=1}^{N} \int_{\mathbb{R}^2} \int_{\mathbb{R}^2} \left(\frac{\nabla \cdot \mathbf{m}_p^\perp(\mathbf{r}) \nabla \cdot \mathbf{m}_q^\perp(\mathbf{s})}{4\pi|\mathbf{r}-\mathbf{s}|} \right) d^2r \; d^2s \\
&- \delta \sum_{p=1}^{N} \sum_{q=1}^{N} \int_{\mathbb{R}^2} \int_{\mathbb{R}^2} \left(\frac{(m_p^\parallel(\mathbf{r}) - m_p^\parallel(\mathbf{s}))(m_q^\parallel(\mathbf{r}) - m_q^\parallel(\mathbf{s}))}{8\pi|\mathbf{r}-\mathbf{s}|^3} \right) d^2r \; d^2s.
\end{aligned}
\tag{5.42}
$$

5.3 Interlayer Stray Field Interaction Energies of Skyrmions

For a system of interacting layers, there are four types of stray field interaction terms that need treatment. The volume (and surface) charge self-interaction, and the volume (and surface) interlayer interactions. Since the skyrmions may be laterally displaced relative to one another, another layer of complexity is introduced compared with skyrmions in the monolayer system. We have

$$E_{\text{vol}}^j = \frac{\delta}{4\pi} \int_{\mathbb{R}^2} \int_{\mathbb{R}^2} \frac{\nabla \cdot \mathbf{m}_{j,\perp}(\mathbf{r}) \nabla \cdot \mathbf{m}_{j,\perp}(\mathbf{r}')}{|\mathbf{r} - \mathbf{r}'|} d^2r d^2r', \tag{5.43}$$

$$E_{\text{surf}}^j = -\frac{\delta}{8\pi} \int_{\mathbb{R}^2} \int_{\mathbb{R}^2} \frac{\left(m_{j,\|}(\mathbf{r}) - m_{j,\|}(\mathbf{r}')\right)^2}{|\mathbf{r} - \mathbf{r}'|^3} d^2r d^2r', \tag{5.44}$$

$$E_{\text{vol}}^{ij} = \frac{\delta}{2\pi} \int_{\mathbb{R}^2} \int_{\mathbb{R}^2} \frac{\nabla \cdot \mathbf{m}_{i,\perp}(\mathbf{r}) \nabla \cdot \mathbf{m}_{j,\perp}(\mathbf{r}')}{|\mathbf{r} - \mathbf{r}'|} d^2r d^2r', \tag{5.45}$$

$$E_{\text{surf}}^{ij} = -\frac{\delta}{4\pi} \int_{\mathbb{R}^2} \int_{\mathbb{R}^2} \frac{\left(m_{i,\|}(\mathbf{r}) - m_{i,\|}(\mathbf{r}')\right)\left(m_{j,\|}(\mathbf{r}) - m_{j,\|}(\mathbf{r}')\right)}{|\mathbf{r} - \mathbf{r}'|^3} d^2r d^2r', \tag{5.46}$$

We proceed to calculate the interaction energy of skyrmions in each layer using the BP-profile ansatz. This will establish their stray field coupling energies and can be used to prove results for skyrmions in multilayer systems in the subsequent chapters. Take the following configuration for the skyrmion in each layer in the same fashion as Equation 3.18, now with a relative translation between the profiles, $\mathbf{r}_i$ and $\mathbf{r}_j$.

$$\mathbf{m}_i(\mathbf{r}) = -f_L\left(\frac{|\mathbf{r} - \mathbf{r}_i|}{\rho_i}\right) R_{\theta_i} \hat{\mathbf{e}}_r + \text{sgn}(\rho_i - |\mathbf{r} - \mathbf{r}_i|)\sqrt{1 - f_L^2\left(\frac{|\mathbf{r} - \mathbf{r}_i|}{\rho_i}\right)} \, \hat{\mathbf{e}}_3, \tag{5.47}$$

$$\mathbf{m}_j(\mathbf{r}) = -f_L\left(\frac{|\mathbf{r} - \mathbf{r}_j|}{\rho_j}\right) R_{\theta_j} \hat{\mathbf{e}}_r + \text{sgn}(\rho_j - |\mathbf{r} - \mathbf{r}_j|)\sqrt{1 - f_L^2\left(\frac{|\mathbf{r} - \mathbf{r}_j|}{\rho_j}\right)} \, \hat{\mathbf{e}}_3. \tag{5.48}$$

with R_{θ_i} being the rotation matrix defining the skyrmion's Néel -Bloch quality. The self-interactions are the same as calculated in monolayers, (3.23)-(3.24), and does not depend on the position of the skyrmions. The relative displacement will, in the end, only matter in magnitude, so define $l_{ij} = |\mathbf{r}_i - \mathbf{r}_j|$.

5.3.1 Interlayer stray field coupling energy of BP profiles

Take the following regrouping of the parameters:

$$\beta_{ij} = \sqrt{\rho_i \rho_j} \ , \quad \alpha_{ij} = \sqrt{\frac{\rho_j}{\rho_i}} \ , \quad \lambda_{ij} = \frac{l_{ij}}{\beta_{ij}}. \tag{5.49}$$

Since we are only analyzing the coupling of two layers here, we may revert to the shorthand $\beta = \beta_{ij}$, $\alpha = \alpha_{ij}$, and $\lambda = \lambda_{ij}$.

Insert the ansatz (5.47), (5.48) into equations (5.45) and (5.46). By strenuous application of Fourier analysis (Subsection 5.3.2), one may compute the coupling energies to the leading order for $L \gg 1$ as

$$E_{\text{vol}}^{ij} = \frac{3\pi^3}{4} \delta\beta \cos\theta_1 \cos\theta_2 F_v(\alpha, \lambda), \tag{5.50}$$

$$E_{\text{surf}}^{ij} = -\zeta \frac{\pi^3}{4} \delta\beta F_s(\alpha, \lambda), \tag{5.51}$$

where

$$F_v(\alpha, \lambda) = \frac{32}{3\pi^2} \int_0^\infty k^2 J_0(\lambda k) K_1(\alpha k) K_1(k/\alpha) dk, \tag{5.52}$$

$$F_s(\alpha, \lambda) = \frac{32}{\pi^2} \int_0^\infty k^2 J_0(\lambda k) K_0(\alpha k) K_0(k/\alpha) dk. \tag{5.53}$$

With these definitions, F_v and F_s take a maximum value of 1. They are symmetric about $\alpha = 1$, in the sense that they are invariant with interchanges of $\alpha \leftrightarrow \alpha^{-1}$. Of note is that F_s will take small negative values for large enough values of λ and $\alpha = 0$, see Figures 5.2 and 5.3.

Analyzing these integrals is a critical feature of the project at hand. They may be calculated numerically for any (α, λ) pair, but in the case of perfect symmetry, $\alpha = 1$, or in the case of concentric pairs, $\lambda = 0$, they do admit analytical expressions in terms of quadratic combinations of the complete elliptic integrals $E(z)$, $K(z)$, [1]. Furthermore, it is advantageous to introduce a new asymmetry parameter, $\omega = \log(\alpha)$.
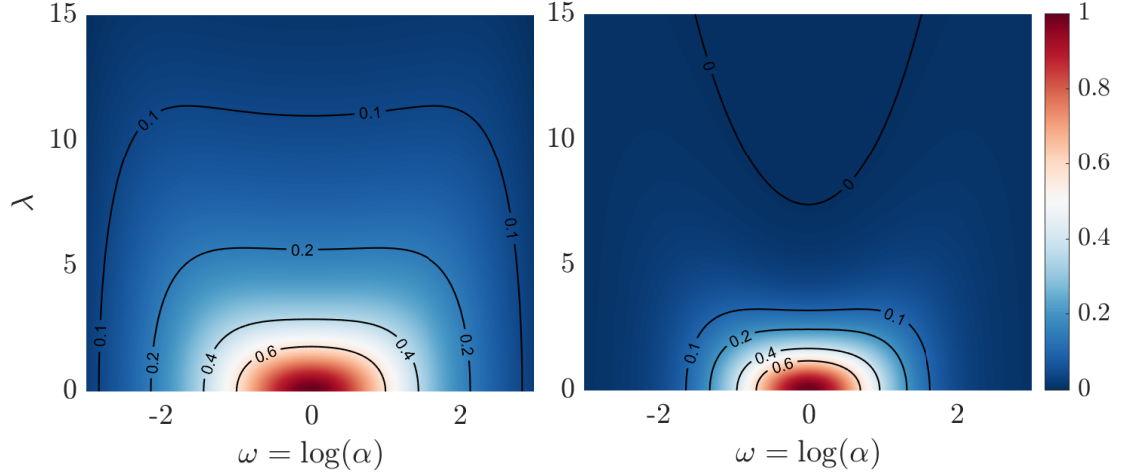
Figure 5.2 Stray field interaction integrals as a function of radius asymmetry, ω, and normalized core distance, λ. Note the rapid decay for either ω or λ tending away from zero. Left: $F_v(e^\omega, \lambda)$, this is always positive. Right: $F_s(e^\omega, \lambda)$, note the presence of the zero contour in the center of the upper half plane.

Then $\omega = 0$ represents perfect symmetry of skyrmion size, and F_v and F_s become even functions of ω.

5.3.2 Study of the stray field coupling integrals

The stray field coupling energy of skyrmions in the bilayer system has terms for volume and surface charges. Respectively, they are:

$$E_{vol}(\mathbf{m}_i, \mathbf{m}_j) = \frac{\delta}{2\pi} \int_{\mathbb{R}^2} \int_{\mathbb{R}^2} \frac{\nabla \cdot \mathbf{m}_{i,\perp}(\mathbf{r}) \nabla \cdot \mathbf{m}_{j,\perp}(\mathbf{r}')}{|\mathbf{r} - \mathbf{r}'|} d^2 r d^2 r', \tag{5.54}$$

$$E_{surf}(\mathbf{m}_i, \mathbf{m}_j) = -\frac{\delta}{4\pi} \int_{\mathbb{R}^2} \int_{\mathbb{R}^2} \frac{\left(m_{i,\|}(\mathbf{r}) - m_{i,\|}(\mathbf{r}')\right) \left(m_{j,\|}(\mathbf{r}) - m_{j,\|}(\mathbf{r}')\right)}{|\mathbf{r} - \mathbf{r}'|^3} d^2 r d^2 r'. \tag{5.55}$$

We shall derive expressions for the energy using the ansatz based calculation of two Belavin-Polyakov profiles a la Section 3.2.

First, use the following convention for the Fourier transform.

$$\hat{f}(\mathbf{k}) = \int_{\mathbb{R}^2} f(\mathbf{r}) e^{-i\mathbf{k}\cdot\mathbf{r}} d^2 r , \quad f(\mathbf{r}) = \int_{\mathbb{R}^2} \hat{f}(\mathbf{k}) e^{i\mathbf{k}\cdot\mathbf{r}} \frac{d^2 k}{(2\pi)^2}. \tag{5.56}$$

Based on theorem 7.12 in the book by Lieb and Loss [67], we may define the conjugate linear form for any two functions $f, g \in H^{1/2}(\mathbb{R}^2)$, for an operator $|p|$ which acts on the functions in Fourier space.

$$(f, |p|g) = \int_{\mathbb{R}^2} |\mathbf{k}| \hat{f}(\mathbf{k}) \overline{\hat{g}}(\mathbf{k}) \frac{d^2 k}{(2\pi)^2}. \tag{5.57}$$

The assertion is that it may be represented as a real space integral like so,

$$(f, |p|g) = \frac{1}{4\pi} \int_{\mathbb{R}^2} \int_{\mathbb{R}^2} \frac{(f(\mathbf{r}) - f(\mathbf{r}'))\overline{(g(\mathbf{r}) - g(\mathbf{r}'))}}{|\mathbf{r} - \mathbf{r}'|^3} \, d^2 r \, d^2 r'. \tag{5.58}$$

for when $f = g$ we recover Thm. 7.12 [67]. Then owing to the fact that $m_{\infty,\parallel} + 1 \in H^1(\mathbb{R}^2)$ and the inclusion $H^1(\mathbb{R}^2) \subseteq H^{1/2}(\mathbb{R}^2)$ we may render the surface-surface interaction energy more easily in Fourier space.

Representing both energy terms in Fourier space, we attain the following:

$$E_{vol}(\mathbf{m}_i, \mathbf{m}_j) = \delta \int_{\mathbb{R}^2} \frac{\mathbf{k} \cdot \hat{\mathbf{m}}_{i,\perp}(\mathbf{k}) \, \overline{\mathbf{k} \cdot \hat{\mathbf{m}}_{j,\perp}(\mathbf{k})}}{|\mathbf{k}|} \frac{d^2 k}{(2\pi)^2}, \tag{5.59}$$

$$E_{surf}(\mathbf{m}_i, \mathbf{m}_j) = -\delta \int_{\mathbb{R}^2} |\mathbf{k}| \hat{m}_{i,\parallel}(\mathbf{k}) \overline{\hat{m}_{j,\parallel}}(\mathbf{k}) \frac{d^2 k}{(2\pi)^2}. \tag{5.60}$$

Now supposing these profiles $\mathbf{m}_i$ take the form of BP profiles, with the further stipulation that they are not concentric. Let $\mathbf{m}_i$ be shifted by a distance $\mathbf{r}_i$. Then the profiles may be given in terms of the canonical Néel profile $\mathbf{m}_\infty$:

$$\mathbf{m}_i(\mathbf{r}) = R_{\theta_i} \mathbf{m}_{\infty,\perp} \left(\frac{\mathbf{r} - \mathbf{r}_i}{\rho_i} \right) + m_{\infty,\parallel} \left(\frac{\mathbf{r} - \mathbf{r}_i}{\rho_i} \right) \hat{\mathbf{e}}_z. \tag{5.61}$$

Then represent the profile by decomposing it into its Néel and Bloch components,

$$R_\theta \mathbf{m}_{\infty,\perp} = \cos(\theta) \mathbf{m}_{\infty,\perp} + \sin(\theta) \mathbf{m}_{\infty,\perp}^\perp. \tag{5.62}$$

The second term has zero divergence since $\mathbf{m}_{\infty,\perp}^{\perp} = f(r)\hat{\mathbf{e}}_\phi$, and as such will not factor into the volume charge energy. Using results from [9] we know

$$i\mathbf{k} \cdot \hat{\mathbf{m}}_{\infty,\perp}(\mathbf{k}) = -4\pi|\mathbf{k}|K_1(|\mathbf{k}|), \tag{5.63}$$

$$\hat{m}_{\infty,\|}(\mathbf{k}) = 4\pi K_0(|\mathbf{k}|). \tag{5.64}$$

Combining everything, the energy becomes (to leading order as $L \to \infty$):

$$E_{vol}(\mathbf{m}_i, \mathbf{m}_j) \simeq (4\pi)^2 \delta \rho_i^2 \rho_j^2 \cos\theta_i \cos\theta_j$$
$$\cdot \int_{\mathbb{R}^2} e^{-i\mathbf{k}\cdot(\mathbf{r}_i-\mathbf{r}_j)} |\mathbf{k}| K_1(\rho_i|\mathbf{k}|) K_1(\rho_j|\mathbf{k}|) \frac{d^2k}{(2\pi)^2}, \tag{5.65}$$

$$E_{surf}(\mathbf{m}_i, \mathbf{m}_j) \simeq -(4\pi)^2 \delta \rho_i^2 \rho_j^2 \int_{\mathbb{R}^2} e^{-i\mathbf{k}\cdot(\mathbf{r}_i-\mathbf{r}_j)} |\mathbf{k}| K_0(\rho_i|\mathbf{k}|) K_0(\rho_j|\mathbf{k}|) \frac{d^2k}{(2\pi)^2}. \tag{5.66}$$

We plan to represent the integrand in polar coordinates. Without loss of generality, let the displacement vector lie along the x-axis, and denote the magnitude $|\mathbf{r}_i - \mathbf{r}_j| = l_{ij}$. We have $\mathbf{k}$ represented by magnitude k and angle ϕ. Then $\mathbf{k} \cdot (\mathbf{r}_i - \mathbf{r}_j) = kl_{ij}\cos\phi$ and $d^2k = kd\phi dk$. Only one factor of the integrand depends on the angle, and we may integrate it separately,

$$\int_0^{2\pi} e^{-ikl_{ij}\cos\phi}d\phi = 2\pi J_0(kl_{ij}). \tag{5.67}$$

Now renormalize using the parameters defined in 5.49. With this system, one may interpret λ as the separation of the two skyrmions in terms of number of skyrmion radii. Rescale the variable of integration $q = \sqrt{\rho_i\rho_j}k$ and the energies become

$$E_{vol}(\mathbf{m}_i, \mathbf{m}_j) \simeq 8\pi\delta\beta \cos\theta_i \cos\theta_j \int_0^\infty J_0(\lambda q) K_1(\alpha q) K_1(q/\alpha) q^2 dq, \tag{5.68}$$

$$E_{surf}(\mathbf{m}_i, \mathbf{m}_j) \simeq -8\pi\delta\beta \int_0^\infty J_0(\lambda q) K_0(\alpha q) K_0(q/\alpha) q^2 dq. \tag{5.69}$$

Now define F_v and F_s by factoring out the energy value attained for $\lambda = 0$ and $\alpha = 1$. We then get the following representation:

$$E_{vol}(\mathbf{m}_i, \mathbf{m}_j) \simeq \frac{3\pi^3}{4}\delta\beta \cos\theta_i \cos\theta_j F_v(\alpha, \lambda), \tag{5.70}$$

$$E_{surf}(\mathbf{m}_i, \mathbf{m}_i) \simeq -\frac{\pi^3}{4}\delta\beta F_s(\alpha, \lambda). \tag{5.71}$$

And this is such that $F_v(1, 0) = F_s(1, 0) = 1$.

We now want to show some properties of functions F_v and F_s. Let us define

$$h_v(k, \alpha, \lambda) = \frac{32}{3\pi^2}k^2 J_0(\lambda k)K_1(\alpha k)K_1(k/\alpha) \tag{5.72}$$

$$h_s(k, \alpha, \lambda) = \frac{32}{\pi^2}k^2 J_0(\lambda k)K_0(\alpha k)K_0(k/\alpha) \tag{5.73}$$

and therefore

$$F_v(\alpha, \lambda) = \int_0^\infty h_v(k, \alpha, \lambda)dk \quad , \quad F_s(\alpha, \lambda) = \int_0^\infty h_s(k, \alpha, \lambda)dk. \tag{5.74}$$

Proposition: $F_v(\alpha, \lambda) < F_v(\alpha, 0) < F_v(1, 0)$ and $F_s(\alpha, \lambda) < F_s(\alpha, 0) < F_s(1, 0)$ for all $\lambda > 0$ or $0 < \alpha \neq 1$.

Proof. We observe $J_0(x) < J_0(0) = 1$ and $K_0(x) > 0$, $K_1(x) > 0$. Therefore

$$F_v(\alpha, \lambda) = \int_0^\infty h_v(k, \alpha, \lambda)dk < \int_0^\infty h_v(k, \alpha, 0)dk = F_v(\alpha, 0) \tag{5.75}$$

$$F_s(\alpha, \lambda) = \int_0^\infty h_s(k, \alpha, \lambda)dk < \int_0^\infty h_s(k, \alpha, 0)dk = F_s(\alpha, 0). \tag{5.76}$$

Now we can compute integrals $F_v(\alpha, 0)$ and $F_s(\alpha, 0)$ and show that for both maximum is achieved at $\alpha = 1$. We only do this for F_s. Firstly note, they exhibit an obvious symmetry about unity $F_v(\alpha, \lambda) = F_v(\alpha^{-1}, \lambda)$ (the same for F_s).

Due to the symmetry about $\alpha = 1$, we need only check that $\frac{\partial F_s}{\partial \alpha} < 0$ for $\alpha > 1$. The derivative may be expressed

$$\frac{\partial F_s}{\partial \alpha}\bigg|_{\alpha,0} = -c \int_0^\infty \left\{ K_1(\alpha k) K_0(k/\alpha) - \frac{1}{\alpha^2} K_0(\alpha k) K_1(k/\alpha) \right\} k^3 dk. \tag{5.77}$$

Due to the monotonicity of the bessel functions, $K_n(k)$, we have the ordering

$$K_1(\alpha k) < K_1(k) < K_1(k/\alpha), \tag{5.78}$$

for all $k > 0$ and $\alpha > 1$. Which allows us to get the estimate

$$\frac{\partial F_s}{\partial \alpha}\bigg|_{\alpha,0} \leq -c \int_0^\infty k^3 K_1(k) \left\{ K_0(k/\alpha) - \frac{1}{\alpha^2} K_0(\alpha k) \right\} dk, \tag{5.79}$$

which attains equality at $\alpha = 1$. By the same token, the difference between the two Bessel functions in brackets is positive, and this entire expression must be negative and bounding $\frac{\partial F_s}{\partial \alpha}$ from above. Hence, F_s is monotone decreasing in α and attains its maximum at $\alpha = 1$. Again, due to the monotonicity of $K_0(k)$ the upper bound is never zero except for $\alpha = 1$. Thus, F_s is in fact strictly monotone decreasing for $\alpha > 1$.

Therefore, we obtain that the only critical point of $F_s(\alpha, 0)$ is $\alpha = 1$ and it delivers a maximum.

$$\mathcal{Q.E.D.}$$
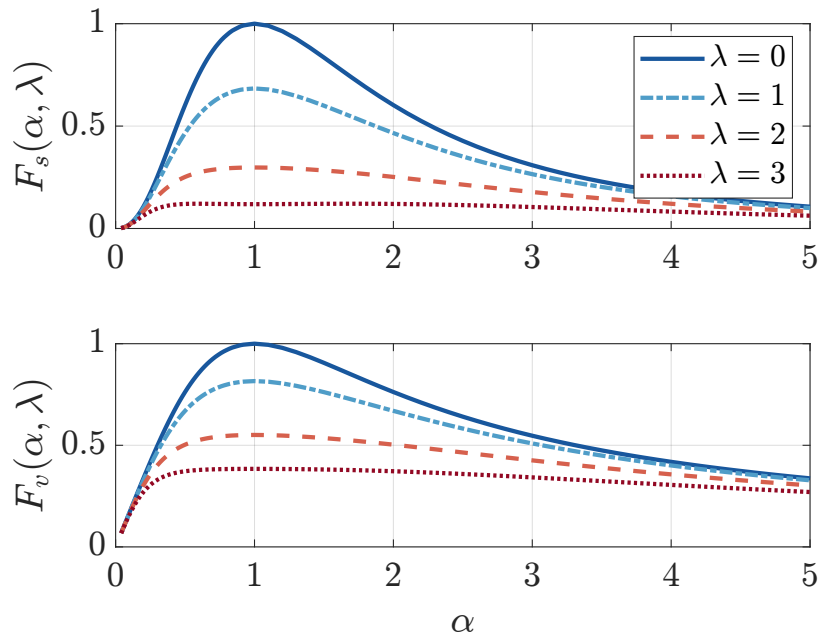
Figure 5.3 Stray field integrals $F_s(\alpha, \lambda)$ and $F_v(\alpha, \lambda)$ for select values of λ.

CHAPTER 6

STRAY FIELD ENABLED SKYRMIONS IN THIN MULTILAYERED MEDIA

We treat the multilayer ferromagnetic system with no DMI, where the layers interact with each other through the stray field only. Having derived the asymptotic model for the multilayer energy in the previous section, we may begin from the energy (5.42) and take $\kappa_i = 0$ and $\sigma = 0$.

We can search for minimizers in the restricted class of skyrmion profiles. This can be shown by ansatz based minimization of the thin film multilayer energy among the class of Belavin-Polyakov profiles. We treat the N layer case to show the existence of same-size skyrmion columns in a system governed by the exchange, anisotropy, and stray field interactions alone. We will also examine the particular case of 2 layers, which allows a more granular look at the energy landscape and gives insight into possible dynamics when skyrmions in different layers are separated by a nonzero distance. This reveals a saddle point in the skyrmion separation parameter, above a critical value the interaction is repulsive rather than attractive.

Beginning with the model energy equation of the thin multilayer system, having undergone asymptotic expansion in the layer thickness parameter δ, the stray field energy will be given by equation (5.41). Let the energy be represented in terms of the parameters defined in (2.29) by setting $\bar{\delta} = \delta/\sqrt{Q-1}$, and then we have the system

energy as follows:

$$E\left(\{\mathbf{m}_i\}\right) = \sum_{i=1}^{N} \int_{\mathbb{R}^2} \left(|\nabla \mathbf{m}_i|^2 + |\mathbf{m}_{i,\perp}|^2\right) d^2r$$

$$-\frac{\bar{\delta}}{8\pi} \sum_{i=1}^{N} \sum_{j=1}^{N} \int_{\mathbb{R}^2} \int_{\mathbb{R}^2} \frac{\left(m_{i,\parallel}(\mathbf{r}) - m_{i,\parallel}(\mathbf{r}')\right)\left(m_{j,\parallel}(\mathbf{r}) - m_{j,\parallel}(\mathbf{r}')\right)}{|\mathbf{r}-\mathbf{r}'|^3} d^2r d^2r' \quad (6.1)$$

$$+\frac{\bar{\delta}}{4\pi} \sum_{i=1}^{N} \sum_{j=1}^{N} \int_{\mathbb{R}^2} \int_{\mathbb{R}^2} \frac{\nabla \cdot \mathbf{m}_{i,\perp}(\mathbf{r}) \nabla \cdot \mathbf{m}_{j,\perp}(\mathbf{r}')}{|\mathbf{r}-\mathbf{r}'|} d^2r d^2r'$$

In Section 3.3, we illustrated how mono-layers are already known to support a Bloch skyrmion under these conditions [9].

6.1 Bloch Skyrmions in Multilayers Coupled Through Stray Field Alone

One obtains the reduced energy by calculating each of the integrals for the thin multilayer system energy on the set of Belavin-Polyakov profiles. These are shown in Section 3.3 for the layer self-interactions and the interlayer stray field interactions are given by Equations (5.70) and (5.71). Recall each of the parameters, ρ_i are the radius of the skyrmion in each layer, and θ_i their in-plane angle. l_{ij} is the lateral separation distance between skyrmion centers. The resultant reduced energy is

$$E = \sum_{i=1}^{N} \left[8\pi + \frac{4\pi}{L_i^2} + 4\pi\rho_i^2 \log\left(\frac{4L_i^2}{e^{2(1+\gamma)}}\right) + \bar{\delta}\frac{\pi^3}{8}\rho_i(3\cos^2\theta_i - 1) \right]$$

$$+ \sum_{i=1}^{N} \sum_{j<i} \bar{\delta}\frac{\pi^3}{4}\sqrt{\rho_i\rho_j} \left[3\cos\theta_i \cos\theta_j F_v\left(\sqrt{\frac{\rho_j}{\rho_i}}, \frac{l_{ij}}{\sqrt{\rho_i\rho_j}}\right) - F_s\left(\sqrt{\frac{\rho_j}{\rho_i}}, \frac{l_{ij}}{\sqrt{\rho_i\rho_j}}\right) \right].$$

$$\quad (6.2)$$

We now proceed to minimize the energy. We can prove the following result.

Theorem 2 *Let $i, N \in \mathbb{N}$ with $1 \leq i \leq N$ and $\rho_i \in \left(0, \frac{2}{e^{2+\gamma}}\right)$. Then the minimizers of the energy E defined in (6.2) satisfy*

1. *$\rho_i = \rho = -\frac{B}{2W(-\frac{B\sqrt{A}}{2})}$, where $A = \frac{e^{2+2\gamma}}{4}$, $B = \frac{\bar{\delta}\pi^2}{32}$ and W is a Lambert W function;*

2. *for $1 \leq j < i \leq N$ it holds $l_{ij} = 0$;*

3. $L_i = \rho^{-1}$;

4. $\sum_{i=1}^{N} \cos \theta_i = 0$.

Proof. We split the proof in several steps, separately minimizing in all variables.

Step 1. We first want to minimize in angles θ_i, $1 \leq i \leq N$. Keeping only meaningful terms depending on angles θ_i in the energy (6.2) we define the following function

$$h_0(\cos \theta_i, \cos \theta_j) = \sum_{i=1}^{N} \rho_i \cos^2 \theta_i + 2 \sum_{i=1}^{N} \sum_{j<i} \sqrt{\rho_i \rho_j} F_v(\alpha_{ij}, \lambda_{ij}) \cos \theta_i \cos \theta_j. \qquad (6.3)$$

We observe that $h_0 \geq 0$. Indeed, using definition of F_v one can show that $F_v(\alpha, \lambda) > 0$ and $F_v(\alpha, \lambda) \leq 1$ with equality achieved only at $(\alpha, \lambda) = (1, 0)$ (see Subsection 5.3.2). Therefore, it follows that quadratic form $h_0 \geq 0$. There are exactly two cases when $h_0(\cos \theta_i, \cos \theta_j) = 0$

1. $\theta_i = \frac{\pi}{2} + \pi n_i$ for some $n_i \in \mathbb{N}$;

2. $(\alpha_{ij}, \lambda_{ij}) = (1, 0)$ and $\sum_{i=1}^{N} \cos \theta_i = 0$ (note that $\alpha_{i,j} = 1$ implies $\rho_i = \rho_j$).

Therefore, minimization in θ_i yields $h_0 = 0$.

Step 2. Using Step 1 the energy minimization reduces to minimizing

$$E = \sum_{i=1}^{N} \left[8\pi + \frac{4\pi}{L_i^2} + 4\pi \rho_i^2 \log \left(\frac{4L_i^2}{e^{2(1+\gamma)}} \right) - \bar{\delta} \frac{\pi^3}{8} \rho_i \right.$$
$$\left. - \sum_{j<i} \bar{\delta} \frac{\pi^3}{4} \sqrt{\rho_i \rho_j} F_s \left(\sqrt{\frac{\rho_j}{\rho_i}}, \frac{l_{ij}}{\sqrt{\rho_i \rho_j}} \right) \right]. \qquad (6.4)$$

We now proceed to minimizing in L_i. Let $t_i = L_i^{-2}$ and define the following function

$$h_1(t_i) = t_i - \rho_i^2 \log t_i. \qquad (6.5)$$

The function is strictly convex and is minimized at $t_i = \rho_i^2$. Hence, the minimizing L_i is

$$L_i^\star = \rho_i^{-1}. \tag{6.6}$$

Recalling the asymptotic considerations, we require that L_i be large and ρ_i be small and hence their relationship is perfectly in order.

Step 3. After minimizing in θ_i and L_i the energy becomes

$$E = 8\pi N - \sum_{i=1}^{N} \left[4\pi \rho_i^2 \log\left(\frac{e^{(1+2\gamma)}}{4} \rho_i^2 \right) + \bar{\delta} \frac{\pi^3}{8} \rho_i + \sum_{j<i} \bar{\delta} \frac{\pi^3}{4} \sqrt{\rho_i \rho_j} F_s\left(\sqrt{\frac{\rho_j}{\rho_i}}, \frac{l_{ij}}{\sqrt{\rho_i \rho_j}} \right) \right]. \tag{6.7}$$

We now note that $F_s(\alpha, \lambda) < F_s(\alpha, 0)$ for all $\lambda > 0$ (see Subsection 5.3.2). Therefore, minimizing in l_{ij} we obtain $l_{ij} = 0$ and minimal energy simplifies even further.

$$E = 8\pi N - \sum_{i=1}^{N} \left[4\pi \rho_i^2 \log\left(\frac{e^{(1+2\gamma)}}{4} \rho_i^2 \right) + \bar{\delta} \frac{\pi^3}{8} \rho_i + \sum_{j<i} \bar{\delta} \frac{\pi^3}{4} \sqrt{\rho_i \rho_j} F_s\left(\sqrt{\frac{\rho_j}{\rho_i}}, 0 \right) \right]. \tag{6.8}$$

We now proceed to minimizing the above energy in ρ_i. Using $F_s(\alpha, 0) \leq 1$ we observe

$$\sum_{i=1}^{N} \sum_{j<i} \sqrt{\rho_i \rho_j} F_s\left(\sqrt{\frac{\rho_j}{\rho_i}}, 0 \right) \leq \sum_{i=1}^{N} \sum_{j<i} \sqrt{\rho_i \rho_j} \leq \frac{N-1}{2} \sum_{i=1}^{N} \rho_i, \tag{6.9}$$

with equality achieved only at $\rho_i = \rho_j = \rho$. Therefore we obtain

$$E \geq 8\pi N - \sum_{i=1}^{N} \left[4\pi \rho_i^2 \log\left(\frac{e^{(1+2\gamma)}}{4} \rho_i^2 \right) + \bar{\delta} \frac{N\pi^3}{8} \rho_i \right] = \sum_{i=1}^{N} F(\rho_i), \tag{6.10}$$

where

$$F(\rho) = 8\pi - 4\pi \rho^2 \log\left(\frac{e^{1+2\gamma}}{4} \rho^2 \right) - \bar{\delta} \frac{N\pi^3}{8} \rho, \tag{6.11}$$

as is shown in Figure 6.2. It is now clear that

$$\inf E = N \inf_{\rho} F(\rho). \tag{6.12}$$

We can now minimize $F(\rho)$ in the interval of model validity $\rho \in \left(0, \frac{2}{e^{2+\gamma}}\right)$. Due to convexity of $F(\rho)$ on this interval we just need to find its critical point by solving

$$F'(\rho) = -8\pi\rho \left(\ln\left(\rho^2 \frac{e^{1+2\gamma}}{4}\right) + 1\right) - \frac{N\bar{\delta}\pi^3}{8} = 0. \tag{6.13}$$

We rewrite this equation in the form

$$-2\rho \ln \rho - \rho \ln\left(\frac{e^{2+2\gamma}}{4}\right) = \frac{N\bar{\delta}\pi^2}{64}. \tag{6.14}$$

The solution is (taking $A = \frac{e^{2+2\gamma}}{4}$, $B = \frac{N\bar{\delta}\pi^2}{64}$)

$$\rho = -\frac{B}{2W\left(-\frac{B\sqrt{A}}{2}\right)}, \tag{6.15}$$

where W is a Lambert W function [1].

$$\mathcal{Q.E.D.}$$

Having established the existence of skyrmion columns we now wish to be able to determine the effect of displacement in one of the $\mathbf{r}_i$ parameters. On one hand, this helps to verify that the skyrmion column will not immediately collapse under perturbations, and on the other hand it leads the way toward more exploration of the energy landscape, which will be treated in the next section. Therefore, pose the minimization problem for skyrmions of a fixed position, $\{\mathbf{r}_i\}$, not necessarily equal to each other, and we obtain the next theorem.

Theorem 3 *Let $i, N \in \mathbb{N}$ with $1 \leq i \leq N$, $\rho_i \in \left(0, \frac{2}{e^{2+\gamma}}\right]$ and*

$$F(\{\rho_i\}, \{\mathbf{r}_i\}) = 8\pi N - \sum_{i=1}^{N} \left[4\pi \rho_i^2 \log\left(\frac{e^{(1+2\gamma)}}{4}\rho_i^2\right) + \bar{\delta}\frac{\pi^3}{8}\rho_i \right.$$
$$\left. + \sum_{j<i} \bar{\delta}\frac{\pi^3}{4}\sqrt{\rho_i\rho_j}F_s\left(\sqrt{\frac{\rho_j}{\rho_i}}, \frac{|\mathbf{r}_i - \mathbf{r}_j|}{\sqrt{\rho_i\rho_j}}\right) \right]. \tag{6.16}$$

Then there exists $\delta_0 > 0$ such that for any fixed $\{\mathbf{r}_i\}$ and all $\delta < \delta_0$ there exists a minimizer of the problem

$$\inf_{0 < \rho_i < \frac{2}{e^{2+\gamma}}} F(\{\rho_i\}, \{\mathbf{r}_i\}). \tag{6.17}$$

Proof. Step 1. We first need to show that the infimum is not equal $-\infty$. It follows, using $F_s(\alpha, \lambda) < F_s(1, 0) < 1$, that

$$\sum_{i=1}^{N}\sum_{j<i} \sqrt{\rho_i\rho_j}F_s\left(\sqrt{\frac{\rho_j}{\rho_i}}, \frac{|\mathbf{r}_i - \mathbf{r}_j|}{\sqrt{\rho_i\rho_j}}\right) \leq \frac{N-1}{2}\sum_{i=1}^{N}\rho_i. \tag{6.18}$$

Therefore, as in Step 3 of the proof of Theorem 2 we obtain

$$F(\{\rho_i\}, \{\mathbf{r}_i\}) \geq 8\pi N - \sum_{i=1}^{N}\left[4\pi\rho_i^2\log\left(\frac{e^{(1+2\gamma)}}{4}\rho_i^2\right) + \bar{\delta}\frac{N\pi^3}{8}\rho_i\right] = NF(\rho) \geq -NC.$$
$$\tag{6.19}$$

Step 2. Now we need to show that minimizing sequences $\rho_{i,n}$ do not converge to 0 for some i. Assume this is not true and, without loss of generality, that $\rho_{N,n} \to 0$ as

$n \to \infty$. In this case we see that the infimum of the energy is

$$F(\{\rho_i\}, \{\mathbf{r}_i\}) = 8\pi N - \sum_{i=1}^{N-1} \left[4\pi \rho_i^2 \log\left(\frac{e^{(1+2\gamma)}}{4} \rho_i^2 \right) + \bar{\delta} \frac{\pi^3}{8} \rho_i \right.$$
$$\left. + \sum_{j<i} \bar{\delta} \frac{\pi^3}{4} \sqrt{\rho_i \rho_j} F_s \left(\sqrt{\frac{\rho_j}{\rho_i}}, \frac{|\mathbf{r}_i - \mathbf{r}_j|}{\sqrt{\rho_i \rho_j}} \right) \right]. \tag{6.20}$$

Therefore, we only need to show that there exists $\rho_N \neq 0$ such that

$$G = 4\pi \rho_N^2 \log\left(\frac{e^{(1+2\gamma)}}{4} \rho_N^2 \right) + \bar{\delta} \frac{\pi^3}{8} \rho_N + \bar{\delta} \frac{\pi^3}{4} \sum_{j=1}^{N-1} \sqrt{\rho_N \rho_j} F_s \left(\sqrt{\frac{\rho_j}{\rho_N}}, \frac{|\mathbf{r}_N - \mathbf{r}_j|}{\sqrt{\rho_N \rho_j}} \right) > 0. \tag{6.21}$$

We will take $0 < \rho_N \ll 1$ and investigate

$$F_s(\alpha, \lambda) \sim \int_0^\infty k^2 J_0(\lambda k) K_0(\alpha k) K_0(k/\alpha) dk$$
$$= \frac{1}{\lambda^3} \int_0^\infty x^2 J_0(x) K_0(\alpha x/\lambda) K_0(x/(\alpha\lambda)) dx, \tag{6.22}$$

where

$$\alpha/\lambda = \frac{\rho_j}{|\mathbf{r}_N - \mathbf{r}_j|}, \qquad \alpha\lambda = \frac{|\mathbf{r}_N - \mathbf{r}_j|}{\rho_N}. \tag{6.23}$$

We observe that $\alpha/\lambda > 0$ is fixed, moreover $\beta = \frac{1}{\alpha\lambda} \ll 1$. We have estimates on $K_0(x)$ [1] such that

$$K_0(x) < h(x) = \max\{-\ln(x) + 1, 1\}. \tag{6.24}$$

It is now clear that we can estimate

$$\left| \int_0^\infty x^2 J_0(x) K_0(\alpha x/\lambda) K_0(x/(\alpha\lambda)) dx \right| \leq \int_0^\infty x^2 K_0(\alpha x/\lambda) h(\beta x) dx \leq C |\ln \rho_N|. \tag{6.25}$$
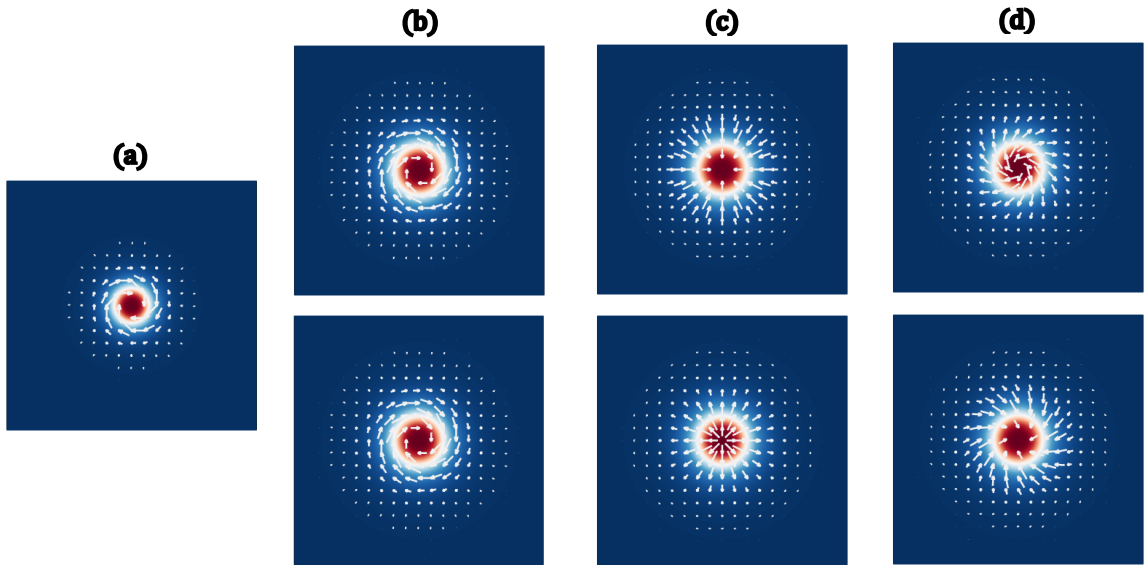
Figure 6.1 Comparison of several species of bilayer skyrmions represented by plots of BP-profiles with all layers of thickness $\bar{\delta}$ and radii obtained from (6.15). (a) Monolayer Bloch skyrmion. (b-c-d) Bilayer skyrmions. (b-c-d) Result in skyrmions of larger radii than would be obtained by a monolayer of depth $\bar{\delta}$. A bilayer system with concentric skyrmions in each layer admits precession of the in-plane angle, such that the radial components of the magnetization in each layer will be opposite. Thus one may have (b) concentric Bloch skyrmions, (c) opposite Néel skyrmions, (d) hybrid skyrmions having opposite radial components.

Therefore we obtain

$$G > 4\pi\rho_N^2 \log\left(\frac{e^{(1+2\gamma)}}{4}\rho_N^2\right) + \bar{\delta}\frac{\pi^3}{8}\rho_N - C\bar{\delta}\frac{\pi^3}{4}\rho_N^2|\ln\rho_N| > 0 \tag{6.26}$$

for $\rho_N \ll 1$.

Step 3. Now we need to show that minimizer $\rho_{i,n} \neq \frac{2}{e^{2+\gamma}}$. Assume this is not true and, without loss of generality, there is a minimizer with $\rho_{N,n} = \frac{2}{e^{2+\gamma}}$. In this case we see that the infimum of the energy is

$$
\begin{aligned}
F(\{\rho_i\}, \{\mathbf{r}_i\}) = 8\pi N - \sum_{i=1}^{N-1} &\left[4\pi\rho_i^2 \log\left(\frac{e^{(1+2\gamma)}}{4}\rho_i^2\right) + \bar{\delta}\frac{\pi^3}{8}\rho_i \right. \\
&\left. + \sum_{j<i} \bar{\delta}\frac{\pi^3}{4}\sqrt{\rho_i\rho_j}F_s\left(\sqrt{\frac{\rho_j}{\rho_i}}, \frac{|\mathbf{r}_i - \mathbf{r}_j|}{\sqrt{\rho_i\rho_j}}\right) \right] \\
&- 4\pi\rho_N^2 \log\left(\frac{e^{(1+2\gamma)}}{4}\rho_N^2\right) - \bar{\delta}\frac{\pi^3}{8}\rho_N \\
&- \sum_{j<N} \bar{\delta}\frac{\pi^3}{4}\sqrt{\rho_N\rho_j}F_s\left(\sqrt{\frac{\rho_j}{\rho_N}}, \frac{|\mathbf{r}_N - \mathbf{r}_j|}{\sqrt{\rho_N\rho_j}}\right)
\end{aligned}
\tag{6.27}
$$

The last term of the energy can be estimated as ($F_s < 1$ and $\rho_j \leq \rho_N$)

$$
\begin{aligned}
-4\pi\rho_N^2 \log&\left(\frac{e^{(1+2\gamma)}}{4}\rho_N^2\right) - \bar{\delta}\frac{\pi^3}{8}\rho_N - \sum_{j<N} \bar{\delta}\frac{\pi^3}{4}\sqrt{\rho_N\rho_j}F_s\left(\sqrt{\frac{\rho_j}{\rho_N}}, \frac{|\mathbf{r}_N - \mathbf{r}_j|}{\sqrt{\rho_N\rho_j}}\right) \\
&> 12\pi\frac{4}{e^{4+2\gamma}} - \bar{\delta}N\frac{\pi^3}{2e^{2+\gamma}}.
\end{aligned}
\tag{6.28}
$$

It is clear that for small enough $\bar{\delta}$ this term is positive. However, taking $\rho_N \to 0$ we observe that this term converges to 0 and so the minimum cannot be achieved at the boundary point.

<div align="right">$\mathcal{Q.E.D.}$</div>

It is clear that it is enough to characterize $F(\rho)$ to describe the minimizers of the multilayer energy among BP profiles (equation 6.2), and the resulting analysis decouples the ρ_i dependence on one another. The obtained solutions exhibit dependence only on
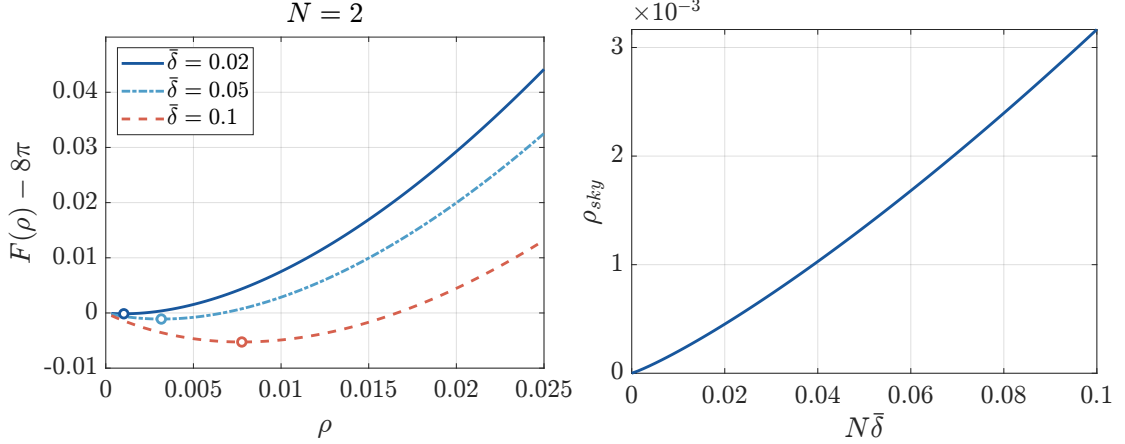
Figure 6.2 Left: $F(\rho)$ defined in equation 6.11, marked with its minimizing ρ values. Right: Energy minimizing ρ_{sky} obtained as a function of the universal parameter $N\bar{\delta}$.

the universal parameter $N\bar{\delta}$, as shown in Figure 6.2, reducing the multilayer system to a rescaling of the monolayer problem in this narrow sense. This suggests more stable or larger skyrmions can be engineered as a part of the coupled multilayer system, with more layers resulting in an increased surface charge interaction, promoting skyrmions, but retaining all the properties of the asymptotically thin system. However, this too should have its limits, as multiple layers would eventually create a stack of layers tall enough to exhibit genuine independence in the vertical coordinate, and one would have to revert to using the finite thickness equations.

More broadly, it has also been shown that the concentric skyrmion column is stable with respect to lateral displacement, l_{ij}, and the skyrmions do not tend to drift apart in the neighborhood of this minimizer. The analysis also reveals several degrees of freedom leftover, as when in the concentric phase, the skyrmion's angles are not uniquely determined by the energy minimization, as with a single layer, but rather obey a constraint equation given in Theorem 2. The consequence is that these systems may exhibit many different orientations of skyrmion with freely precessing angles, so long as they continue to obey the constraint. We can further understand these peculiarities in a reduced analysis of an $N = 2$ layer system presented in the subsequent section.

6.2 Stray Field Coupled Skyrmions in Bilayers

In the bilayer system, the simplest example of a non-trivial multilayer system, the energy minimization procedure may be replicated as was done in the preceeding section for the N layer system, so we present it in a brief form, and highlight particular features of the energy landscape as they appear.

One may write the full energy of two BP-profile skyrmions (Equations (5.47), (5.48)) using calculations from previous sections. We take a far field ferromagnetic alignment in all layers, since the antiferromagnetic case is not stable under dipolar action alone. Exchange coupling is not used, so $\bar{\sigma} = 0$. Using the symmetry parameters defined in (5.49), obtain the following reduced energy:

$$
\begin{aligned}
E = {} & 16\pi + \frac{4\pi}{L_1^2} + \frac{4\pi}{L_2^2} + 4\pi \left(\frac{\beta}{\alpha}\right)^2 \log\left(\frac{4L_1^2}{e^{2(1+\gamma)}}\right) + 4\pi(\alpha\beta)^2 \log\left(\frac{4L_2^2}{e^{2(1+\gamma)}}\right) \\
& + \bar{\delta}\frac{\pi^3}{8}\beta\bigg(3\left[\alpha^{-1}\cos^2\theta_1 + \alpha\cos^2\theta_2 + 2\cos\theta_1\cos\theta_2 F_v(\alpha, \lambda)\right] \\
& - \left[\alpha^{-1} + \alpha + 2F_s(\alpha, \lambda)\right]\bigg).
\end{aligned}
\tag{6.29}
$$

The desired result may be achieved by sequential minimizations of each of the variables. Immediately, $L_j^\star = 1/\rho_j$. Then the volume charge terms present another piece of information. As discussed, all terms featuring θ_j are volume charge energies. The volume charge is quadratic with $\cos\theta_j$, always positive, and is zero in the following scenarios: Either $\theta_j = \pm\pi/2$, then the $\mathbf{m}_j$'s are Bloch skyrmions. However, the quadratic system degenerates when the skyrmions are the same size, and perfectly concentric, $\alpha = 1$, $\lambda = 0$, in this case it accepts a family of minimizers $\theta_2 = \pi \pm \theta_1$, thereby aligning $\mathbf{m}_{j,\perp}$ antiparallel with one another. Remarkably, the angles are free to precess, maintaining this relationship, without being constrained by any other interaction. This enables a family of equivalently stable configurations for which the skyrmion in one layer has the same angular component as its partner in the other layer, while having opposite radial components, as shown in Figure 6.1c.
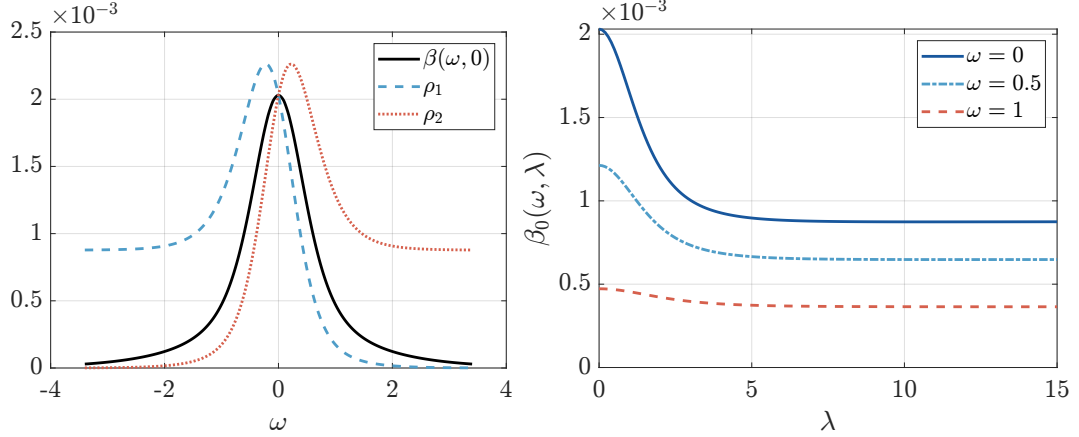
Figure 6.3 Skyrmion mean radii, (6.33), in the bilayer system depending on ω and λ after minimizing in all other variables, with $\bar{\delta} = 0.07$. Left: Schematic of skyrmion radii for $\lambda = 0$ as a function of ω. Right: radius β as a function of skyrmion separation, λ. When perfectly concentric with one another, the two skyrmions will strongly interact through the stray field and expand.

In all cases, it is clear that the surface charges are responsible for stabilizing the skyrmion structure. Write $G_s(\omega, \lambda) = F_s(e^\omega, \lambda)$, and let

$$\bar{\varepsilon}(\omega, \lambda, \delta) = \frac{\bar{\delta}\pi^3}{16}[\cosh(\omega) + G_s(\omega, \lambda)]. \tag{6.30}$$

$$\eta(\omega) = \frac{e^{1+\gamma+\omega\tanh(2\omega)}}{8\cosh(2\omega)}. \tag{6.31}$$

Next, represent the energy in terms of the remaining parameters

$$h(\beta, \omega, \lambda) = \frac{E - 16\pi}{4\pi} = -2\beta^2 \left(\cosh(2\omega)\log\left(e^{\frac{1+\gamma}{2}}\beta/2\right) + \omega\sinh(2\omega)\right) - \beta\bar{\varepsilon}(\omega, \lambda, \delta). \tag{6.32}$$

after minimizing over the mean radius, β, it may be expressed parametrically in terms of the remaining parameters:

$$\beta_0(\omega, \lambda) = \frac{-\bar{\varepsilon}(\omega, \lambda, \delta)}{4\cosh(2\omega)W_{-1}(-\eta(\omega)\bar{\varepsilon}(\omega, \lambda, \delta))}, \tag{6.33}$$

where, W_{-1} is the negative branch of the Lambert W function [1]. The bulk radius, β_0, attains its largest value for $\omega = 0$. For $\lambda = 0$ and increasing ω, the skyrmion
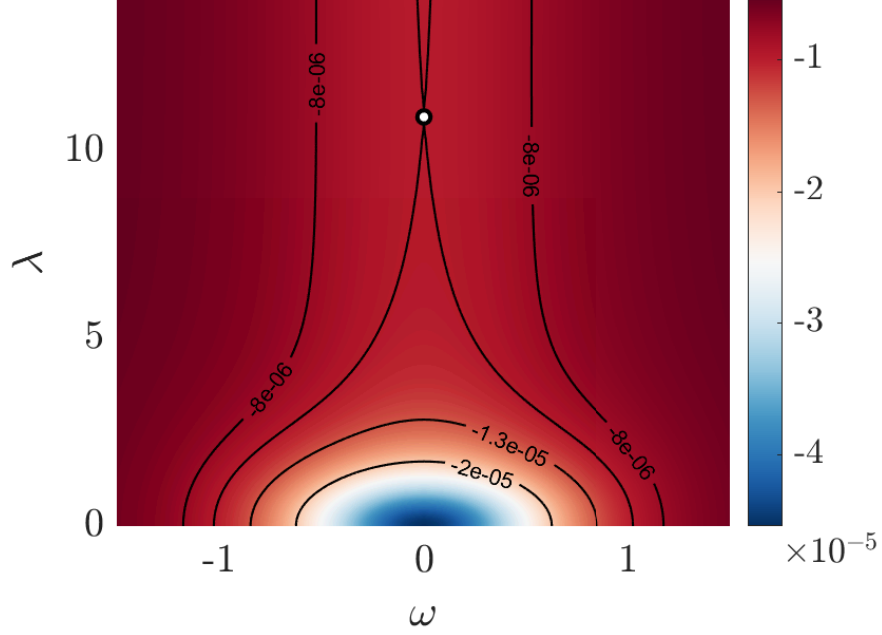
Figure 6.4 Energy $h(\beta, \omega, \lambda)$ after minimizing in β. Parameter values are $\bar{\kappa} = 0$, $\bar{\sigma} = 0$, $\bar{\delta} = 0.07$. The system favors a bound state where the skyrmions are concentric and perfectly symmetric $(\omega, \lambda) = (0, 0)$. Alternatively, note the presence of a saddle at $(\omega, \lambda) = (0, 10.9)$ beyond which, the skyrmion interaction is repulsive.

in one layer will reduce in size, while its counterpart will shrink to zero (see Figure 6.3). After substituting the result back into $h(\beta_0(\omega, \lambda), \omega, \lambda)$, the energy acquires a minimum for $\omega = \lambda = 0$, and the skyrmions form a bound pair and have the same size (see Figure 6.4). Same size skyrmions are clearly favored in all cases, but for λ larger than $\lambda_s = 10.9$, the energy crosses a saddle point, beyond which the skyrmions would experience a repulsive interaction, and run away to infinity. The value of λ_s is universal in this system and does not depend on $\bar{\delta}$.

CHAPTER 7

SKYRMIONS IN EXCHANGE COUPLED BILAYERS

Consider the case for multilayers with exchange coupling between layers. The coupling is represented as a "nearest neighbor" interaction between adjacent layers, with strength characterized by the constant σ given in dimensional form by the energy (5.2). This is a local interaction unlike the stray field, and could model both ferromagnetically coupled and antiferromagnetically coupled systems depending on the sign of J_{ec} [57, 84]. We shall proceed within the restricted class of skyrmion profiles, and examine the effect of both the ferromagnetic and antiferromagnetic exchange coupling interaction on a two layer system with skyrmions in each layer. We essentially treat the exchange coupling as the dominant interlayer interaction and regard stray field interlayer coupling as a perturbation. Therefore, we only consider skyrmions which are enabled by DMI, finally concluding under which circumstances these systems admit Néel skyrmions as energy minimizers.

Take the model energy equation, (5.1) for a thin multilayered ferromagnetic system with the asymptotic formulation of the stray field energy according to (5.41). Recall this is nondimensionalized such that $\sigma = J_{ec}/K_d$. Furthermore, for this section we take the regrouped constants defined in (2.29). This additionally yields the constant

$$\bar{\sigma} = \frac{\sigma}{\sqrt{Q-1}}. \tag{7.1}$$

The energy may thus be written as

$$
\begin{aligned}
E\left(\{\mathbf{m}_i\}\right) = &\sum_{i=1}^{N} \int_{\mathbb{R}^2} \left(|\nabla \mathbf{m}_i|^2 + |\mathbf{m}_{i,\perp}|^2 - 2\bar{\kappa}_i \mathbf{m}_{i,\perp} \cdot \nabla m_{i,\|} \right) d^2 r \\
&- \frac{\bar{\delta}}{8\pi} \sum_{i=1}^{N} \sum_{j=1}^{N} \int_{\mathbb{R}^2} \int_{\mathbb{R}^2} \frac{\left(m_{i,\|}(\mathbf{r}) - m_{i,\|}(\mathbf{r}') \right) \left(m_{j,\|}(\mathbf{r}) - m_{j,\|}(\mathbf{r}') \right)}{|\mathbf{r} - \mathbf{r}'|^3} d^2 r d^2 r' \\
&+ \frac{\bar{\delta}}{4\pi} \sum_{i=1}^{N} \sum_{j=1}^{N} \int_{\mathbb{R}^2} \int_{\mathbb{R}^2} \frac{\nabla \cdot \mathbf{m}_{i,\perp}(\mathbf{r}) \nabla \cdot \mathbf{m}_{j,\perp}(\mathbf{r}')}{|\mathbf{r} - \mathbf{r}'|} d^2 r d^2 r' \\
&+ \bar{\sigma} \sum_{i=1}^{N-1} \int_{\mathbb{R}^2} |\mathbf{m}_{i+1} - \mathbf{m}_i|^2 d^2 r
\end{aligned}
\tag{7.2}
$$

We restrict the analysis to a bilayer system ($N = 2$) and one where $|\bar{\sigma}|$ and $|\bar{\kappa}_j|$ are small, and yet large enough that the nonlocal component of the stray field interaction is negligible (in other words, let $\bar{\delta} = 0$).

7.1 Interlayer Exchange Coupling Energy of BP profiles

Exchange coupling between layers may be alternately defined depending on whether the layers are coupled ferromagnetically or antiferromagnetically ($\bar{\sigma} > 0$ or $\bar{\sigma} < 0$). Define an alignment parameter, $\zeta \in \{-1, 1\}$, which will stand in for the ferromagnetic ($\zeta = 1$) and antiferromagnetic ($\zeta = -1$) cases. The allowance of an antiferromagnetic order motivates the following redefinition of the ansatz:

$$
\mathbf{m}_1(\mathbf{r}) = -f_L\left(\frac{|\mathbf{r} - \mathbf{r}_1|}{\rho_1} \right) R_{\theta_1} \hat{\mathbf{e}}_r + \text{sgn}(\rho_i - |\mathbf{r} - \mathbf{r}_1|)\sqrt{1 - f_L^2\left(\frac{|\mathbf{r} - \mathbf{r}_1|}{\rho_1} \right)} \, \hat{\mathbf{e}}_3,
\tag{7.3}
$$

$$
\mathbf{m}_2(\mathbf{r}) = -f_L\left(\frac{|\mathbf{r} - \mathbf{r}_2|}{\rho_2} \right) R_{\theta_2} \hat{\mathbf{e}}_r + \zeta\,\text{sgn}(\rho_j - |\mathbf{r} - \mathbf{r}_2|)\sqrt{1 - f_L^2\left(\frac{|\mathbf{r} - \mathbf{r}_2|}{\rho_2} \right)} \, \hat{\mathbf{e}}_3.
\tag{7.4}
$$

We will also refer to the parameters α, β, λ defined in (5.49).

In the case of ferromagnetic coupling take the energy as written, and let $\zeta = 1$:

$$E_{ec}^+ = \bar{\sigma} \int_{\mathbb{R}^2} |\mathbf{m}_1 - \mathbf{m}_2|^2 d^2r. \tag{7.5}$$

Otherwise, one needs to introduce a constant offset to the integrand such that the energy might result in a bounded integral. So if $\bar{\sigma} < 0$, take $\zeta = -1$ and define instead:

$$E_{ec}^- = |\bar{\sigma}| \int_{\mathbb{R}^2} \left(4 - |\mathbf{m}_1 - \mathbf{m}_2|^2 \right) d^2r. \tag{7.6}$$

These integrals have yet to be calculated for the truncated BP-profiles; however, supposing the skyrmions centers are close to one another on the scale of the core, i.e. $\lambda \sim 1$, the calculation of the energy of untruncated BP-profiles, will capture the energy to leading order. Notice that it takes a similar form as the anisotropy energy $\int |\mathbf{m}_\perp|^2 d^2r$, and therefore may be a divergent integral. Therefore, we calculate this energy for $L \to \infty$.

When supposing perfect symmetry $\alpha = 1$, however, the cancellation of the tails of $\mathbf{m}_{j,\perp}$ will lead to a bounded result in this L-limit. One may therefore interpret this as a strong energy penalty on asymmetry, since E_{ec} is always positive. This forces $\beta = \rho_1 = \rho_2$ and the same in-plane angle $\theta_1 = \theta_2$. Formally, this can be calculated in Fourier space using Plancharel's theorem.

Begin by assuming $\bar{\sigma} > 0$, and so $\zeta = 1$. The other case assuming $\bar{\sigma} < 0$, $\zeta = -1$ will obtain the same result by trivial modification of the following derivation. Split the exchange coupling energy apart into contributions by in-plane and out-of-plane components

$$E_{ec}^+ = \bar{\sigma} \int_{\mathbb{R}^2} |\mathbf{m}_{1,\perp} - \mathbf{m}_{2,\perp}|^2 d^2r + \bar{\sigma} \int_{\mathbb{R}^2} \left(m_{1,\|} - m_{2,\|} \right)^2 d^2r. \tag{7.7}$$

We denote these integrals as $F_{12}^{\perp}$ and $F_{12}^{\parallel}$ respectively. Continuing, we have

$$F_{12}^{\perp} = \int_{\mathbb{R}^2} |\mathbf{m}_{1,\perp}(\mathbf{r}) - \mathbf{m}_{2,\perp}(\mathbf{r})|^2 d^2 r. \tag{7.8}$$

Then Plancharel's theorem finds

$$F_{12}^{\perp} = \int_{\mathbb{R}^2} |\hat{\mathbf{m}}_{1,\perp}(\mathbf{k}) - \hat{\mathbf{m}}_{2,\perp}(\mathbf{k})|^2 \frac{d^2 k}{(2\pi)^2}. \tag{7.9}$$

Note that these fields, $\mathbf{m}_j$ are conservative and admit a scalar potential (before rotation), therefore define

$$\Phi_\infty(\mathbf{r}) = \log\left(1 + |\mathbf{r}|^2\right). \tag{7.10}$$

$$\mathbf{m}_{\infty,\perp}(\mathbf{r}) = -\nabla\Phi_\infty(\mathbf{r}). \tag{7.11}$$

It then follows after introducing the BP symmetries see (3.5), for the first profile we have

$$\mathbf{m}_{1,\perp}(\mathbf{r}) = -\rho_1 R_{\theta_1} \nabla\Phi_\infty\left(\frac{\mathbf{r} - \mathbf{r}_1}{\rho_1}\right), \tag{7.12}$$

$$\mathbf{m}_{2,\perp}(\mathbf{r}) = -\rho_2 R_{\theta_2} \nabla\Phi_\infty\left(\frac{\mathbf{r} - \mathbf{r}_2}{\rho_2}\right). \tag{7.13}$$

Formally, we have the Fourier transform

$$\hat{\Phi}_\infty(\mathbf{k}) = -4\pi \frac{K_1(|\mathbf{k}|)}{|\mathbf{k}|}. \tag{7.14}$$

without loss of generality, suppose $\mathbf{r}_2 = 0$, and having already determined the radii must be identical, i.e. $\rho_1 = \rho_2 = \beta$, we arrive at the transformed profiles

$$\hat{\mathbf{m}}_{1,\perp}(\mathbf{k}) = 4\pi\beta^2 e^{-i\mathbf{k}\cdot\mathbf{r}_1}\frac{R_{\theta_1}\mathbf{k}}{|\mathbf{k}|}K_1(\beta|\mathbf{k}|). \tag{7.15}$$

$$\hat{\mathbf{m}}_{2,\perp}(\mathbf{k}) = 4\pi\beta^2\frac{R_{\theta_2}\mathbf{k}}{|\mathbf{k}|}K_1(\beta|\mathbf{k}|). \tag{7.16}$$

We may decompose these profiles into Néel and Bloch components.

$$\hat{\mathbf{m}}_{j,\perp}(\mathbf{k}) = \beta^2\cos\theta_j\left(\hat{\mathbf{m}}_{\infty,\perp}(\beta\mathbf{k})\right) + \beta^2\sin\theta_j\left(R_{\pi/2}\hat{\mathbf{m}}_{\infty,\perp}(\beta\mathbf{k})\right). \tag{7.17}$$

When expanding out the integrand in dot-products, the construction above exploits orthogonality; many of the terms are zero. The integral can be reduced to the following

$$F_{12}^{\perp} = 2\int_{\mathbb{R}^2}\left(1 - \cos(\theta_1 - \theta_2)\cos(\mathbf{k}\cdot\mathbf{r}_1)\right)\left|\hat{\mathbf{m}}_{\infty,\perp}(\beta\mathbf{k})\right|^2\frac{d^2k}{(2\pi)^2}. \tag{7.18}$$

In polar coordinates $\mathbf{k} = (k,\phi)$ let $\mathbf{k}\cdot\mathbf{r}_1 = kl_{12}\cos\phi$. Integration can be performed over the angular coordinate, ϕ_k. Then rescale as follows

$$\lambda = \frac{l_{12}}{\beta} \;\; ; \;\; s = \beta k, \tag{7.19}$$

where $|\mathbf{r}_1| = l_{12}$. We arrive at

$$F_{12}^{\perp} = 16\pi\int_0^\infty\left(1 - \cos(\theta_1 - \theta_2)J_0(\lambda s)\right)K_1^2(s)sds. \tag{7.20}$$

Observe the character of singularity in the integrand; for $s \to 0$ we have the singularity

$$\left(1 - \cos(\theta_1 - \theta_2)J_0(\lambda s)\right)K_1^2(s)s \simeq \pi\left(\frac{1 - \cos(\theta_1 - \theta_2)}{s}\right) + \mathcal{O}\left(s(c + \log(s))\right). \tag{7.21}$$

Therefore, this integral is only bounded when the skyrmion in both layers has the same in-plane angle θ_j. In such a case, we may finally calculate

$$F_{12}^{\perp}(\lambda) = 8\pi \left(\frac{2\left(\lambda^2 + 2\right)\sinh^{-1}\left(\frac{\lambda}{2}\right)}{\lambda\sqrt{\lambda^2 + 4}} - 1 \right). \tag{7.22}$$

As for the other term relating the out of plane components, we shall denote

$$F_{12}^{\parallel} = \frac{1}{\rho_1\rho_2} \int_{\mathbb{R}^2} \left((m_{1,\parallel}(\mathbf{r}) + 1) - (m_{2,\parallel}(\mathbf{r}) + 1) \right)^2 d^2r, \tag{7.23}$$

using the untruncated profile, $m_{j,\parallel}(\mathbf{r}) = m_{\infty,\parallel}\left(\frac{\mathbf{r} - \mathbf{r}_j}{\rho_j}\right)$ and following up with Plancharel's theorem. These profiles transform as follows,

$$\mathcal{F}\left\{m_{\infty,\parallel} + 1\right\} = 4\pi K_0(|\mathbf{k}|). \tag{7.24}$$

$$\mathcal{F}\left\{m_{1,\parallel} + 1\right\} = 4\pi\rho_1^2 e^{-i\mathbf{k}\cdot\mathbf{r}_1} K_0(\rho_1|\mathbf{k}|). \tag{7.25}$$

$$\mathcal{F}\left\{m_{2,\parallel} + 1\right\} = 4\pi\rho_2^2 K_0(\rho_2|\mathbf{k}|). \tag{7.26}$$

We have then

$$F_{12}^{\parallel} = \frac{4}{\rho_1\rho_2} \int_{\mathbb{R}^2} \left| \rho_1^2 e^{-i\mathbf{k}\cdot\mathbf{r}_1} K_0(\rho_1|\mathbf{k}|) - \rho_2^2 K_0(\rho_2|\mathbf{k}|) \right|^2 d^2k. \tag{7.27}$$

Again, we regroup the parameters using (5.49), and rescale the variable of integration $\beta\mathbf{k} = \mathbf{s}$. This integral becomes

$$F_{12}^{\parallel} = 4 \int_{\mathbb{R}^2} \left| e^{-i\mathbf{s}\cdot\mathbf{r}_1/\beta} \alpha^{-2} K_0(\alpha^{-1}|\mathbf{s}|) - \alpha^2 K_0(\alpha|\mathbf{s}|) \right|^2 d^2s. \tag{7.28}$$

After changing to polar coordinates and integrating in the angular variable this evaluates to the following.

$$F_{12}^{\parallel} = 8\pi \int_0^\infty \left(\alpha^{-4} K_0^2(\alpha^{-1}s) + \alpha^4 K_0^2(\alpha s) - 2J_0(\lambda s)K_0(\alpha^{-1}s)K_0(\alpha s) \right) s\,ds. \quad (7.29)$$

The symmetry in the first two terms which allows further simplification, yielding

$$F_{12}^{\parallel} = 8\pi \int_0^\infty \left((\alpha^{-2} + \alpha^2)K_0^2(s) - 2J_0(\lambda s)K_0(\alpha^{-1}s)K_0(\alpha s) \right) s\,ds. \quad (7.30)$$

For now this can be made compatible with the previously calculated $F_{12}^{\perp}$ by taking $\alpha = 1$ and consequently $\beta = \rho_1 = \rho_2$. We arrive at

$$F_{12}^{\parallel}(\lambda) = 16\pi \int_0^\infty \left(1 - J_0(\lambda s) \right) K_0^2(s)s\,ds \quad (7.31)$$

$$= 8\pi \left(1 - \frac{4\sinh^{-1}\left(\frac{\lambda}{2}\right)}{\lambda\sqrt{\lambda^2 + 4}} \right). \quad (7.32)$$

Now combining the above results to obtain the exchange coupling energy, we have

$$E_{ec}^{+} = \bar{\sigma}\beta^2 (F_{12}^{\perp}(\lambda) + F_{12}^{\parallel}(\lambda)). \quad (7.33)$$

Having given suitable treatment to the integrals for $\bar{\sigma} > 0$, this is immediately extendable to the case $\bar{\sigma} < 0$ by taking E_{ec}^{-} and computing it with the ansatz for $\zeta = -1$. One obtains the almost the same expressions for $F_{12}^{\perp}$ and $F_{12}^{\parallel}$. To summarize, we may define $F_{ec}^{\zeta}(\lambda)$ in Fourier space:

$$F_{ec}^{\zeta}(\lambda) = \int_0^\infty (1 - \zeta\cos(\theta_1 - \theta_2)J_0(\lambda k))K_1^2(k)k\,dk + \int_0^\infty (1 - J_0(\lambda k))K_0^2(k)k\,dk. \quad (7.34)$$

The energy is then,

$$E_{ec}^{\zeta} = 16\pi|\bar{\sigma}|\beta^2 F_{ec}^{\zeta}(\lambda), \quad (7.35)$$

which covers both cases, $\zeta = \pm 1$.

Recall, due to the cross interaction for the in-plane components, the first integral in (7.34) has a nonintegrable singularity for almost every choice of θ_j. The reason is the same reason which requires $\alpha = 1$, so θ_j must be such that the integrand decays rapidly enough for large $\mathbf{r}$. This fixes the relationship between the in-plane angles:

$$\zeta = 1 \;\Rightarrow\; \theta_1 = \theta_2,$$
$$\zeta = -1 \;\Rightarrow\; \theta_1 = \theta_2 + \pi. \tag{7.36}$$

Under this framework, we get

$$F_{ec}^{\zeta}(\lambda) = F_{ec}(\lambda) = \frac{\lambda \sinh^{-1}(\lambda/2)}{\sqrt{\lambda^2 + 4}}. \tag{7.37}$$

In conclusion, the skyrmions will have the same size, and the in-plane components will be parallel (or antiparallel when $\zeta = -1$) but their Néel or Bloch character will be determined by other interactions. Using this may be rather restrictive, but also advantageous as it immediately simplifies to same-size configurations before even considering the total energy. Such a simplification allows room to focus on the effects of displacement, λ.

7.2   Néel Skyrmions in DMI dominant Bilayers with Exchange Coupling

Consider a bilayer system where the stray field is negligible, $\bar{\delta} = 0$. Then the interlayer exchange will be the only interaction coupling the two layers. As shown in the previous result result, (3.27), for $\bar{\delta}$ small enough compared to $\bar{\kappa}$ a single-layer configuration will have a Néel skyrmion as its minimizer. This will be the same for the bilayer system. The exchange coupling effect results in a stable concentric pairing of same-size Néel skyrmions in (anti)ferromagnetically coupled layers. Early on in the analysis the energy discriminates between certain configurations of DMI, $\bar{\kappa}_j$, and permits stable
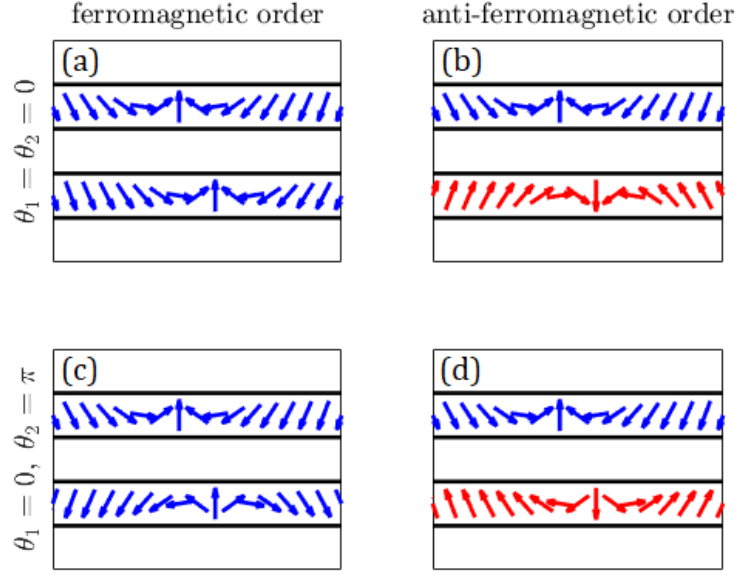
Figure 7.1 Schematic cases of Néel skyrmion pairs in bi-layers. The pictured skyrmions have in-plane angles which would be selected by the following DMI strengths: in the top layer $\bar{\kappa}_1 > 0$, (a,d) has $\bar{\kappa}_2 = \bar{\kappa}_1$, leading to two counterclockwise Néel skyrmions. (b,c) has $\bar{\kappa}_2 = -\bar{\kappa}_1$ resulting in one counterclockwise and one clockwise Néel skyrmion. Cases (c) and (d) fail to yield valid energy minimizers.

skyrmions only in the case of ferromagnetic coupling and same-sign DMI, or in the case of antiferromagnetic coupling and opposite-sign DMI.

Take the micromagnetic energy defined in (7.2) for $N = 2$ thin layers restricted to a system where both layers have DMI strength of identical magnitude, $|\bar{\kappa}_1| = |\bar{\kappa}_2| = \bar{\kappa}$, though they may take the same or opposite signs. Now compute the energies for the BP-profiles (Equations (7.3) and (7.4)). From the previous analysis of the exchange coupling energy, already $\alpha = 1$ must hold for $L \gg 1$, and the angles must satisfy (7.36) for this to be valid. Thus,

$$\theta_1 = \theta_2 + \frac{1+\zeta}{2}\pi, \tag{7.38}$$

and the energy may be written as,

$$E_{\rho,\theta,L,\lambda} = 16\pi + \sum_{j=1}^{2} \left[\frac{4\pi}{L_j^2} + 4\pi\beta^2 \log\left(\frac{4L_j^2}{e^{2(1+\gamma)}} \right) - 8\pi \operatorname{sgn}(\bar{\kappa}_j)\bar{\kappa}\beta \cos\theta_j \right] + 16\pi\bar{\sigma}\beta^2 F_{ec}(\lambda).$$

$$(7.39)$$

Upon inspection, only the DMI energy depends on the in-plane angles θ_j. Should the layers be coupled ferromagnetically, $\zeta = 1$, and if the DMI terms have opposite-sign, there is a problem. If $\theta_1 = \theta_2$, the total DMI energy is canceled out; therefore, it will not be possible to stabilize a skyrmion without this energy term present. The anisotropy interaction would minimize to $\beta = 0$. Therefore, we must discard this case before advancing. The same is true for two layers coupled antiferromagnetically, $\zeta = -1$, and same-sign DMI terms. These two failure cases are characterized in Figure 7.1.c and 7.1.d respectively. We proceed by cataloging all remaining choices for ζ, $\bar{\kappa}_1$, and $\bar{\kappa}_2$. If $\zeta = 1$, $\bar{\kappa}_1 = \bar{\kappa}_2 > 0$ (Figure 7.1.a), then the energy may be minimized by choosing

$$\theta_j^\star = 0. \tag{7.40}$$

In the case where $\zeta = 1$, $\bar{\kappa}_1 = \bar{\kappa}_2 < 0$ the same result is achieved by taking the opposite angle

$$\theta_j^\star = \pi. \tag{7.41}$$

Now, in the case of antiferromagnetic coupling, $\zeta = -1$, $\bar{\kappa}_1 > 0$, and $\bar{\kappa}_2 = -\bar{\kappa}_1$ (Figure 7.1.b), we get

$$\begin{aligned} \theta_1^\star &= 0, \\ \theta_2^\star &= \pi, \end{aligned} \tag{7.42}$$

and when $\zeta = -1$, $\bar{\kappa}_1 < 0$, $\bar{\kappa}_2 = -\bar{\kappa}_1$, we get

$$\begin{aligned} \theta_1^\star &= \pi, \\ \theta_2^\star &= 0. \end{aligned} \tag{7.43}$$
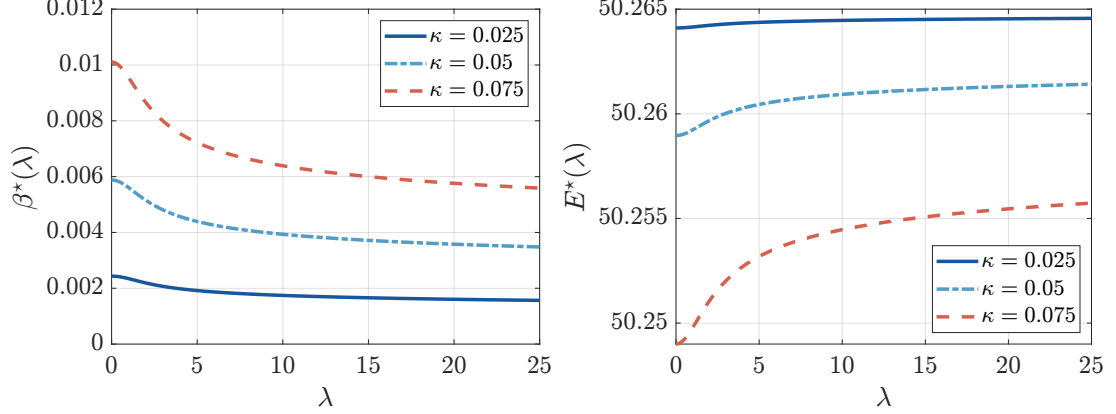
Figure 7.2 Left: skyrmion radius vs λ. Right: skyrmion energy vs λ, for select values of DMI strength $\bar{\kappa}$. Here we take $\bar{\sigma} = 0.75$. Note that the energy is minimized for $\lambda = 0$ when the skyrmions in each layer are concentric with one another. This is also where their radii take their largest values.

In all cases, the DMI energy resolves to the same value, $\sum_{j=1}^{2} E_{DMI}(\mathbf{m}_j) = -16\pi\bar{\kappa}\beta$.

The energy may then be minimized with parametric dependence on λ. We obtain

$$a(\bar{\sigma}, \lambda) = \exp\left[\gamma + 1 - \bar{\sigma}F_{12}(\lambda)\right], \tag{7.44}$$

$$\beta^{\star}(\lambda) = \frac{-|\bar{\kappa}|}{2W_{-1}\left(-\frac{1}{4}|\bar{\kappa}|\exp\left[\gamma + 1 - \bar{\sigma}F_{12}(\lambda)\right]\right)}, \tag{7.45}$$

$$E_{\beta^{\star}(\lambda),\theta^{\star},L^{\star},\lambda} = 16\pi\left[1 + \bar{\kappa}^2\left(\frac{1 + 2W_{-1}\left(-\frac{1}{4}a(\bar{\sigma}, \lambda)|\bar{\kappa}|\right)}{8W_{-1}^2\left(-\frac{1}{4}a(\bar{\sigma}, \lambda)|\bar{\kappa}|\right)}\right)\right]. \tag{7.46}$$

These are plotted in Figure 7.2. The resultant energy is monotonically increasing with λ, and takes its minimum at zero. Then it follows that the skyrmion size does not depend on $\bar{\sigma}$. Thus the role of the interlayer exchange coupling, in the final solution, is only to penalize deviations from $\lambda = 0$.

Take $\lambda = 0$ and we arrive at the final results, which are shown in Figure 7.3:

$$E^{\star} = 16\pi\left[1 + \bar{\kappa}^2\left(\frac{1 + 2W_{-1}\left(-\frac{1}{4}e^{1+\gamma}|\bar{\kappa}|\right)}{8W_{-1}^2\left(-\frac{1}{4}e^{1+\gamma}|\bar{\kappa}|\right)}\right)\right], \tag{7.47}$$
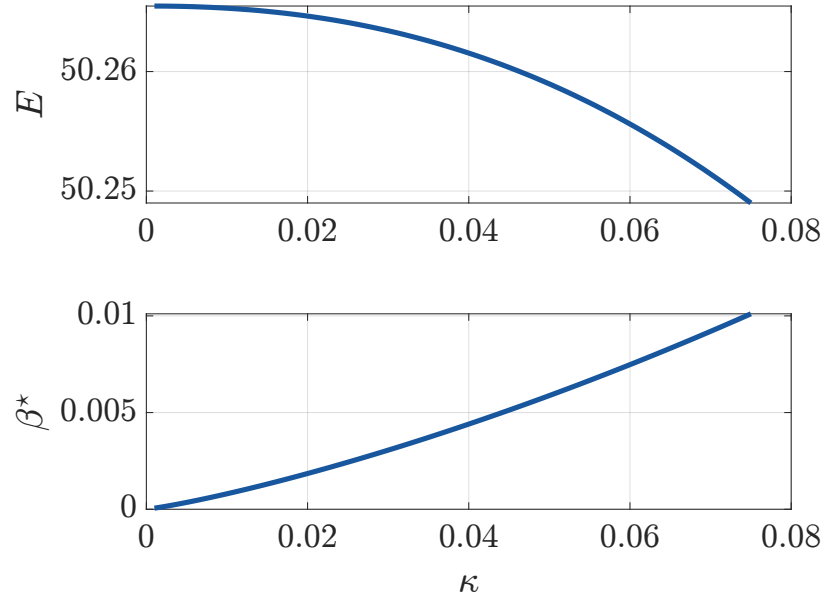
Figure 7.3 The energy, $E^\star$, and radius, $\beta^\star$, of a concentric bound pair of skyrmions in (anti)ferromagnetically coupled layers with $\bar{\delta} = 0$. The result does not depend on $\bar{\sigma}$.

$$\beta^\star = \frac{-|\bar{\kappa}|}{2W_{-1}\left(-\frac{1}{4}e^{1+\gamma}|\bar{\kappa}|\right)}. \tag{7.48}$$

CHAPTER 8

SUMMARY AND OUTLOOK

The problem of skyrmions in thin ferromagnetic multilayers has been addressed from the point of view of perturbations of harmonic maps and other analytical tools. The restricted class $\mathcal{A}$, and the Belavin-Polyakov profile based ansatz enable precise estimates and calculations of the micromagnetic energy necessary for this study. The methodology has also offered a straightforward framework within which to treat the stray field energy of the skyrmion in a plethora of physical systems.

The study of the finite thickness model gives further insight into the competition between stray field and anisotropy interactions in a monolayer. By analyzing the system without passing to the asymptotic limit, one observes strong two-parameter dependence on Q and δ. The model predicts a bifurcation after which skyrmion solutions fail to exist, a phenomenon which is not revealed in the asymptotic model [9]. The complementary analysis of numerical simulation corroborates the general trends among skyrmion solutions in this system.

Due to the form of the stray field interaction energy studied in the finite thickness model, a hypothetical reintroduction of the DMI would give rise to parameter combinations which have two local minimizers. This represents one avenue for continued study, and could lead to new understanding of how stray field and DMI compete or complement each other in the stabilization of skyrmions.

The numerical simulations allow some gesture toward the phase of skyrmion bursting or strip-out, and estimate the critical thickness $\bar{\delta}_b$ of strip-out. The direct simulation of the LLG equations remains valid in the thicker film regimes for which the use of the restricted class, $\mathcal{A}$, and the assumptions of vertical uniformity would become more dubious for use in a theoretical calculation. Still more can be done in

simulation to refine the estimate of the strip out thickness by attempting to bisect the material parameters across strip-out and non-strip-out regimes.

All this combined begins to form the complete picture of stray field enabled skyrmions in PMA materials, as it bounds the existence of skyrmions in a compact set in the (Q, δ) plane. Thus, the difficulty of engineering stray field enabled skyrmions in practice cannot be understated, as this analysis assumes very ideal conditions without thermal noise. This treatment therefore contextualizes the other results obtained for multilayer systems using the asymptotic models.

The derivation of the thin multilayer stray field energy is accomplished first by exactly solving Maxwell's equations in the system geometry for finite thickness, and then passing to the asymptotic form. This derivation sheds fundamental insight on the nature of interactions in the layered system such as characterizing the roles, and the origins of, the local shape-anisotropy, and surface and volume charges, and the often neglected surface-volume interaction energy. Arranging the interactions in their exact form as integral kernels gives a simple and adaptable scheme for calculation. This classification also establishes a clear asymptotic hierarchy of interactions, with the local interactions at leading order, at the next order the surface-surface and volume-volume interactions, and beginning at the third order are the surface-volume interactions.

In the case of a multilayer system with no DMI, where the layers interact with each other through the stray field only, we have found the existence of bound concentric skyrmion solutions using the asymptotic model as it applies to the class of Belavin-Polyakov profiles of the thin film multilayer energy. The presence of several interacting ferromagnetic layers leads to multiple nontrivial effects. In particular, the appearance of a distance threshold beyond which the interaction between skyrmions in each layer will switch to repulsion, and the existence of degrees of freedom among the rotation angles facilitated by the volume charge interactions. Furthermore, the added

stability acquired in multilayer systems compared to that of a stray field stabilized skyrmion in a monolayer represents one avenue for applied scientists to study these objects in experiment.

The results suggest a continuation in the form of a dynamical study of the bilayer system a la Thiele [57, 100]. Dynamically, skyrmions in coupled bilayer systems are known to exhibit different effects than that of the monolayer skyrmions when driven by electric current [112], but in the analyzed stray field coupled system, it is not yet known how the additional degree of freedom in the skyrmion rotation angle will affect the dynamics. This will be important to understand when viewing the stray field coupled multilayer system as a candidate for skyrmion-electronic applications.

We have also treated a bilayer system with DMI and $\delta = 0$, where the layers are coupled locally through a reduced exchange interaction. This system will also admit bound concentric skyrmion solutions for certain parameter values. Preliminary work suggests that adding the stray field back to this system as a perturbation could create a metastable state consisting of a bound skyrmion pair where the cores are slightly off-center. Investigation may be continued along these lines until a complete picture of the bilayer problem can be formed.

REFERENCES

[1] M. Abramowitz and I. Stegun. *Handbook of Mathematical Functions*. National Bureau of Standards, Gaithersburg, MD, USA, 10th edition, 1972.

[2] A. Aharoni. Magnetostatically coupled néel walls. *Journal of Applied Physics*, 38:2252–2253, 5, 1967. ISSN: 00218979.

[3] P. F. B. anf G. P. Müller, I. S. Lobanov, F. N. Rybakov, N. S. Kiselev, H. Jónsson, V. M. Uzdin, S. Blügel, L. Bergqvis, and A. Delin. Lifetime of racetrack skyrmion. *Scientific Reports*, 8:3433.

[4] V. Baltz, A. Manchon, M. Tsoi, T. Moriyama, T. Ono, and Y. Tserkovnyak. Antiferromagnetic spintronics. *Reviews of Modern Physics*, 90, 1, Feb. 2018. ISSN: 15390756.

[5] J. Barker and O. A. Tretiakov. Static and dynamical properties of antiferromagnetic skyrmions in the presence of applied current and temperature. *Physical Review Letters*, 116, 14, Apr. 2016. ISSN: 10797114.

[6] A. A. Belavin and A. M. Polyakov. Metastable states of two-dimensional isotropic ferromagnets. *Journal of Experimental and Theoretical Physics Letters*:245–247, 1975.

[7] K. V. Bergmann, A. Kubetzka, O. Pietzsch, and R. Wiesendanger. Interface-induced chiral domain walls, spin spirals and skyrmions revealed by spin-polarized scanning tunneling microscopy. *Journal of Physics Condensed Matter*, 26, 39, Oct. 2014. ISSN: 1361648X.

[8] A. Bernand-Mantel, C. B. Muratov, and T. M. Simon. A quantitative description of skyrmions in ultrathin ferromagnetic films and rigidity of degree ±1 harmonic maps from $R2$ to $S2$. *Archive for Rational Mechanics and Analysis*:219–299, 2021.

[9] A. Bernand-Mantel, C. B. Muratov, and T. M. Simon. Unraveling the role of dipolar versus dzyaloshinskii-moriya interaction in stabilizing compact magnetic skyrmions. *Physical Review B*:045416, 2020.

[10] A. Bernand-Mantel, L. Camosi, A. Wartelle, N. Rougemaille, M. Darques, and L. Ranno. The skyrmion-bubble transition in a ferromagnetic thin film. *SciPost Physics*, 4:27, 5, 2018.

[11] A. Bernand-Mantel, N. J. Dubicki, C. B. Muratov, and T. M. Simon. Stray field enabled skyrmions in ferromagnetic films of finite thickness, 2024. Manuscript in Preparation.

[12] A. Bernand-Mantel, N. J. Dubicki, C. B. Muratov, and V. V. Slastikov. Bloch skyrmions in stray field coupled magnetic multilayers, 2024. Manuscript in Preparation.

[13] A. Bernand-Mantel, A. Fondet, S. Barnova, T. M. Simon, and C. B. Muratov. Theory of magnetic field stabilized compact skyrmions in thin-film ferromagnets. *Physical Review B*, 108:L161405, 16, Oct. 2023. ISSN: 2469-9950.

[14] A. Bernand-Mantel, C. B. Muratov, and V. V. Slastikov. A micromagnetic theory of skyrmion lifetime in ultrathin ferromagnetic films. *Proceedings of the National Academy of Sciences of the United States of America*, 119:29, 2022.

[15] M. Bode, M. Heide, K. V. Bergmann, P. Ferriani, S. Heinze, G. Bihlmayer, A. Kubetzka, O. Pietzsch, S. Blügel, and R. Wiesendanger. Chiral magnetic order at surfaces driven by inversion asymmetry. *Nature*, 447:190–193, 7141, May 2007. ISSN: 14764687.

[16] A. Bogdanov and A. Hubert. The stability of vortex-like structures in uniaxial ferromagnets. *Journal of Magnetism and Magnetic Materials*, 195:182–192, 1999.

[17] A. Bogdanov and A. Hubert. Thermodynamically stable magnetic vortex states in magnetic crystals. *Journal of Magnetism and Magnetic Materials*, 138:255–269, 1994.

[18] A. N. Bogdanov and D. A. Yablonskii. Thermodynamically stable "vortices" in magnetically ordered crystals. the mixed state of magnets. *Soviet Journal of Experimental and Theoretical Physics*, 95:178–182, 1989.

[19] A. Bogdanov, M. Kudinov, and D. Yablonskii. Theory of magnetic vortices in easy-axis ferromagnets. *Soviet Physics Solid State*, 31:1707–1710, Oct. 1989.

[20] O. Boulle, J. Vogel, H. Yang, S. Pizzini, D. D. S. Chaves, A. Locatelli, T. O. Menteş, A. Sala, L. D. Buda-Prejbeanu, O. Klein, M. Belmeguenai, Y. Roussigné, A. Stashkevich, S. M. Chérif, L. Aballe, M. Foerster, M. Chshiev, S. Auffret, I. M. Miron, and G. Gaudin. Room-temperature chiral magnetic skyrmions in ultrathin magnetic nanostructures. *Nature Nanotechnology*, 11:449–454, 5, May 2016. ISSN: 17483395.

[21] H.-B. Braun. Topological effects in nanomagnetism: from superparamagnetism to chiral quantum solitons. *Advances in Physics*, 61(1):1–116, 2012.

[22] W. F. Brown. *Micromagnetics*. Interscience Tracts of Physics and Astronomy. Interscience Publishers (Wiley and Sons), New York, NY, USA, 1963.

[23] F. Büttner, B. Krüger, S. Eisebitt, and M. Kläui. Accurate calculation of the transverse anisotropy of a magnetic domain wall in perpendicularly magnetized multilayers. *Physical Review B*, 92, 5, Aug. 2015. ISSN: 1550235X.

[24] F. Büttner, I. Lemesh, and G. S. Beach. Theory of isolated magnetic skyrmions: from fundamentals to room temperature applications. *Scientific Reports*, 8, 1, Dec. 2018. ISSN: 20452322.

[25] L. Caretta, M. Mann, F. Büttner, K. Ueda, B. Pfau, C. M. Günther, P. Hessing, A. Churikova, C. Klose, M. Schneider, D. Engel, C. Marcus, D. Bono, K. Bagschik, S. Eisebitt, and G. S. Beach. Fast current-driven domain walls and small skyrmions in a compensated ferrimagnet. *Nature Nanotechnology*, 13:1154–1160, 12, Dec. 2018. ISSN: 17483395.

[26] S. Chikazumi. *Physics of Ferromagnetism*. Oxford University Press, Oxford, UK, 2nd edition, 2009.

[27] A. Crèpieux and C. Lacroix. Dzyaloshinsky-moriya interactions induced by symmetry breaking at a surface. *Journal of Magnetism and Magnetic Materials*, 182:341–349, 1998.

[28] H. T. Diep. Phase transition in frustrated magnetic thin film-physics at phase boundaries. *Entropy*, 21, 2, Feb. 2019. ISSN: 10994300.

[29] H.-D. Dietze and H. Thomas. Bloch und neel-wande in dunnen ferromagnetischen schichten. *Zeitschrift fur Physik*, 163:523–534, 1961.

[30] L. Döring and C. Melcher. Compactness results for static and dynamic chiral skyrmions near the conformal limit. *Calculus of Variations and Partial Differential Equations*, 56, Nov. 2017.

[31] Y. Dovzhenko, F. Casola, S. Schlotter, T. X. Zhou, F. Büttner, R. L. Walsworth, G. S. Beach, and A. Yacoby. Magnetostatic twists in room-temperature skyrmions explored by nitrogen-vacancy center spin texture reconstruction. *Nature Communications*, 9, 1, Dec. 2018. ISSN: 20411723.

[32] I. Dzyaloshinskii. A thermodynamic theory of "weak" ferromagnetism of antiferromagnetics. *Journal of Physics and Chemistry of Solids*, 4(4):241–255, 1958. ISSN: 0022-3697.

[33] S. Erokhin, D. Berkov, and A. Michels. Micromagnetics of ferromagnetic/ antiferromagnetic nanocomposite materials. i. towards a mesoscopic approach. *Physical Review B*, 108:214425, 21, Dec. 2023.

[34] A. Fert, V. Cros, and J. Sampaio. Skyrmions on the track. *Nature Nanotechnology*, 8:152–156, 3, 2013. ISSN: 17483395.

[35] A. Fert, N. Reyren, and V. Cros. Magnetic skyrmions: advances in physics and potential applications. *Nature Reviews Materials*, 2, June 2017. ISSN: 20588437.

[36] G. D. Fratta, C. B. Muratov, F. N. Rybakov, and V. V. Slastikov. Variational principles of micromagnetics revisited. *Society of Industrial and Applied Mathematics Journal on Mathematical Analysis*, 52:3580–3599, 4, 2020. ISSN: 10957154.

[37] G. D. Fratta, C. B. Muratov, and V. V. Slastikov. Reduced energies for thin ferromagnetic films with perpendicular anisotropy. *Mathematical Models and Methods in Applied Sciences*, 2024. To appear.

[38] C. J. García-Cervera. *Magnetic domains and magnetic domain walls*. PhD thesis, Courant Institute of Mathematical Sciences, New York University, New York, NY, USA, 1999.

[39] C. J. García-Cervera. Numerical micromagnetics: a review. *Boletin de la Sociedad Española de Matematica Aplicada*, 39:103–135, 2007.

[40] T. Gilbert. A phenomenological theory of damping in ferromagnetic materials. *IEEE Transactions on Magnetics*, 40(6):3443–3449, 2004.

[41] G. Gioia and R. D. James. Micromagnetics of very thin films. *Proceedings of the Royal Society of London. Series A: Mathematical, Physical and Engineering Sciences*, 453(1956):213–223, 1997.

[42] B. Göbel, I. Mertig, and O. A. Tretiakov. Beyond skyrmions: review and perspectives of alternative magnetic quasiparticles. *Physics Reports*, 895:1–28, 2021. ISSN: 0370-1573.

[43] S. Gustafson and L. Wang. Co-rotational chiral magnetic skyrmions near harmonic maps. *Journal of Functional Analysis*, 280, 4, Feb. 2021. ISSN: 10960783.

[44] J. Hagemeister, N. Romming, K. von Bergmann, E. Y. Vedmedenko, and R. Wiesendanger. Stability of single skyrmionic bits. *Nature Communications*, 6:8455, 2015.

[45] B. Heinrich and J. F. Cochran. Ultrathin metallic magnetic films: magnetic anisotropies and exchange interactions. *Advances in Physics*, 42:523–639, 5, Jan. 1993. ISSN: 14606976.

[46] S. Heinze, K. V. Bergmann, M. Menzel, J. Brede, A. Kubetzka, R. Wiesendanger, G. Bihlmayer, and S. Blügel. Spontaneous atomic-scale magnetic skyrmion lattice in two dimensions. *Nature Physics*, 7:713–718, 9, 2011. ISSN: 17452481.

[47] F. Hélein and J. C. Wood. Harmonic maps. In D. Krupka and D. Saunders, editors, *Handbook of Global Analysis*, pages 417–491. Elsevier, Amsterdam, The Netherlands, 2008. ISBN: 978-0-444-52833-9.

[48] A. Hubert and R. Schäfer. *Magnetic Domains: The Analysis of Magnetic Micro structures*. Springer, Berlin, Germany, 1998. ISBN: 9783540641087.

[49] B. Ivanov, V. Stephanovich, and A. Zhmudskii. Magnetic vortices: the microscopic analogs of magnetic bubbles. *Journal of Magnetism and Magnetic Materials*, 88(1):116–120, 1990. ISSN: 0304-8853.

[50] T. Jungwirth, X. Marti, P. Wadley, and J. Wunderlich. Antiferromagnetic spintronics. *Nature Nanotechnology*, 11:231–241, 3, Mar. 2016. ISSN: 17483395.

[51] S. K. Kim, G. S. Beach, K. J. Lee, T. Ono, T. Rasing, and H. Yang. Ferrimagnetic spintronics. *Nature Materials*, 21:24–34, 1, Jan. 2022. ISSN: 14764660.

[52] H. Knüpfer, C. B. Muratov, and F. Nolte. Magnetic domains in thin ferromagnetic films with strong perpendicular anisotropy. *Archive for Rational Mechanics and Analysis*, 232:727–761, 2, May 2019. ISSN: 14320673.

[53] R. V. Kohn and V. V. Slastikov. Effective dynamics for ferromagnetic thin films: a rigorous justification. *Proceedings of the Royal Society A: Mathematical, Physical and Engineering Sciences*, 461:143–154, 2053, Jan. 2005. ISSN: 14712946.

[54] A. G. Kolesnikov, M. E. Stebliy, A. S. Samardak, and A. V. Ognev. Skyrmionium – high velocity without the skyrmion hall effect. *Scientific Reports*, 8, 1, Dec. 2018. ISSN: 20452322.

[55] S. Komineas, C. Melcher, and S. Venakides. The profile of chiral skyrmions of small radius. *Nonlinearity*, 33:3395–3408, 2020.

[56] W. Koshibae and N. Nagaosa. Theory of antiskyrmions in magnets. *Nature Communications*, 7, Jan. 2016. ISSN: 20411723.

[57] W. Koshibae and N. Nagaosa. Theory of skyrmions in bilayer systems. *Scientific Reports*, 7:42645, Feb. 2017. ISSN: 20452322.

[58] T. Lancaster. Skyrmions in magnetic materials. *Contemporary Physics*, 60(3):246–261, July 2019.

[59] L. D. Landau and E. M. Lifshitz. *Electrodynamics of Continuous Media*. Pergamon Press Ltd., Oxford, UK, 1960.

[60] L. D. Landau and E. M. Lifshitz. On the theory of the dispersion of magnetic permeability in ferromagnetic bodies. *Physikalische Zeitschrift der Sowjetunion*, 8:153–169, 1935.

[61] W. Legrand, J.-Y. Chauleau, D. Maccariello, N. Reyren, S. Collin, K. Bouzehouane, N. Jaouen, V. Cros, and A. Fert. Hybrid chiral domain walls and skyrmions in magnetic multilayers. *Science Advances*, 4, 7, 2018.

[62] L. Leindler. On a certain converse of hölder's inequality ii. *Acta Scientiarum Mathematicarum*:217–223, 1972.

[63] L. Lemaire. Applications harmoniques de surfaces riemanniennes. *Journal of Differential Geometry*:51–78, 1978.

[64] I. Lemesh, F. Büttner, and G. S. Beach. Accurate model of the stripe domain phase of perpendicularly magnetized multilayers. *Physical Review B*, 95, 17, May 2017. ISSN: 24699969.

[65] A. O. Leonov, U. K. Rößler, and M. Mostovoy. Target-skyrmions and skyrmion clusters in nanowires of chiral magnets. *European Physical Journal Web of Conferences*, 75:05002, 2014.

[66] S. Li, J. Xia, X. Zhang, M. Ezawa, W. Kang, X. Liu, Y. Zhou, and W. Zhao. Dynamics of a magnetic skyrmionium driven by spin waves. *Applied Physics Letters*, 112:142404, Feb. 2018.

[67] E. H. Lieb and M. Loss. *Analysis*. American Mathematical Society, Providence, RI, USA, 2nd edition, 2002.

[68] I. S. Lobanov, H. Jónsson, and V. M. Uzdin. Mechanism and activation energy of magnetic skyrmion annihilation obtained from minimum energy path calculations. *Physical Review B*, 94:174418, 2016.

[69] C. T. Ma, X. Li, and S. J. Poon. Micromagnetic simulation of ferrimagnetic tbfeco films with exchange coupled nanophases. *Journal of Magnetism and Magnetic Materials*, 417:197–202, Nov. 2016. ISSN: 0304-8853.

[70] A. Manchon and S. Zhang. Theory of nonequilibrium intrinsic spin torque in a single nanomagnet. *Physical Review B*, 78:212405, 21, Dec. 2008.

[71] J. McCord. Progress in magnetic domain observation by advanced magneto-optical microscopy. *Journal of Physics D: Applied Physics*, 48:333001, 33, Aug. 2015. ISSN: 13616463.

[72] C. Melcher. Chiral skyrmions in the plane. *Proceedings of the Royal Society A: Mathematical, Physical and Engineering Sciences*, 470, 2172, Dec. 2014. ISSN: 14712946.

[73] C. Moreau-Luchaire, C. Moutafis, N. Reyren, J. Sampaio, C. A. Vaz, N. V. Horne, K. Bouzehouane, K. Garcia, C. Deranlot, P. Warnicke, P. Wohlhüter, J. M. George, M. Weigand, J. Raabe, V. Cros, and A. Fert. Additive interfacial chiral interaction in multilayers for stabilization of small individual skyrmions at room temperature. *Nature Nanotechnology*, 11:444–448, 5, May 2016. ISSN: 17483395.

[74] T. Moriya. Anisotropic superexchange interaction and weak ferromagnetism. *Physical Review*, 120:91–98, 1, Oct. 1960.

[75] S. Mühlbauer, B. Binz, F. Jonietz, C. Pfleiderer, A. Rosch, A. Neubauer, R. Georgii, and P. Böni. Skyrmion lattice in a chiral magnet. *Science*, 323:915, 2009.

[76] J. Müller. Magnetic skyrmions on a two-lane racetrack. *New Journal of Physics*, 19:025002, 2, Feb. 2017. ISSN: 13672630.

[77] C. B. Muratov and V. V. Slastikov. Domain structure of ultrathin ferromagnetic elements in the presence of Dzyaloshinskii-Moriya interaction. *Proceedings of the Royal Society A*, 473:20160666, 2017.

[78] C. B. Muratov. A universal thin film model for ginzburg–landau energy with dipolar interaction. *Calculus of Variations and Partial Differential Equations*, 58:52, 2, Apr. 2019. ISSN: 09442669.

[79] N. Nagaosa and Y. Tokura. Topological properties and dynamics of magnetic skyrmions. *Nature Nanotechnology*, 8:899–911, 12, 2013. ISSN: 17483395.

[80] A. K. Nayak, V. Kumar, T. Ma, P. Werner, E. Pippel, R. Sahoo, F. Damay, U. K. Rößler, C. Felser, and S. S. Parkin. Magnetic antiskyrmions above room temperature in tetragonal heusler materials. *Nature*, 548:561–566, 7669, Aug. 2017. ISSN: 14764687.

[81] F. Nolte. *Optimal scaling laws for domain patterns in thin ferromagnetic films with strong perpendicular anisotropy*. PhD thesis, Heidelberg University, Heidelberg, Germany, 2017.

[82] S. Novikov and A. Fomenko. *Basic Elements of Differential Geometry and Topology*. Springer Nature B.V., Berlin, Germany, 2010. ISBN: 9789048140800.

[83] H. Oezelt, A. Kovacs, F. Reichel, J. Fischbacher, S. Bance, M. Gusenbauer, C. Schubert, M. Albrecht, and T. Schrefl. Micromagnetic simulation of exchange coupled ferri-/ferromagnetic heterostructures. *Journal of Magnetism and Magnetic Materials*, 381:28–33, May 2015. ISSN: 03048853.

[84] S. Panigrahy, S. Mallick, J. Sampaio, and S. Rohart. Skyrmion inertia in synthetic antiferromagnets. *Physical Review B*, 106:144405, 14, Aug. 2022.

[85] M. Potkina, I. Lobanov, H. Jonsson, and V. Uzdin. Lifetime of skyrmions in discrete systems with infinitesimal lattice constant. *Journal of Magnetism and Magnetic Materials*, 549:168974, Jan. 2022.

[86] A. Prékopa. Logarithmic concave measures with applications to stochastic programming. *Acta Scientiarum Mathematicarum*:301–316, 1971.

[87] D. Prychynenko, M. Sitte, K. Litzius, B. Krüger, G. Bourianoff, M. Kläui, J. Sinova, and K. Everschor-Sitte. Magnetic skyrmion as a nonlinear resistive element: a potential building block for reservoir computing. *Physical Review Applied*, 9, 1, Jan. 2018. ISSN: 23317019.

[88] S. Rohart and A. Thiaville. Skyrmion confinement in ultrathin film nanostructures in the presence of dzyaloshinskii-moriya interaction. *Physical Review B*, 88:184422, 18, Nov. 2013.

[89] N. Romming, C. Hanneken, M. Menzel, J. E. Bickel, B. Wolter, K. von Bergmann, A. Kubetzka, and R. Wiesendanger. Writing and deleting single magnetic skyrmions. *Science*, 341(6146):636–639, 2013.

[90] N. Romming, A. Kubetzka, C. Hanneken, K. von Bergmann, and R. Wiesendanger. Field-dependent size and shape of single magnetic skyrmions. *Physical Review Letters*, 114:177203, 17, May 2015.

[91] U. K. Rößler, A. N. Bogdanov, and C. Pfleiderer. Spontaneous skyrmion ground states in magnetic metals. *Nature*, 442:797–801, 7104, Aug. 2006. ISSN: 14764687.

[92] M. Ruderman and C. Kittel. Indirect exchange coupling of nuclear magnetic moments by conduction electrons. *Physical Review*:99, 1954.

[93] M. Rupflin. Sharp quantitative rigidity results for maps from S^2 to S^2 of general degree, 2023. arXiv: 2305.17045.

[94] F. N. Rybakov and N. S. Kiselev. Chiral magnetic skyrmions with arbitrary topological charge. *Physical Review B*, 99, 6, Feb. 2019. ISSN: 24699969.

[95] L. Sánchez-Tejerina, R. Tomasello, V. Puliafito, B. Azzerboni, M. Carpentieri, and G. Finocchio. Unified framework for micromagnetic modeling of ferro-, ferri-, and antiferromagnetic materials at mesoscopic scale: domain wall dynamics as a case study. *IEEE Magnetics Letters*, 11:1–5, 2020.

[96] R. Schoen and K. Uhlenbeck. Boundary regularity and the dirichlet problem for harmonic maps. *Journal of Differential Geometry*, 18:253–268, 1983.

[97] M. Schott, A. Bernand-Mantel, L. Ranno, S. Pizzini, J. Vogel, H. Béa, C. Baraduc, S. Auffret, G. Gaudin, and D. Givord. The skyrmion switch: turning magnetic skyrmion bubbles on and off with an electric field. *Nano Letters*, 17(5):3006–3012, 2017. PMID: 28437086.

[98] T. H. R. Skyrme. A non-linear field theory. *Proc. Roy. Soc. London Ser. A*, 260:127–138, 1961. ISSN: 0962-8444,2053-9169.

[99] A. Suna. Perpendicular magnetic ground state of a multilayer film. *Journal of Applied Physics*, 59:313–316, 2, 1986. ISSN: 00218979.

[100] A. A. Thiele. Steady-state motion of magnetic domains. *Physical Review Letters*, 30:230–233, 6, Feb. 1973.

[101] Y. Tokura and N. Kanazawa. Magnetic skyrmion materials. *Chemical Reviews*, 121:2857–2897, 5, Mar. 2021. ISSN: 15206890.

[102] R. Tomasello, E. Martinez, R. Zivieri, L. Torres, M. Carpentieri, and G. Finocchio. A strategy for the design of skyrmion racetrack memories. *Scientific Reports*, 4:6784, Oct. 2014. ISSN: 20452322.

[103] L. N. Trefethen. Exactness of quadrature formulas. *SIAM Review*, 64(1):132–150, 2021.

[104] V. M. Uzdin, M. N. Potkina, I. S. Lobanov, and H. Jónsson. Energy surface and lifetime of magnetic skyrmions. *Journal of Magnetism and Magnetic Materials*, 459:236, 2018.

[105] A. Vansteenkiste, J. Leliaert, M. Dvornik, M. Helsen, F. Garcia-Sanchez, and B. Van Waeyenberge. The design and verification of mumax3. *American Institute of Physics Advances*, 4(10):107133, 2014.

[106] J. M. Winter. Bloch wall excitation. application to nuclear resonance in a bloch wall. *Physical Review*, 124:452–459, 2, Oct. 1961.

[107] S. Woo, K. Litzius, B. Krüger, M. Y. Im, L. Caretta, K. Richter, M. Mann, A. Krone, R. M. Reeve, M. Weigand, P. Agrawal, I. Lemesh, M. A. Mawass, P. Fischer, M. Kläui, and G. S. Beach. Observation of room-temperature magnetic skyrmions and their current-driven dynamics in ultrathin metallic ferromagnets. *Nature Materials*, 15:501–506, 5, May 2016. ISSN: 14764660.

[108] J. C. Wood. *Harmonic mappings between surfaces : some local and global properties*. PhD thesis, University of Warwick, Coventry, UK, June 1974.

[109] X. Yu, D. Morikawa, T. Yokouchi, K. Shibata, N. Kanazawa, F. Kagawa, T.-h. Arima, and Y. Tokura. Aggregation and collapse dynamics of skyrmions in a non-equilibrium state. *Nature Physics*, 14:832–836, 8, Aug. 2018. ISSN: 17452481.

[110] J. Zázvorka, F. Jakobs, D. Heinze, N. Keil, S. Kromin, S. Jaiswal, K. Litzius, G. Jakob, P. Virnau, D. Pinna, K. Everschor-Sitte, L. Rózsa, A. Donges, U. Nowak, and M. Kläui. Thermal skyrmion diffusion used in a reshuffler device. *Nature Nanotechnology*, 14:658–661, 7, July 2019. ISSN: 17483395.

[111] X. Zhang, J. Xia, Y. Zhou, D. Wang, X. Liu, W. Zhao, and M. Ezawa. Control and manipulation of a magnetic skyrmionium in nanostructures. *Physical Review B*, 94, 9, Sept. 2016. ISSN: 24699969.

[112] X. Zhang, Y. Zhou, and M. Ezawa. Magnetic bilayer-skyrmions without skyrmion hall effect. *Nature Communications*, 7:10293, Jan. 2016. ISSN: 20411723.

[113] X. Zhang, Y. Zhou, K. M. Song, T.-E. Park, J. Xia, M. Ezawa, X. Liu, W. Zhao, G. Zhao, and S. Woo. Skyrmion-electronics: writing, deleting, reading and processing magnetic skyrmions toward spintronic applications. *Journal of Physics: Condensed Matter*, 32(14):143001, Jan. 2020.